EFFECTS OF NANOPARTICLE FUNCTIONALIZATION, SHAPE & SIZE ON LUNG FUNCTION & INFLAMMATION.

By

DANIELLE JOY BOTELHO

A dissertation submitted to the

Graduate School-New Brunswick

Rutgers, The State University of New Jersey

And

The Graduate School of Biomedical Sciences

In partial fulfillment of the requirements

For the degree of

Doctor of Philosophy

Joint Graduate Program in Toxicology

Written under the direction of

Andrew J. Gow

And approved by

_____

_____

_____

_____

_____

New Brunswick, New Jersey

October 2015

ABSTRACT OF THE DISSERTATION

Effects of Nanoparticle Functionalization, Shape & Size on Lung Function & Inflammation

By DANIELLE JOY BOTELHO

Dissertation Director:

Andrew J. Gow, Ph.D.

With the rise of nanoparticle use in commercial products, industry, and medicine, there is a need to better understand the consequences of nanoparticle exposure. Due to their nano-scale size, the lung is a primary route of exposure. To study the effects of nanoparticle functionalization, shape and size on the lung, an organ-level toxicological approach was taken. To achieve an organ-level approach, respiratory mechanics were first evaluated. Following ventilation, bronchoalveolar lavage was performed to obtain cells and lung lining fluid for cellular, cytokine, protein, and lipid analysis. Lastly, the lungs were harvested for assessment of tissue structure and immunohistochemistry. The collection of these endpoints allowed for a more complex approach that relates both molecular and physiological endpoints, which provides the foundation for more translational work to be done that addresses both environmental and occupational exposure risks to the public concerning nanomaterials. The data provided within this thesis validates that the primary driving factors in organ level respiratory response to nanoparticle exposure are: core composition (metal v. carbon), zeta potential, shape, and host inflammatory state. These factors affect injury and inflammation, surfactant composition and lung function. Overall, this work examines how nanoparticle biophysics alters both lung function and inflammation.

ACKNOWLEDGEMENTS

The road to completing my dissertation was challenging, and I could not have done it without the support of my committee members, mentor, family, friends, and labmates. While this experience has been challenging it has also been extremely rewarding. I am grateful to those who helped me along the way, although I am not sure I have the words to adequately express exactly how much I appreciate everyone involved…but I will do my best.

Before thanking those directly involved in my day-to-day work, I would like to acknowledge the Graduate School-New Brunswick Staff. Barbara, Alex, Gary, and your whole team—you have been a great and constant support these last years. You work so hard "behind the scenes," thank you for everything!

To my thesis committee—Dr. Robert Laumbach, Dr. Stephan Schwander, Dr. Junfeng (Jim) Zhang, and Dr. Jeffrey Laskin: collaborating with you all has been my absolute pleasure. Your insightful questions and guidance as I developed my studies was invaluable. To Dr. Debra Laskin—thank you for all of your encouragement over the years. Although you were not a part of my committee, you were always there encouraging collaboration and pushing the graduate students to do their best work. I am honored to have worked alongside you. You all have set an inspiring and positive example for me as I move forward with my career in science.

To my mentor—Dr. Andrew Gow, thank you. You have always pushed me to think critically, provided me numerous opportunities that have shaped me as a scientist, and supported me through both successes and trials. I am a more confident and capable scientist

largely due to your support. Working as part of the Gow Lab was by far the best part of my graduate school experience.

To my labmates—Dr. CJ Guo, Dr. Helen Abramova, Dr. Christopher Massa, and Dr. Thea Golden, it was an amazing experience working with each of you. I'll miss being able to turn in my chair and start up conversations with you all. Words fail me here, I just feel so privileged to know you. I'm happy to leave the lab not just as colleagues, but as friends.

To all of my friends and church family—your prayers and encouragement have sustained me through all of this. These last years have been grueling, and I have missed so many calls, rescheduled so many trips/meetings, but you stuck by me...that's true friendship. You have cared so well for not only myself, but for my husband too. You are all a true blessing to me.

Lastly, I would like to acknowledge my family. To my cousins, aunts, and uncles—each of you have shared in a piece of this journey with me, and it was a great comfort to know that I had you all in my corner. To my parents—thank you for all of your sacrifice and support. I know you both thought I would be the forever professional student, but this dissertation is the culmination of everything you watched me strive for from the sidelines. I love you both so much, and am so thankful that you always pushed me to work hard, and to never give up. To my siblings—Kaitlynn, Holly, and Andrew, you all mean the world to me. Thank you for always encouraging me, letting me destress over dinner and drinks, and for loving me even when it was not so easy. To my nieces—Rian, Payton & Hannah, I never realized how much I could love and laugh until you all came along. Without your hugs and laughter after a long day at the lab, I am not sure I would have made it to the end

of this journey…or at least not with my sanity. Rian, some of my favorite days were when you would visit the lab and we would look at slides together. I love that you question everything. Being an aunt to each of you is my most favorite "job" in the world. To my husband—Nick, this is as much an accomplishment for you as it is myself. You have loved and supported me unconditionally every step of the way. I'll never forget all the dinners you made me, the coffees you dropped me in the morning after I pulled an all-nighter at the lab, the times you sat in the office with me when I took breaks between assays, and how you pushed me even when I wanted to so badly to quit. I can only hope that one day I may do the same for you. I love you madly. Finally, I dedicate this work to my grandparents, Henry & Thelma Rohmann. Without you I would not be the woman I am today. All that I have, I owe to you both.

TABLE OF CONTENTS

LIST OF FIGURES

LIST OF TABLES

INTRODUCTION

Use of engineered nanomaterials in commercial products is increasing across the globe. The lung is a primary route of exposure, and experimental design needs to be directed toward understanding effects of nanoparticles on lung function and inflammation. Numerous studies have focused on particle interactions with components of the lung lining fluid *in vitro* [1-5]. The difficulty in an *in vitro* approach is that the lung is a highly complex and integrated system. Type II alveolar epithelial cells produce and secrete surfactant components that form the hypophase along alveoli [6]. These components influence lung function and inflammatory responses. Invading materials that reach the hypophase may interact with individual components, leading to indirect consequences on the surrounding environment; but none of the hypophase components act in isolation. This makes *in vivo* examination of nanoparticle exposures crucial.

Our laboratory uses intratracheal instillations to deliver nanoparticles at varied dose, functionalization, shape and size. The greatest obstacle facing *in vivo* studies is particle delivery due to the complexity of particle biophysics. Intratracheal instillation allows for increased control of maintaining nano-scale size before delivery as well as decreasing particle-particle interactions prior to delivery; better ensuring nanoparticles reach the alveolar system at the delivered dose. This is in contrast to inhalation studies with which it is difficult to determine the dose of nanoparticles that reach the alveolar system, if at all.

The biophysical characteristics of the nanoparticles will effect interactions with cells (Type II epithelial cells, macrophages), surfactant proteins, as well as surfactant

lipids; all of which are involved in lung function and respiratory immunity. These cells, proteins, and lipids work together in maintaining low surface tension and innate immune response. Interactions with one subset will likely affect the others. We predict that the biophysical properties of nanoparticles (functionalization, shape and size) will determine interactions with alveolar epithelial cells, macrophages, surfactant proteins, and lipids which will alter lung function and inflammatory responses.

BACKGROUND

RELEVANCE OF NANOPARTICLES

Engineered nanomaterials—any particle <100nmin one dimension—have many uses. Silver nanoparticles (AgNPs) are in high demand for their antimicrobial properties, and multi-walled carbon nanotubes (MWCNTs) are valued for their high aspect ratio and thermal conductivity [7-11]. Industrial AgNPs are used in air purifiers, aerosol sprays, water purifiers, washing machines and as a component for inks used in inkjet printers [8-10]; and MWCNTs are used in conductive fuel lines, conductive inks, electronics as well as in targeted drug delivery [7, 11]. As the commercial and medical use of nanoparticles has grown, multiple studies have been aimed at determining the toxic effects arising from high doses of nanoparticles in both *in vitro* and *in vivo* systems [12-16]. The respiratory system is a primary target for exposure [1]. Although numerous studies have examined particle-particle interactions in various media and particle-surfactant interactions *in vitro* and *in vivo* [16-18], potential effects on the organ-level physiology and toxicity at lower doses are still poorly understood.

PREVIOUS STUDIES: *IN VITRO* & *IN VIVO* APPROACHES/LIMITATIONS

Nanoparticles are readily deposited into the lower airways of the lung, and the lung lining fluid is a highly absorptive surface, which can uptake those particles. *In vitro* work has already shown that nano-scale particles can become coated by the lipid portion of the lung lining fluid causing the particles to form strands in a manner dependent upon surfactant protein-B (SP-B) [1, 16]. This interaction leads to an increase in surface tension and a decrease in the absorptive properties of the synthetic lipid layer *in vitro* [1]. Though many early studies focused on the lipid portion interactions and changes to surface tension,

more recent studies have begun examining particle-collectin specific interactions. Surfactant proteins A & D (SP-A & D), often termed collectins, are key regulators of the innate immune system within the lung. It has been demonstrated that SP-A & D bind to functionalized carbon nanotubes in a calcium dependent manner [15]. It is reasonable to postulate that collectin association to NPs may facilitate phagocytosis and clearance of these particles by the cells of the lung lining. This is supported by recent research examining macrophage clearance of nanoparticles; in the presence of SP-A and SP-D particle clearance was increased, but particle functionalization and composition played a role in the affinity for SP-A versus SP-D, as well as efficiency of clearance [19, 20]. Further study of MWCNTs has demonstrated that a negatively charged surface increases interaction and binding with SP-D, as well as nanospheres; size was shown to also be a predominate factor in SP-D binding in the same study [21]. Larger (100nm), more negatively charged nanoparticles are more likely to bind and interact with SP-D [21]. Marchetti et al. (2015) proposes this affinity for negatively charged MWCNTs is due to a positively charged area located within the carbohydrate-binding region of SP-D [22]. This particle-collectin binding may also affect surfactant recycling and/or secretion by the Type II alveolar cells [15, 21].

In vivo studies have mainly focused on cytotoxicity as a consequence of nanoparticle inhalation and instillation within the lung, using both rat and mouse models [23-25]. Typically, high dose nanoparticle exposures are used in inhalation toxicity [26, 27]. In the case of AgNPs, evidence of organ damage and adverse effects has proved limited despite findings of particle accumulation as long as 56 days post a single exposure

[28]. Conversely, MWCNT exposures have led to induction of inflammation and fibrosis [29-32].

There are limitations that have been acknowledged in both inhalation and instillation studies, which may affect the translation of rodent nanoparticle studies to human environmental and occupational nanoparticle exposures. Inhalation studies with rodent models are typically performed at higher doses because rodents have more complex nasal turbinates than humans and particles can become trapped within the nasal passageways [33], potentially unable to reach the lung; a higher dose is needed to elicit particle effects. Additionally, unlike humans which breathe nasally and orally, rodents are limited to nasal breathing [33]. While instillation studies provide the ability for more targeted delivery, assuring that the delivered dose is reaching the lung, particles must be suspended first into solution. This does not mimic environmental and occupational exposure (inhalation), and since many types of nanomaterials are poorly soluble and have a propensity for aggregation (ex, carbon nanomaterials), manipulation of the sample for delivery by addition of surfactants to the solution is often necessary. It is important to note that relating inhalation and instillation data of similar dosing schemes and particle exposure provides the most comprehensive picture of *in vivo* nanoparticle effects.

SP-D$^{-/-}$ MICE: A MODEL OF INFLAMMATION

Mice lacking SP-D have been shown to alter surfactant homeostasis, clearance of bacteria, and display chronic pulmonary inflammation [34, 35]. SP-D$^{-/-}$ mice have been characterized and documented at baseline with increased alveolar macrophage count and size, as well as abnormal Type II cell morphology (contain giant intracellular lamellar bodies) [36]. Additionally, structures may accumulate in the alveolar spaces, there is

overall increased phospholipid content, and increased total protein concentration (collectins and surfactant proteins) in the lung lining [36]. Accumulation of surfactant within the alveolar spaces occurs due to impaired uptake by the Type II cells [21]. While this knockout model displays chronic inflammation, it is fairly low-level inflammation. SP-$D^{-/-}$ mice have been used to examine the effects of exposure to different materials up to 80 weeks of age [37]. These factors make the SP-$D^{-/-}$ model an ideal candidate for assessing nanomaterial effects in an inflamed respiratory system.

LUNG FUNCTION & THE ALVEOLAR SYSTEM

It has been well established that estimates of resistance and elastance serve as a determination of lung function [38]. Mechanical ventilation with forced oscillation maneuvers are used to measure impedance. Broadband signal (0.5-20Hz) respiratory impedance [Z(f)] is a sensitive indicator of pathology of the airways and tissues [39]. To measure impedance, a known broadband flow is applied at the tracheal opening and transduces pressure. The flow [V(t)] is a known value input into the system while pressure [P(t)] output is unknown. As mechanical function varies with frequency of oscillation, a Fourier Transform is utilized so that impedance can be expressed as a function of frequency, $Z(f) = P(f)/ V(f)$. Output impedance spectra are used to generate resistance (R_L) and elastance (E_L) spectra across the frequency range, and fit to a model of heterogeneous lung function using the following equations [37, 40, 41]:

$$RL = (a + bf)/(c + f) \text{ and } EL = E0 + \Delta E\ (1\text{-}e\text{-}\beta f)$$

These measures of lung function can become altered due to changes occurring in the alveolar system. The alveolar system is comprised of 3 major cell types: Type I & II alveolar epithelial cells, as well as alveolar macrophages. Type I cells largely provide

structure and barrier function for alveoli, while Type II cells are more dynamic. If Type I cells become damaged Type II cells differentiate into Type I cells, however, Type I cells cannot differentiate into Type II cells [42]. Protein and lipid components of the lung lining fluid are also produced and secreted by Type II cells. Lipids comprise approximately 90% of the lung lining fluid, while the remaining 10% is surfactant collectins and proteins. The primary lipid found in the lung lining fluid is dipalmitoylphosphatidylcholine (DPPC); others include phosphatidylglycerol (PG) and phosphatidylcholine (PC). Surfactant collectins include surfactant proteins-A and D (SP-A & SP-D) which are calcium-dependent lectins involved in the innate immune responses of the lung. These collectins are similar in structure in their monomeric form: (N-terminus) a collagenous domain, neck, and carbohydrate recognition domain (C-terminus). Though similar in monomeric form, the monomers form different higher-order structures to create trimers, dodecamers, octadecamers, and multimers.

SP-D is involved in both anti-and pro-inflammatory responses within the lung lining fluid. Under physiological conditions, SP-D acts to suppress transcription of macrophage pro-inflammatory genes; while in the presence of increasing nitric oxide levels, the cysteine residues of SP-D can become S-nitrosylated leading to a proinflammatory response [37, 43]. SP-D is also involved in maintaining surfactant homeostasis and it effects surfactant ultrastructure [44, 45]. It has been demonstrated that orphan receptor, Ig-Hepta/GPR116 is expressed on alveolar Type II cells and is involved in detecting SP-D levels within the surfactant to trigger SP-D recycling and maintain surfactant homeostasis [46]. Surfactant proteins-B and C (SP-B & SP-C) are more hydrophobic proteins than SP-A & D. They are involved in maintaining surface tension

near zero to lessen respiratory effort. SP-B interacts with lung lining fluid lipids (mechanism unknown) to facilitate the formation of the mono-lipid layer along the surface of the alveoli. SP-A, B and D are also synthesized (but not recycled) by the bronchiolar Clara cells, while SP-C is thought to be synthesized solely by Type II cells [6, 47].

Previous studies have correlated changes in lung function with reduction of SP-B or SP-D expression and surfactant dysfunction [37, 48]. Acute lung injury induced via exposure to aerosolized endotoxin lipopolysaccharide (LPS) led to decreased SP-B expression and surfactant dysfunction which was correlated with increased tissue stiffness [48]. Additionally, mice deficient in SP-D (SP-D$^{-/-}$) exposed to ozone have demonstrated increases in both measures of elastance as well as resistance [37]. In other models, lung function changes are correlated with increases in SP-D expression; this may be due to differences in inflammatory profiles between different animal and exposure models.

Therefore, we examine within this manuscript the relationship between molecular and physiological endpoints and hypothesize that biophysical characteristics of AgNPs & MWCNTs will affect particle-lung lining fluid interactions.

SPECIFIC AIMS

SPECIFIC AIM 1

In this study, we aim to determine changes in lung function and inflammation in response to metal nanoparticles. We hypothesize that AgNPs will aggregate and interact with the lipid portion of the lung lining fluid in a divergent manner than its non-metal control, carbon black NP. We propose that metal NPs will increase respiratory effort and will activate divergent inflammatory pathways from non-metal NP exposed mice. To examine potential effects, dose and time point were varied and carbon black nanospheres were used as a size/non-metal control. Following exposure the lung function and inflammatory response was analyzed using the flexivent, bronchoalveolar lavage (BAL), and harvesting of the lungs for histology and molecular studies (1, 3 and 7 days post-single exposure). This will provide an organ level assessment and allow us to correlate respiratory mechanics (flexivent analysis) with changes in alveolar cells, proteins, lipids (BAL analysis) and lung tissue (histology) due to exposure from varied doses of AgNPs (metal) and carbon black NPs (non-metal).

SPECIFIC AIM 2

In this study, we aim to determine how different AgNP functionalization and size affects lung function and inflammation. We propose that larger, polymer-stabilized AgNP exposure will result in increased alveolar system interactions versus all sizes of citrate-stabilized AgNPs and demonstrate more pronounced changes in lung function and inflammation due to their increased particle stability. A low dose of AgNPs was used to reduce possible injury and inflammation, and allow for determination of the relationship between particle biophysics and lung function. Four different types of AgNPs with

combinations of two diameters (20nm vs. 110nm) and two capping agents (citrate and PVP) were intratracheally instilled for *in vivo* assessment, while the interaction between each type of AgNP and a model surfactant was measured *in vitro*. 1, 7, and 21 days post-exposure the lung function and inflammatory response were analyzed using the flexivent, bronchoalveolar lavage (BAL), and harvesting of the lungs for histology and molecular studies. This provided an organ level assessment and allowed for correlation of respiratory mechanics (flexivent analysis) with changes in alveolar cells, proteins, lipids (BAL analysis) and lung tissue (histology) due to exposure of AgNPs of varied functionalization and size.

SPECIFIC AIM 3

In this study, we aim to determine how nanoparticle shape and functionalization affects lung function and inflammation under physiological as well as inflammatory conditions. We propose that MWCNTs will elicit a persistent anti-inflammatory response to remove the nanomaterial over time, but will not alter work of breathing under physiological conditions; while when exposed to a baseline inflammatory environment, the MWCNTs will not be effectively cleared and increase the work of breathing. When a single high dose of carbon black nanospheres was delivered into the lung previously, there was an acute inflammatory response without a detectable change in lung function (Aim 1); in this study a similar dose of MWCNTs was administered (determined by surface area to volume ratio). Following exposure the lung function and inflammatory response was analyzed using the flexivent, bronchoalveolar lavage (BAL), and harvesting of the lungs for histology and molecular studies (1, 3, and 7 days post-single exposure). This provided an organ level assessment and allowed for correlation of respiratory mechanics (flexivent

analysis) with changes in alveolar cells, proteins, lipids (BAL analysis) and lung tissue (histology) due to exposure from MWCNTs of varied functionalization.

EXPERIMENTAL PLAN

SPECIFIC AIM 1: EFFECTS OF METAL NANOPARTICLES

In this study, we aim to determine changes in lung function and inflammation in response to metal nanoparticles. We hypothesize that AgNPs will aggregate and interact with the lipid portion of the lung lining fluid in a divergent manner than its non-metal control, carbon black NP. We propose that metal NPs will increase respiratory effort and will activate divergent inflammatory pathways from non-metal NP exposed mice. To examine potential effects, dose and time point were varied and carbon black nanospheres were used as a size/non-metal control. Following exposure the lung function and inflammatory response was analyzed using the flexivent, bronchoalveolar lavage (BAL), and harvesting of the lungs for histology and molecular studies (1, 3 and 7 days post-single exposure). This will provide an organ level assessment and allow us to correlate respiratory mechanics (flexivent analysis) with changes in alveolar cells, proteins, lipids (BAL analysis) and lung tissue (histology) due to exposure from varied doses of AgNPs (metal) and carbon black NPs (non-metal).

RATIONALE

AgNPs are valued for their antimicrobial properties and are used in a growing number of commercial products. Many previous studies have focused on the *in vitro* interactions of metal NPs and lung lining proteins, lipids, and cells [1, 2, 4, 5]. The study of gold nanoparticles in the presence of dipalmitoyl phosphatidylcholine (DPPC), palmitoyl-oleoyl-phosphatidylglycerol, and surfactant protein B (SP-B) demonstrated that the metal NPs become coated by lipids and form aggregated strands [1]. This coating and consequent aggregation led to increased surface tension measurements, indicating potential

for increased work of breathing when metal NPs are inhaled [1]. Herzog et al. (2014) used AgNPs and a complex triple cell culture with an air-liquid interface to mimic the conditions of the lung. Data from this study indicated differential particle interactions depending upon AgNP interactions at the air-liquid interface versus AgNPs submerged in the liquid phase. AgNPs aggregated with cells at the air-liquid interface, but did not trigger a cytotoxic response, while AgNPs immersed in the liquid phase led to cytotoxicity. Findings from these previous *in vitro* studies indicate potential for pronounced mechanical and inflammatory responses by the lung due to metal NP exposure. Yet, while these studies closely mimic respiratory conditions, the complex organ level toxicology must be assessed *in vivo* for NP exposures.

A carbon black nanosphere is of Buckminster Fullerene structure, while AgNPs are stabilized using citrate, reduced using sodium borohydride and are redox reactive [14]. These differences in surface composition allow for differential interactions with components of the lung lining fluid. By using carbon black NPs of the same size and geometry as a control, it will be possible to determine if organ level effects are due to the functionalization/metal properties of the nanoparticle. Additionally, with the use of a silver nitrate solution as a control, it will be possible to determine if organ level effects are due to silver ion interactions or if they are specific to AgNPs. Changes in pH and the ionic environment have been shown to disrupt AgNPs and cause them to dissolve into their ionic form, but Imperial College London has characterized this set of AgNPs as displaying limited dissolution over time under varying conditions [14].

METHODS

PARTICLE SPECIFICATIONS

Carbon black NPs and silver nanospheres (AgNPs) (15nm) were designed and characterized by Department of Materials and London Centre for Nanotechnology, Imperial College London [14]. AgNPs were stabilized using citrate and reduced using sodium borohydride [14].

MURINE MODEL AND PARTICLE INSTILLATION

Nine-week-old C57-BL6 Jackson wild-type male mice were intratracheally instilled with either Hank's Balanced Salt solution (HBSS), silver nitrate solution, carbon black NPs or AgNPs following anesthesia using a ketamine/xylazine combination. 0.05µg or 0.5µg particle/g body weight were suspended into HBSS to a final volume of 50µl. Probe sonication of NPs was utilized immediately before intratracheal instillation. Mice were left for 1, 3, or 7 days before being anesthetized, attached to a ventilator having their mechanical function assessed (see below). Low dose particle treated mice (0.05 µg/g body weight) were only examined 1 day post-instillation, while silver nitrate instillations were given at a high dose (0.5µg/g body weight) and mice were examined only at 7 days post-instillation. Following ventilator protocol, tissues were harvested and analyzed as described below.

This protocol was approved by the Rutgers University Institutional Animal Care and Use Committee (IACUC) (Protocol Number: 06-028). The study was conducted in accordance with the recommendations in the Guide for the Care and Use of Laboratory Animals of the National Institutes of Health. Intratracheal instillations and mechanical ventilation were conducted under ketamine/xylazine anesthesia, and all efforts were made

to minimize suffering. Animals were sacrificed using a lethal dose of ketmine/xylazine and exsanguination.

Bronchoalveolar Lavage

A bronchoalevolar lavage of the whole lung was performed using with 10mM HEPES buffered saline in 1mL increments four times (prior to inflation fixing with paraformaldehyde). Cells (~30,000) from the bronchoalveolar lavage fluid (BAL) were then centrifuged (300xg, 10 minutes) on a glass microscope slide. The supernatant was collected for protein and phospholipid assays. The cell pellet was re-suspended in 1mL buffered saline for cell count, cytology and RT-PCR analysis [36, 40, 49].

Histology

Using a 3% paraformaldehyde/2% sucrose solution, the left lung was inflation fixed. The tissue was then embedded in paraffin, sectioned and stained with hematoxylin and eosin (H&E). The Olympus VS120-SL Virtual Slide System was used for imaging lung sections [40, 49].

Cell Counts and Cytology

Using the Beckman CoulterTM MultisizerTM 3 Coulter Counter®, the cell number from BAL samples was assessed. Approximately 30,000 cells were centrifuged onto a glass slide at 800xg for 3 minutes, air dried, and stained with Diff-Quik buffered modified Wright-Giemsa stain. Cell differentials were performed manually using a light microscope (1-way ANOVA, t-test) [36, 40, 49].

Real-Time Polymerase Chain Reactions

RNA was prepared from BAL cells using a QIAshredderTM kit and converted to cDNA. The cell samples for each treatment group were pooled into one larger sample for analysis. Thermocycling was used to analyze mRNA expression of CCL2, IL1B, IL6,

CXCL10, IL10 and IL12B in the treated mice. Fold expression was calculated by the ΔΔCT method normalizing to the HBSS (control) treatment group [50].

Protein and Phospholipid Assay

Whole BAL protein concentration was determined using a Low Protein BCA Assay kit by Lamda Biotech, Inc (St. Louis, MO). To estimate phospholipid content whole BAL was fractionated into small and large aggregate portions by centrifugation at 17,000xg for one hour at 4^0C. The supernatant is the protein-rich small aggregate fraction, while the pellet can be re-suspended in a small volume of saline (35µl) and was the lipid-rich large aggregate fraction. Inorganic phosphate from the lipid-rich fractions was measured as an estimate of the phospholipid content (1-way ANOVA, Holm-Sidak method) [49, 51].

Immunoblotting

To determine surfactant protein content, reducing NuPAGE was performed using individual BAL samples. Gels were transferred to BioRad Immun-blot® PDVF membranes, incubated with SP-D or SP-B antibody (M.F. Beers, University of Pennsylvania), goatαrabbit linked to horseradish peroxidase, and imaged using Amersham™ ECL™ Prime Western Blotting Detection Reagent. Densitometry was performed to quantify the chemiluminescent signal (1-way ANOVA, Holm-Sidak method). Whole BAL was used for SP-D analysis; and sample load was normalized to volume. Large aggregate BAL (LA BAL) was used for SP-B analysis and sample load was normalized to phospholipid content as determined by the phospholipid assay [49].

Capillary Surfactometry

Surface tension was measured using a capillary surfactometer (Calmia Medical, Inc). Samples were loaded at a consistent phospholipid concentration of 1.0µg/µl. Following sample loading, compressed air was applied to the capillary at increasing

pressures. Both the initial pressure to disrupt the LA BAL and percent capillary open over the course of two minutes were recorded [49].

Mechanical Ventilation and Respiratory Model

1, 3 or 7 days following particle instillation, mice were anesthetized and ventilated using the flexiVent (SCIREQ, Montreal, Canada) at positive end expiratory pressures (PEEPs) (0, 1, 3, and 6 cmH_2O)—performed prior to harvesting of tissue and BAL for biological assays. Mechanical ventilation with forced oscillation maneuvers was used to measure impedance. Broadband signal (0.5-20Hz) respiratory impedance [Z(f)] is a sensitive indicator of pathology of the airways and tissues [39]. To measure impedance a known broadband flow is applied at the tracheal opening, and transduces pressure. The flow [V(t)] is a known value input into the system while pressure [P(t)] output is unknown. As mechanical function varies with frequency of oscillation, a Fourier Transform was performed so that impedance can be expressed as a function of frequency, $Z(f) = P(f)/ V(f)$. Output impedance spectra were used to generate resistance (R_L) and elastance (E_L) spectra across the frequency range, and fit to a model of heterogeneous lung function using the following equations [40]:

$$R_L = (a + bf)/(c + f) \text{ and } E_L = E0 + \Delta E\ (1\text{-}e^{-\beta f})$$

Model fits were estimated for each treatment group by fitting a non-linear regression curve to the spectra of all mice in a treatment group equally at each PEEP. Spectra were analyzed for significant differences using the null hypothesis that the data can be characterized by one three-parameter relationship or alternatively that the data are distinct enough to be characterized by two three-parameter relationships. The parameters of the R_L and E_L curves were estimated from non-linear regressions fitting to the spectra of each individual mouse within a treatment group at each PEEP. Then a mean and standard

error for each parameter was taken for each treatment group. A two-way analysis of variance (ANOVA) was used to determine significant differences in the mean value of each parameter for treatment groups and PEEP. Pairwise comparisons were made using the Holm-Sidak method.

RESULTS

1 DAY POST-INSTILLATION

There was no evidence of injury in any of the saline (control) or particle treated mice by way of histology (Figure 1). Cytology, however, demonstrated significant invasion of neutrophils in high dose carbon black NP treated mice, as well as obvious uptake of carbon black NPs into macrophages (Figures 2 & 3). This indicates activation of an inflammatory response which is supported by the PCR data where there was an increase in expression of IL1B, IL6, and IL12B as compared to the control (Figure 4); this cytokine profile confirms macrophage activation. However, there was no invasion of inflammatory cells or inflammatory activation indicated by way of cytology or PCR for low dose carbon black NP or AgNP treated mice (low or high dose).

Additionally, there were no significant differences between treatment groups in protein concentration, phospholipid content, SP-D/B ratios, or capillary surfactometry at 1 day post-instillation (Figures 5, 6, & Table 1). Although there was an inflammatory response elicited by high doses of carbon black NPs, there was no significant difference in respiratory mechanics (resistance or elastance) between carbon black NP treated mice (low or high dose) as compared to the saline control (Figure 8). Furthermore, despite a lack of inflammatory response, AgNP treated mice (low and high dose) demonstrated a significant increase in tissue stiffness as compared to the control; but there were no significant differences in airway or tissue resistance (Figure 8, low dose AgNP results not shown).

These significant increases in elastance were restricted to the low frequency end of the spectra indicating changes in the parenchyma (data not shown).

3 Days Post-Instillation

Again at 3 days post single instillation histology demonstrated no signs of injury to the lung as a result of particle exposure (Figure 9). Cytology confirmed persisting neutrophilia in high dose carbon black NP treated mice and continued uptake of carbon black NPs in macrophages (Figure 2 & 3). Additionally, high dose AgNP treated mice cytospins demonstrated an invasion of lymphocytes and an increased number of macrophages (Figure 2). This indicates activation of an inflammatory response in both particle treated groups, but by potentially different pathways. PCR demonstrated continued elevated cytokine expression of IL1B and IL6 as well as an increase in CCL2 and IL10 for high dose carbon black NP treated mice indicating activation of macrophages, a response to inflammation, and recruitment of monocytes (Figure 4). While these same cytokines were expressed in AgNP treated mice, there was a 60 mRNA fold change as compared to the control for IL10 (Figure 4). IL10 is produced by monocytes and lymphocytes, but it's the magnitude of expression of IL10 in AgNP treated mice as compared to carbon black NP treated mice coupled with lymphocyte invasion for AgNP treated mice that indicates a significant difference in inflammatory profiles of the two groups. There was no significant difference in protein concentration between groups (Figure 5), consistent with a lack of lung injury; however, there was a significant increase in phospholipid content for carbon black NP treated mice as compared to the control (Figure 5).

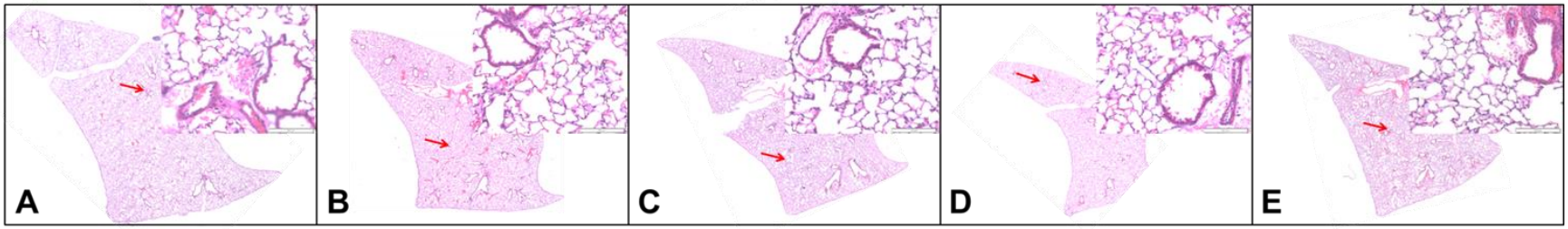

Figure 1. *Histology (H&E) 1 day post-instillation*: **A)** HBSS **B)** LD Carbon Black NP **C)** HD Carbon Black NP **D)** LD AgNP **E)** HD AgNP; histology does not show any significant injury associated with particle treatment (LD = low dose, HD = high dose) (enlarged H&E images 20x, whole lung 0.8x).

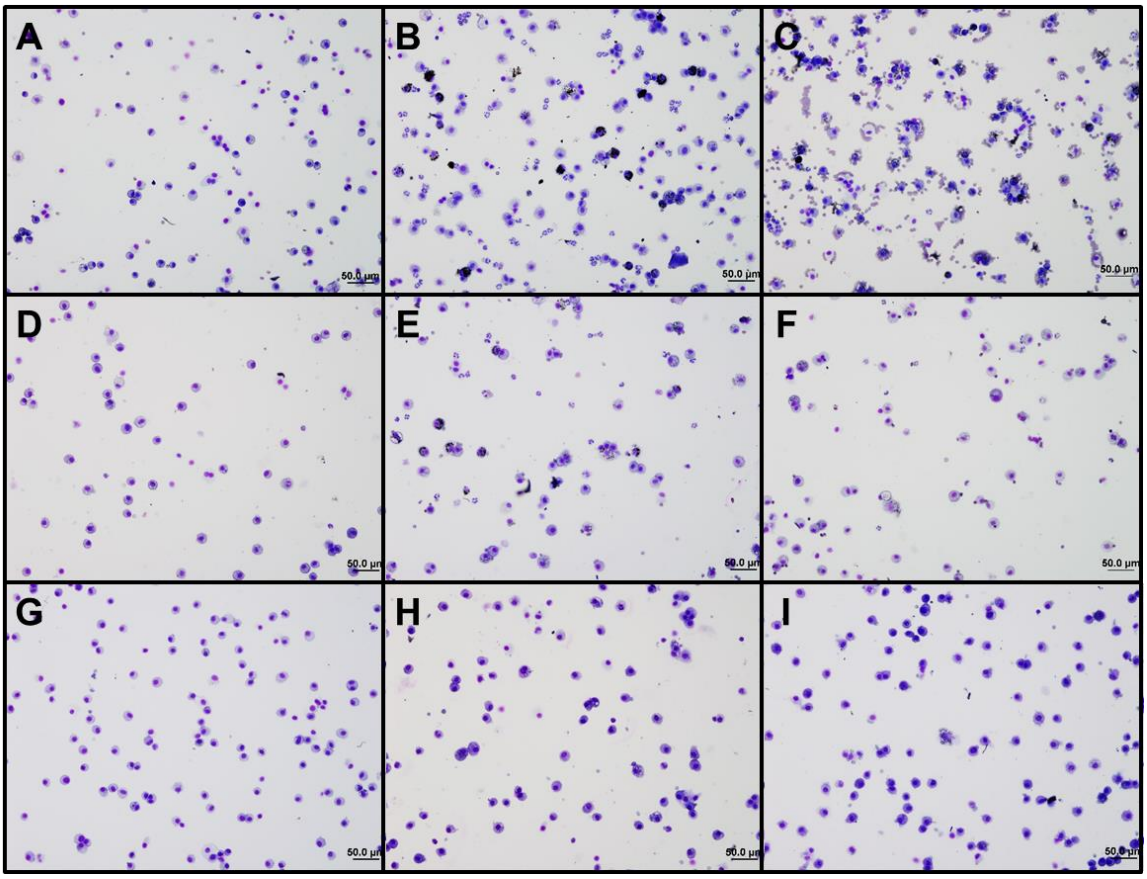

Figure 2. *Cytology High Dose NPs All Time Points*: **A, D & G)** HBSS (1, 3, & 7 days post-instillation) **B, E & H)** HD Carbon Black NPs (1, 3, & 7 days post-instillation) **C, F & I)** HD AgNPs (1, 3, & 7 days post-instillation); demonstrates acutely activated macrophages in both NP treatments, and uptake of Carbon Black NPs into macrophages. No visible Carbon Black NPs in macrophages by 7 days post-instillation (LD = low dose, HD = high dose) (cytology images at 20x).

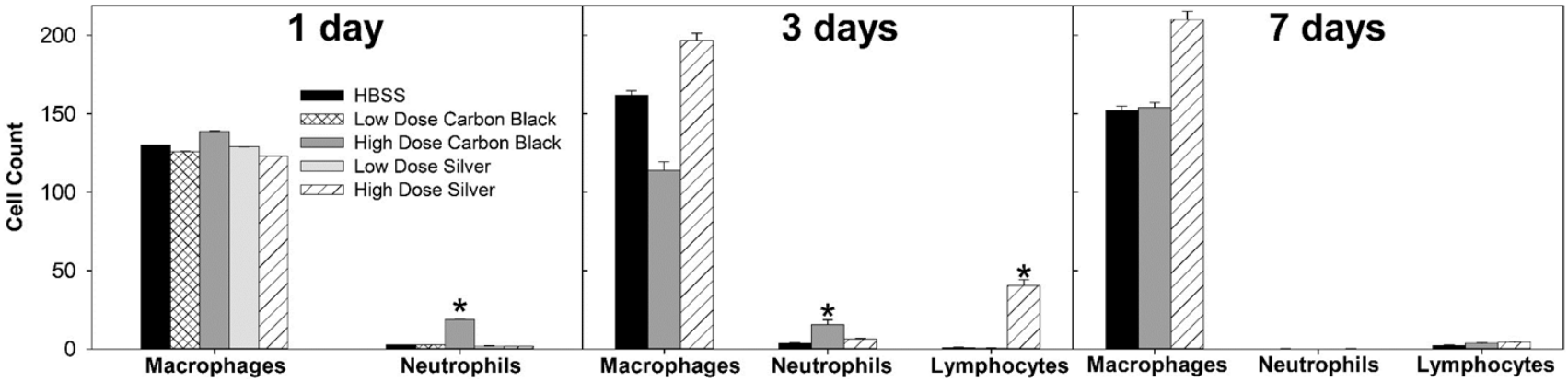

Figure 3. *Cell Differentials*: At 1 day post-instillation, high dose carbon black NP treatment results in neutrophilia. 3 Days post-instillation carbon black NP-mediated neutrophilia begins to resolve, while high dose AgNP treatment results in increased macrophages and lymphocytes. 7 Days post-instillation, persisting elevated macrophages are seen with AgNPs, while neutrophils and lymphocytes have resolved (*****$p<0.05$ compared to the control for that cell type).

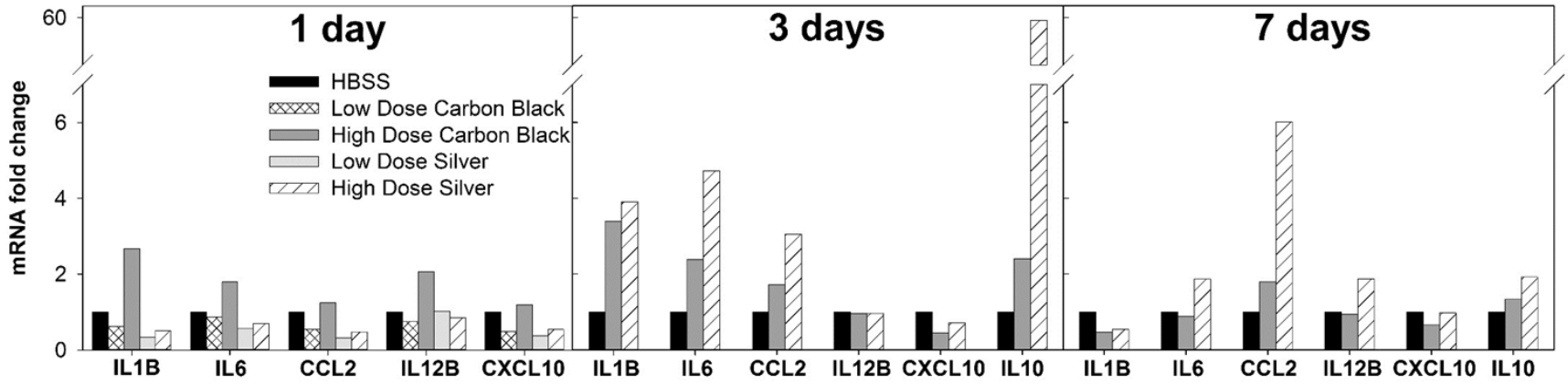

Figure 4. *mRNA expression by PCR*: 1 day post-instillation high dose carbon black NP treated mice demonstrate increased expression of IL-1β, IL-6 and IL-12B as compared to control (HBSS). 3 days post-instillation high dose carbon black NP treated mice persist with elevated IL-1β and IL-6 expression, while AgNP treated mice demonstrate increased expression of IL-1β, IL-6, CCL2, and IL-10. 7 days post-instillation all inflammatory markers have resolved in carbon black NP treated mice, but in AgNP treated mice CCL2 remains elevated (samples were pooled for each treatment group at each time point, n=4-6 mice)

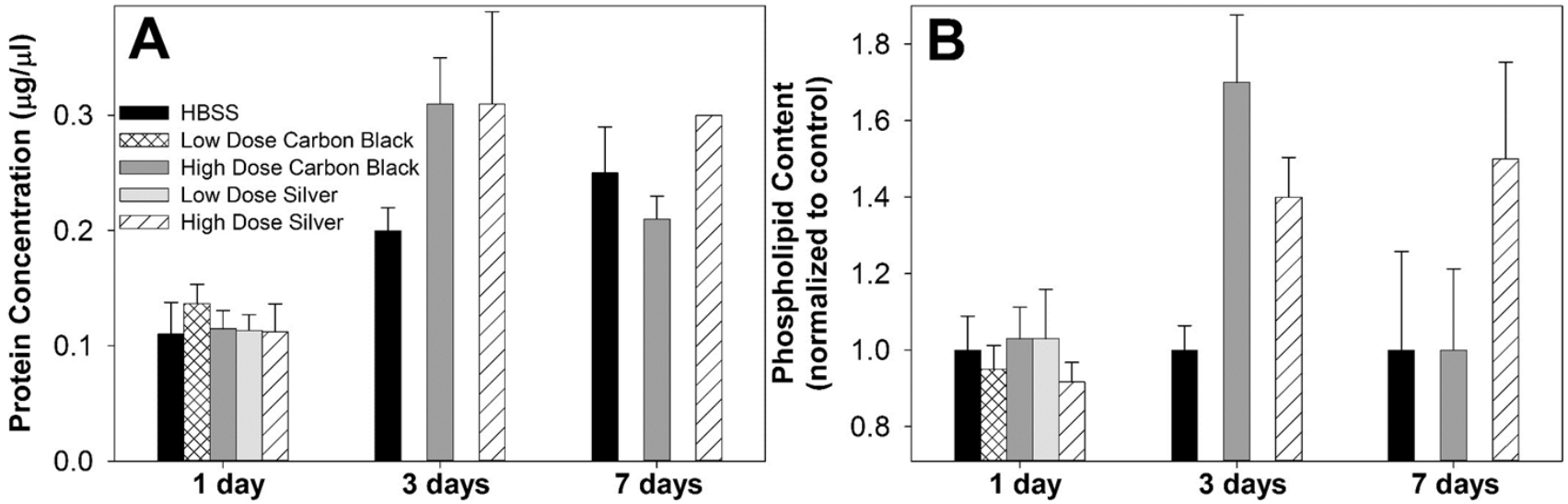

Figure 5. *Protein Concentration & Phospholipid Content in BAL:* **A)** At each time point, treatment groups were not significantly different from control (HBSS). However, at 3 days post-instillation all groups displayed an increase in BAL protein concentration which began to resolve by 7 days in Carbon Black NP treated mice **B)** There was no significant difference between treatment groups at any time point, however at 3 day post-instillation NP treated mice displayed increases in phospholipid content as compared to the control. While this increase resolved by 7 days in Carbon Black NP treated mice, AgNP mice continued to display increases in phospholipid content as compared to the control.

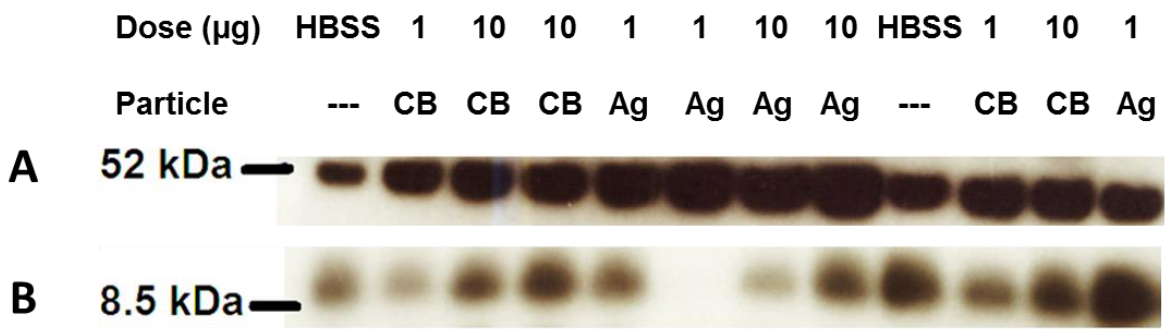

C

Treatment	SP-D/SP-B ratio compared to control	SP-D content compared to control	SP-B content compared to control
HBSS	1.0 ± 0.07	1.0 ± 0.06	1.0 ± 0.08
1µg Carbon Black	1.1 ± 0.09	1.0 ± 0.05	1.0 ± 0.05
10µg Carbon Black	1.1 ± 0.06	1.1 ± 0.07	1.0 ± 0.04
1µg Silver	1.2 ± 0.35	1.0 ± 0.11	1.0 ± 0.13
10µg Silver	1.3 ± 0.20	1.2 ± 0.08	1.0 ± 0.10

Figure 6. *Immnoblotting 1 day post-instillation*: **A)** SP-D Immunoblot **B)** SP-B Immunoblot **C)** SP-D/SP-B ratios; there is considerable variability between individuals within a group, however, the overall trend suggests that nanoparticle treated lungs experience increases in SP-D expression with corresponding decreases in SP-B expression. The greatest differences compared to the control occur with AgNP treatment, though not statistically significant (**CB**= carbon black NPs, **Ag**= silver NPs).

	Treatment	% Capillary Open normalized to control	Initial Pressure normalized to control
1 day	HBSS	1.00 ± 0.01	1.00 ± 0.03
	Low Dose Carbon Black	1.00 ± 0.01	0.99 ± 0.05
	High Dose Carbon Black	0.98 ± 0.008	0.97 ± 0.06
	Low Dose Silver	0.92 ± 0.04	0.92 ± 0.07
	High Dose Silver	0.97 ± 0.03	0.94 ± 0.09
3 days	HBSS	1.00 ± 0.04	1.00 ± 0.06
	High Dose Carbon Black	1.04 ± 0.01	1.02 ± 0.01
	High Dose Silver	1.03 ± 0.02	1.04 ± 0.01
7 days	HBSS	1.00 ± 0.02	1.00 ± 0.03
	High Dose Carbon Black	0.97 ± 0.04	1.04 ± 0.02
	Low Dose Silver	1.00 ± 0.04	0.98 ± 0.02

Table 1. *Capillary Surfactometry*: There was no significant difference between treatment groups in either percent capillary open or initial pressure taken using capillary surfactometry at any time point.

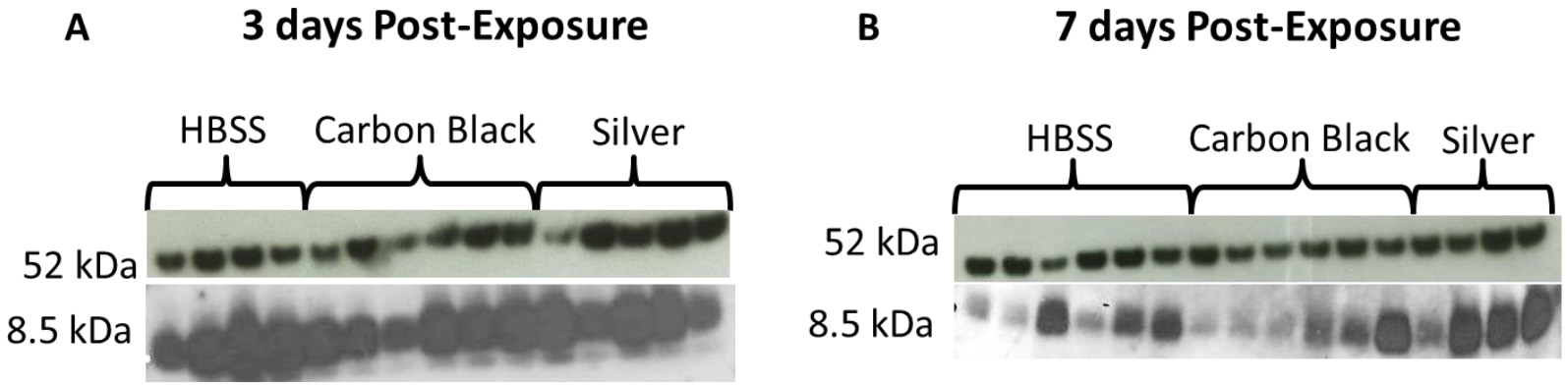

C

	Treatment	SP-D content compared to control	SP-B content compared to control	SP-D/SP-B ratio compared to control
3 days	HBSS	1.00 ± 0.053	1.00 ± 0.15	1.00 ± 0.25
	10µg Carbon Black	0.88 ± 0.045	0.90 ± 0.11	1.07 ± 0.14
	10µg Silver	1.09 ± 0.092	0.89 ± 0.17	1.49 ± 0.37
7 days	HBSS	1.00 ± 0.044	1.00 ± 0.08	1.00 ± 0.13
	10µg Carbon Black	0.96 ± 0.035	1.16 ± 0.06	0.79 ± 0.04
	10µg Silver	1.26 ± 0.045*†	1.21 ± 0.07	1.00 ± 0.06

Figure 7. *Surfactant Protein Immunblotting 3 & 7 days post-instillation*: **A)** SP-D (top) and SP-B (bottom) 3 days-post instillation **B)** SP-D (top) and SP-B (bottom) 7 days-post instillation **C)** Table of densitometry values for SP-D and SP-B content and SP-D/SP-B ratios normalized to the control. No differences in SP-D content until 7 days post-instillation (*****$p<0.001$ compared to the control, †$p<0.001$ compared to carbon black NP treatment).

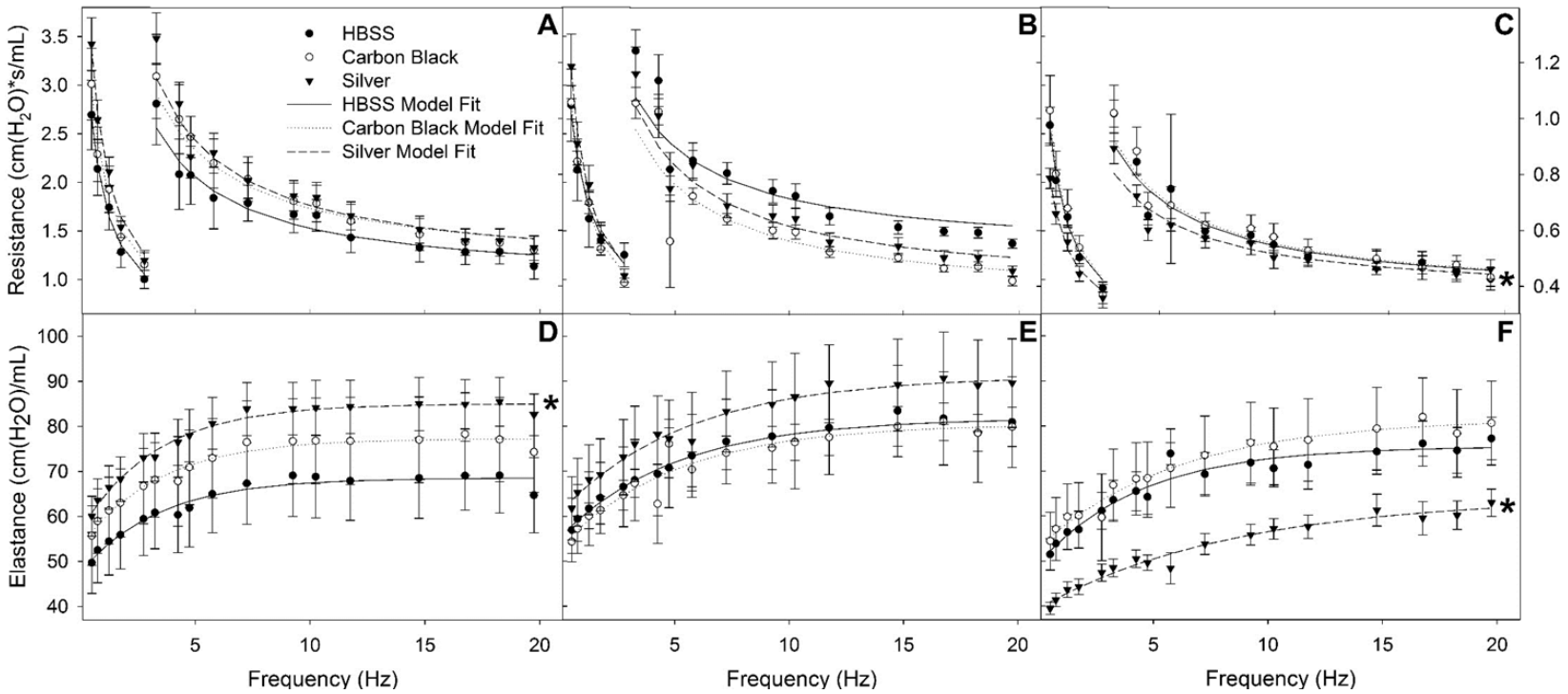

Figure 8. *Resistance (R_L) & Elastance (E_L) Spectra Using Forced Oscillation Technique*: Analysis of impedance measurements at PEEP 3 **A/D)** HBSS R_L/E_L spectra **B/E)** Carbon Black NP R_L/E_L spectra **C/F)** AgNP R_L/E_L spectra at 1, 3, 7 days. Both HBSS & high dose Carbon Black NP mice did not significantly differ in E_L or R_L across time points within treatment groups or when compared to one another. AgNP treated mice displayed acute tissue stiffness. At 7 days post-instillation, AgNP treated mice experienced significantly decreased E_L (decreased tissue stiffness), as well as significantly decreased R_L (as compared to AgNP treated mice 1 & 3 days post-instillation, as well as compared to all other treatments at all other time points). At 1 day post-instillation low dose particle treatments demonstrated no significant differences as compared to the control (*$p<0.05$).

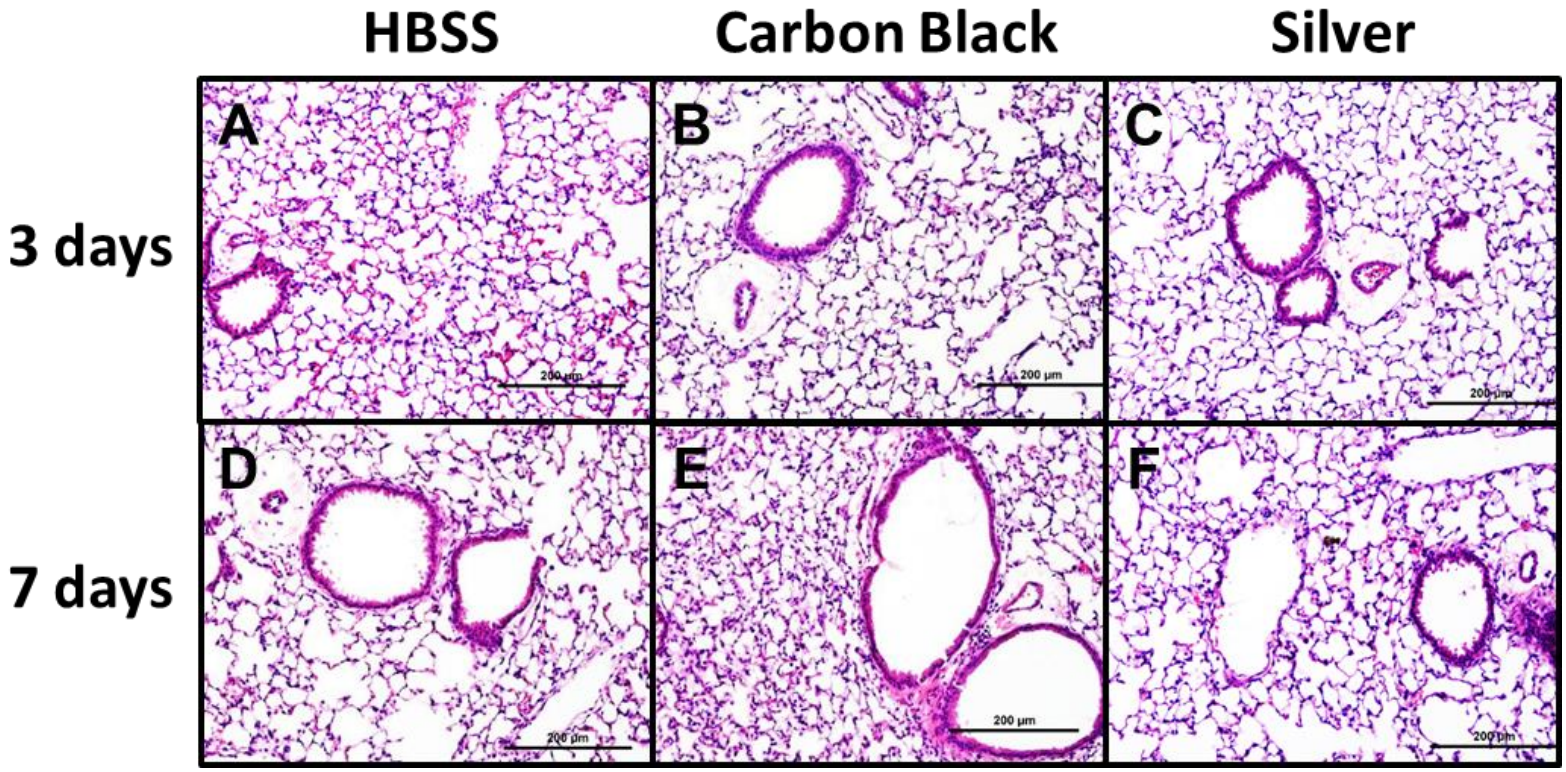

Figure 9. *Histology (H&E) 3 & 7 days post-instillation*: **A)** HBSS 3 days **B)** Carbon Black NP 3 days **C)** AgNP 3 days **D)** HBSS 7 days **E)** Carbon Black NP 7 days **F)** AgNP 7 days (all images – 20x).

Despite changes in the inflammatory profile for AgNP treated mice, and persisting inflammation coupled with a change in phospholipid content for carbon black NP treated mice there were no significant differences between groups for SP-D/SP-B ratios or capillary surfactometry (Figure 7 & Table 1). Lastly, respiratory mechanics analysis revealed no significant differences in elastance or resistance between treatment groups; indicating resolution of tissue stiffness previously demonstrated by AgNP treated mice at 1 day post-instillation.

7 Days Post-Instillation

At 7 days post single instillation there continues to be no sign of lung injury by way of histology (Figure 9). As evidenced by cytology, there is near complete resolution of invading neutrophils and lymphocytes for carbon black NP and AgNP treated mice respectively (Figure 2). PCR indicates near complete resolution of previously increased cytokine expression with minor elevation of CCL2 (1.8 mRNA fold change as compared to the control) for carbon black NP treated mice; also minor elevation of IL6, IL12B, IL10 (1.8 mRNA fold change as compared to the control), and CCL2 (6 mRNA fold change as compared to the control) for AgNP treated mice (Figure 4). This indicates some continued activation of macrophages in both treatment groups, but also a distinct likelihood of continued monocyte recruitment for AgNP treated mice (evidenced by CCL2 expression). There were no significant differences between treatment groups for protein concentration or phospholipid content; again consistent with a lack of tissue injury (Figures 5 & 9). However, there was a significant increase in SP-D content of AgNP treated mice as compared to the control (Figure 7). There were no significant differences between treatment groups for capillary surfactometry as well (Table 1), which is consistent with

phospholipid and SP-B findings (Figures 5 & 7). Analysis of respiratory mechanics revealed significant decreases in elastance and resistance spectra for AgNP treated mice as compared to the control (Figure 8). The differences in spectra were demonstrated to be isolated to the low frequency end of the spectra for both elastance and resistance indicating changes were occurring in the parenchyma (Figure 10). To determine if the results at 7 days post-instillation were due to the nano-scale properties of the AgNPs or ionic silver, a separate group of mice were dosed with silver nitrate solution. This treatment group demonstrated no signs of inflammation or significant differences in respiratory mechanics as compared to the saline control (data not shown).

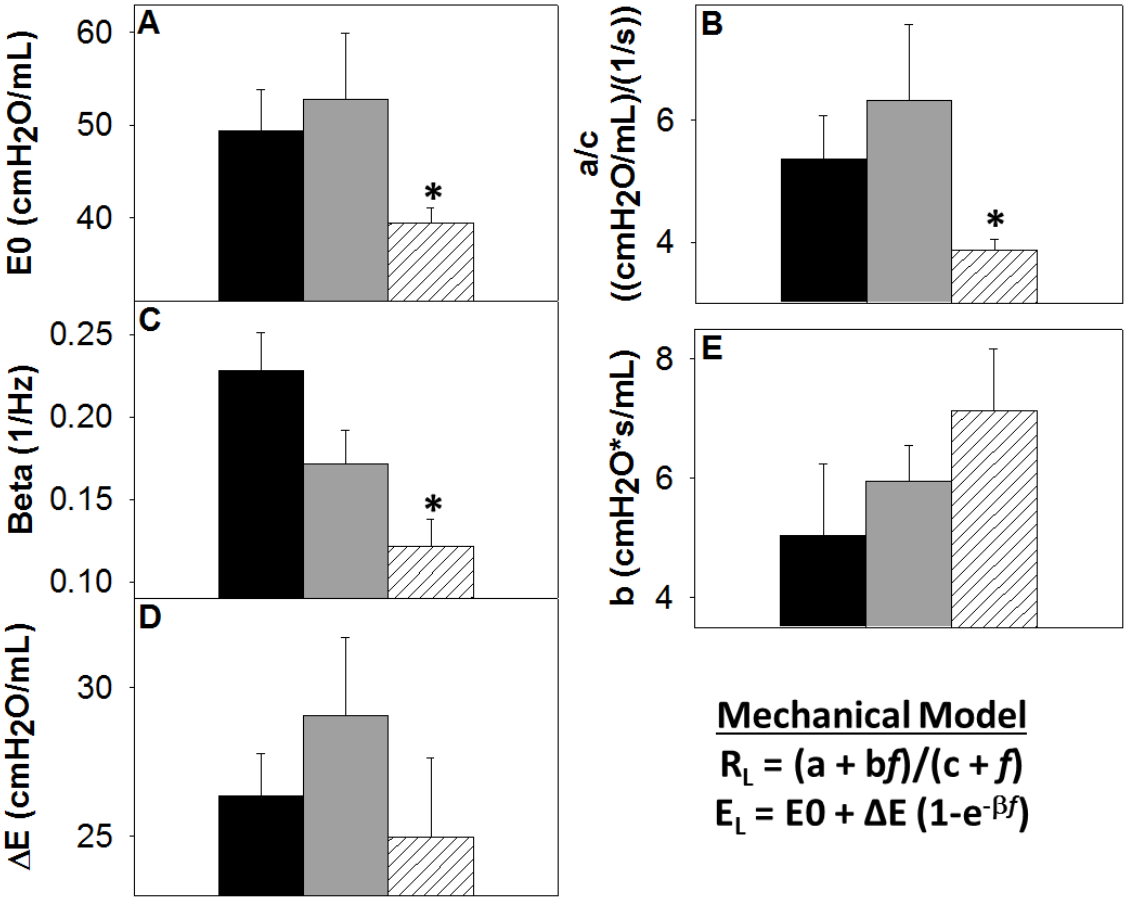

Figure 10. *7 Days Post-Exposure Resistance (R_L) & Elastance (E_L) Model Parameters*: Analysis of model parameters at PEEP 3 **A)** inherent tissue stiffness (E0) **B)** Low frequency resistance (a/c) **C)** rate of change of elastance (beta) **D)** magnitude of change in elastance (ΔE) **E)** high frequency resistance (b) The greatest changes in spectra were seen at 7 days, and these parameters are extracted from the 7 day model for HBSS, high dose Carbon Black NP, and high dose AgNP. The most significant changes are occurring in the low frequency end of the spectra, where AgNP treated mice display a significantly decreased inherent tissue stiffness and resistance in the lower airways as compared to the control. These differences are not resolved with increasing PEEP (*****$p<0.05$ compared to the control).

DISCUSSION

This study documents effects specific to the metal properties of AgNPs. Throughout this study, there were significant differences found in both inflammatory and lung function endpoints between metal and non-metal NP exposures. While high doses of non-metal, carbon black NPs predictably led to acute inflammation (neutrophilia and macrophage activation), the same dose of metal, AgNPs produced no signs of acute inflammation. Though these metal NP treated mice lacked a classic inflammatory response, they experienced significantly increased work of breathing (at low and high doses). At 3 and 7 days post-instillation, inflammation resolved in the non-metal NP treated mice; while the metal NP treated mice experienced delayed inflammatory effects and a persisting decline in lung function. These findings confirm our hypothesis that there are inflammatory and lung function effects specific to the metal properties of AgNPs. These effects are most likely due to modified airway epithelial cell function.

Non-metal NPs elicit a dose-dependent response that demonstrates low doses of carbon black NPs do not lead to inflammation, while high doses of carbon blacks NPs lead to neutrophilic invasion and macrophage activation. The metal, AgNPs do not act in a similar dose-dependent manner. Neither at low or high doses did AgNPs elicit an inflammatory response. This may be due to their difference in affinity for aggregation and consequent interactions with components of the lung lining fluid. Carbon black NPs more easily self-aggregates than AgNPs [14, 52], thus there is a higher probability of formation of larger agglomerates that can be easily phagocytosed by macrophages and trigger inflammatory pathways (as demonstrated by the increased expression of macrophage activation markers and neutrophilic invasion, Figures 3 & 4). AgNPs readily maintain

nanoscale form [14], and are less likely to form large agglomerates than carbon black NPs; however, they still have the capacity to interact with components of the lung lining fluid.

The acute respiratory mechanical effects of metal NPs were isolated to changes in elastance in the low frequency portion of the inspiratory spectrum. These changes are consistent with alterations to the nature of the parenchymal tissue of the lung. This may be due to AgNPs becoming coated by lipid and surfactant protein in the lung lining fluid. Such interactions have been previously reported to mediate the formation of NP strands in the presence of SP-B [1, 14, 53]. This coating and strand formation could disrupt the maintenance of surface tension by the lung lining fluid, not only by their presence, but also by removing available surface-active material. Previously we have reported that 20nm citrate-stabilized AgNPs have a greater propensity for aggregation and dissolution when lipid-coated as compared with both 20 and 110nm PVP-stabilized AgNPs [53].

Lipids comprise the largest percentage of macromolecules within the lung lining fluid (90%-dipalmitoyl phosphatidylcholine (DPPC), phosphatidylcholine (PC) and phosphatidylglycerol (PG)); and how NPs interact with this portion of the lung lining fluid will likely determine further interactions with cells and proteins. AgNPs coated by lipid will increase likelihood of interacting with alveolar macrophages, thus increasing lipid removal from the lung lining fluid. Loss of lipid could produce an increase in the work of breathing [1, 12, 54]. While our capillary surfactometry results did not confirm a change in surface tension, this assay is limited in that it cannot detect localized changes within the lung. Lipid used in the capillary surfactometry assay is procured via a whole lung lavage. Localized changes that can be detected by the lung mechanics model may not be evidenced once examining the whole lung lavage, unless severe, wide-spread injury has occurred.

Thus the data presented here are supportive of a change in surface active function of the lung lining fluid, but are not conclusive. Future studies focusing on using more sensitive assays, such as a pulsating bubble surfactometry, would be valuable in determining potential changes to surface tension and their relative importance to lung function.

The inflammatory response to high doses of non-metal NPs lessened at 3 days and resolved by 7 days post-instillation, which is consistent with an irritant inflammation response. However, mice dosed with AgNPs experienced a delayed inflammatory response. At 3 days post-instillation, AgNP mice demonstrated an invasion of lymphocytes, increasing macrophage count, and increased cytokine expression. While the inflammatory pattern had worsened the initial tissue stiffness appears to resolve 3 days after AgNP exposure. These data are best explained by reasoning that a cellular response has been mounted to compensate for the proposed change in the lung lining fluid lipid content. Further it appears that the lung lining is signaling for cellular recruitment, and that increased lipid production by Type II epithelial cells has lessened the work of breathing. Type II epithelial cells are crucial to maintaining surfactant homeostasis; they are responsible for producing, secreting, and recycling surfactant proteins and lipid. Altered surfactant composition will trigger a Type II cell response to preserve both the immune and surface tension maintenance properties of the lung lining fluid. At 7 days post-instillation, while the inflammatory response had all but resolved in AgNP treated mice, there was a significant decrease in both elastic and resistive components of the lung, specifically in the low frequency end of the spectra. This is potentially a result of an overshoot response by the pulmonary epithelium, in which the Type II cells have begun to

over produce lipid. Additionally at 7 days, AgNP exposed mice demonstrated an increase in SP-D, providing further evidence for changes in Type II cell function.

CONCLUSION

AgNPs elicit metal-specific organ level responses within the lung. AgNP-surfactant interactions lead to altered respiratory function and delayed immune response due to modified airway epithelial cell function.

SPECIFIC AIM 2: EFFECTS OF AGNP FUNCTIONALIZATION & SIZE

In this study, we aim to determine how different AgNP functionalization and size affects lung function and inflammation. We propose that larger, polymer-stabilized AgNP exposure will result in increased alveolar system interactions versus all sizes of citrate-stabilized AgNPs and demonstrate more pronounced changes in lung function and inflammation due to their increased particle stability. A low dose of AgNPs was used to reduce possible injury and inflammation, and allow for determination of the relationship between particle biophysics and lung function. Four different types of AgNPs with combinations of two diameters (20nm vs. 110nm) and two capping agents (citrate and PVP) were intratracheally instilled for *in vivo* assessment, while the interaction between each type of AgNP and a model surfactant was measured *in vitro*. 1, 7, and 21 days post-exposure the lung function and inflammatory response were analyzed using the flexivent, bronchoalveolar lavage (BAL), and harvesting of the lungs for histology and molecular studies. This provided an organ level assessment and allowed for correlation of respiratory mechanics (flexivent analysis) with changes in alveolar cells, proteins, lipids (BAL analysis) and lung tissue (histology) due to exposure of AgNPs of varied functionalization and size.

RATIONALE

Surface chemistry and particle size are key factors that determine nanoparticle interactions within a biological system [55, 56]. These factors determine redox potential, particle-particle interaction, particle-protein interaction, particle-lipid interaction, deposition of particles, and cellular clearance of particles [56]. During the synthesis process, AgNPs are often stabilized by a ‘capping agent’ such as citrate and polyvinylpyrrolidine (PVP). Prior research has demonstrated that PVP binds to the core of

AgNPs by steric interaction producing a stronger association than citrate that binds AgNPs via ionic interactions [1, 10, 57]. PVP-stabilized particles do not readily aggregate or precipitate out of culture media. In contrast, citrate-stabilized particles can rapidly aggregate and precipitate when suspended in high ionic strength buffers due to charge screening effects [57]. How these different stabilization mechanisms affect the AgNP interaction with the lung lining fluid is currently unknown.

METHODS

SILVER NANOSPHERES

All four types of AgNPs were manufactured by nanoComposix, Inc (San Diego, CA) via base-catalyzed reduction of silver nitrate using 5-7nm gold seed as nucleation centers. The size of the particles was measured by the Nanotechnology Characterization Laboratory, National Cancer Institute at Frederick using TEM and ICP-MS. The AgNPs were subsequently provided by the Consortium of NIEHS Centers for Nanotechnology Health Implications Research (NCNHIR). The particles were further characterized, using TEM, energy dispersive X-ray spectroscopy (EDX) and zeta potential ζ measurements. 110nm AgNPs were further characterized using high angle annular dark field scanning transmission electron microscopy (HAADF-STEM). HAADF-STEM combined with EDX analysis were carried out using an FEI Titan 80/300 fitted with a Cs (image) corrector, monochromator and EDX detector (EDAX, Leicester UK) operated at an accelerating voltage of 80kV. For STEM experiments, a convergence semi-angle of 14mrad was used, with an inner and outer HAADF collection angle of 49 and 239mrad, respectively. The probe diameter was <0.5nm.

Stability of AgNPs: Dissolution Kinetics

Aliquots of Ag solutions were taken for inductively coupled plasma-optical emission spectroscopy (ICP-OES) analysis at various time points from 1 hour up to 3 days (72 hours). ICP-OES was used to determine the amount of dissolved Ag at pH 5 and 7. To minimize the impact of anions on the stability of the AgNPs, non-interacting buffers were used and perchloric acid (Sigma-Aldrich) was used to adjust the pH. Each AgNP suspension (PVP or citrate coating) was incubated in a temperature controller at 37°C and then centrifuged at high speed (13 000 rpm) with 2kDa (< 4nm) filter tubes (Sartorius Stedim VIVACON 500) to separate any NPs from the solution. For the control experiment, deionized water (no AgNPs) and supernatant from which the AgNPs had been removed were analyzed to ensure that any residual AgNPs were removed during centrifugation and filtering.

Stability of AgNPs: Morphology Evolution

TEM was performed using a JEOL 2010 instrument operated at an accelerating voltage of 200 kV. The effect of pH, particle size and surface chemistry on the stability of AgNPs (25 mg L^{-1}) was studied in the presence and absence of dipalmitoylphosphatidylcholine (DPPC). This assay was designed to examine lipid-AgNP interactions, not to model the alveolar environment where interactions are complicated by the presence of surfactant proteins [16]. DPPC solutions of 100 mg L^{-1} were prepared in perchlorate acid solutions (pH 5) by sonication for 10 minutes using an ultrasonic bath. The samples were incubated at 37°C for one day (24 hours) in a dri-block heater. TEM samples were prepared by depositing a single drop of the suspension on a 300 Cu Mesh holey support film and were left to dry at room temperature and stored under vacuum.

Murine Model and Particle Instillation

Nine-week-old C57-BL6 Jackson wild-type male mice were intratracheally instilled with AgNPs, or water (50µl) for control, following anesthesia using a ketamine/xylazine combination. Particles, at 0.05µg AgNP/g body weight, were suspended into water to a final volume of 50µl. Citrate-stabilized particles can rapidly aggregate and precipitate in high ionic strength buffers [57]. Therefore AgNPs were suspended in a non-ionic solution (water), at a low dose. Particles were mixed in solution using probe sonication immediately before intratracheal instillation. To determine a particle dose that was sub-toxic, as defined by a failure to increase lung leak 24 hours post administration, mice were instilled with 0.05, 0.15, 0.45, or 1.35µg AgNP/g body weight. At 24 hours post-instillation animals were injected with Evan's Blue Dye (EBD) retro-orbitally. Lungs were lavaged and dye content was measured spectrophotometrically. A dose of 0.05 µg AgNP/g body showed no significant increase in dye content. Mice were left for 1, 7 or 21 days before being anesthetized and mechanical function assessed (see below). Following lung function assessment (described below) the mice were exsanguinated and tissues were harvested and analyzed as described below.

This protocol was approved by the Rutgers University Institutional Animal Care and Use Committee (IACUC) (Protocol Number: 06-028). The study was conducted in accordance with the recommendations in the Guide for the Care and Use of Laboratory Animals of the National Institutes of Health. Intratracheal instillations and mechanical ventilation were conducted under ketamine/xylazine anesthesia, and all efforts were made to minimize suffering. Animals were sacrificed using a lethal dose of ketmine/xylazine and exsanguination.

Bronchoalveolar Lavage

The whole lung of each mouse was lavaged (prior to inflation fixing with paraformaldehyde) with 10mM HEPES buffered saline in 1mL increments four times. Cells from the BAL were then centrifuged (300g, 10 minutes). The supernatant was collected for protein and lipid analysis. The cell pellet was re-suspended in 1mL buffered saline for cytology and RT-PCR [36, 40, 49].

Histology

The left lung was harvested and inflation fixed using a 3% paraformaldehyde in 2% sucrose solution. Lungs were then embedded in paraffin, sectioned and stained with hematoxylin and eosin (H&E). Lung images were captured using the Olympus VS120-SL Virtual Slide System [40, 49].

Cell Counts and Cytology

Cell number was assessed using a Beckman Coulter™ Multisizer™ 3 Coulter Counter®. Approximately 30 000 cells were then centrifuged onto a glass slide at 800g for three minutes, air dried, and then stained with Diff-Quik buffered modified Wright-Giemsa stain. Cell differentials were performed manually using a light microscope at 40x magnification [36, 40, 49].

Lactate Dehydrogenase (LDH) Activity Assay

A LDH assay was performed using BAL fluid to assess general cellular cytotoxicity. Chemicals and protocol were used from an *In Vitro* Toxicology Assay Kit, Lactic Dehydrogenase based by Sigma-Aldrich® (St. Louis, MO, USA) [58, 59].

Real-Time Polymerase Chain Reactions

RNA was prepared from BAL cells using a QIAshredder™ kit and converted to cDNA. The cell samples for each treatment group were pooled into one larger sample for analysis. Thermocycling was used to analyze mRNA expression of CCL2 (mCCL2 1F103: CCT GCT GCT ACT CAT TCA CCA; mCCL2 1R259: GTC TGG ACC CAT TCC TTC TTG), IL1B (mIL1b1F216: TGT GGC AGC TAC CTG TGT CTT; mIL1b1R321: TCC CAT GAG TCA CAG AGG ATG), IL6 (mIL6F23: GAC TTC CAT CCA GTT GCC TTC; mIL6R125: TGG GAG TGG TAT CCT CTG TGA), CXCL10 (mCXCL10F12: AGT GCT GCC GTC ATT TTC TGC; mCXCL10R139: CCT ATG GCC CTC ATT CTC ACT), and IL12B (mIL12bF131: GTG ACA CGC CTG AAG AAG ATG; mIL12bR303: CTT CTT GTG GAG CAG CAG ATG). The ABI 7900HT Fast Real-Time PCR System by Applied Biosystems (Waltham, Massachusetts, USA) was used and primers were designed with OligoPerfect™ Designer (Invitrogen.com). Fold expression was calculated by the ΔΔCT method normalizing to the water (control) treatment group and using actin as the control gene [50].

Immunohistochemistry

To qualitatively assess cellular recruitment in response to AgNP treatment and better define the macrophage population within the lung, paraffin embedded tissue sections were stained using an antibody for Cd11b (ab133357, anti-rabbit, abcam® (Cambridge, MA, USA)). Cd11b serves as a marker for recruited monocytes [60, 61].

Protein & Phospholipid Assay

Whole BAL protein concentration was determined using a Low Protein BCA Assay kit by Lamda Biotech, Inc (St. Louis, MO). To estimate phospholipid content, whole BAL

was fractionated into small and large aggregate portions by centrifugation at 17 000g for one hour at 4^0C. The supernatant was the protein-rich small aggregate fraction. The pellet was re-suspended in a small volume of saline (35µl) and was the lipid-rich large aggregate fraction. Inorganic phosphate from the lipid-rich fractions was measured as an estimate of the phospholipid content [49, 51].

IMMUNOBLOTTING

To determine surfactant protein content, reducing NuPAGE was performed using individual BAL samples. Gels were transferred to BioRad Immun-blot® PDVF membranes, incubated with SP-D or SP-B antibody (M.F. Beers, University of Pennsylvania), goatαrabbit linked to horseradish peroxidase, and imaged using Amersham™ ECL™ Prime Western Blotting Detection Reagent. Densitometry was performed to quantify the chemiluminescent signal. Whole BAL was used for SP-D analysis; and sample load was normalized to protein concentration. Large aggregate BAL (LA BAL) was used for SP-B analysis and sample load was normalized to phospholipid content as determined by the phospholipid assay [49].

CAPILLARY SURFACTOMETRY

Surface tension was measured using a capillary surfactometer (Calmia Medical, Inc). Samples were loaded at a consistent phospholipid concentration of 1.0µg/µl. Following sample loading, compressed air was applied to the capillary at increasing pressures. Both the initial pressure to disrupt the LA BAL and percent capillary open over the course of two minutes were recorded [49].

Mechanical Ventilation and Respiratory Model

Mice were anesthetized and ventilated using the flexiVent (SCIREQ, Montreal, Canada) at increasing positive end expiratory pressures (PEEPs) (0, 1, 3, and 6 cmH_2O) to assay for resolution of lung function [62]. Mechanical ventilation with forced oscillation maneuvers was used to measure impedance broadband signal (0.5-20Hz) respiratory impedance [Z(f)] [39]. The flow [V(t)] is a known value input into the system while pressure [P(t)] output is unknown. As mechanical function varies with frequency of oscillation, a Fourier Transform was performed so that impedance could be expressed as a function of frequency, $Z(f) = P(f)/ V(f)$. Output impedance spectra were used to generate resistance (R_L) and elastance (E_L) spectra across the frequency range, and fit to a model of heterogeneous lung function using the following equations [37, 40, 41]:

$$R_L = (a + bf)/(c + f) \text{ and } E_L = E0 + \Delta E\ (1\text{-}e^{-\beta f})$$

Statistical Analysis

All data (excluding respiratory mechanics) were analyzed using 1-way ANOVA and the Holm-Sidak Method, a p value of < 0.05 was considered statistically significant. In the case of respiratory modeling, model fits were estimated for each treatment group by fitting a non-linear regression curve to the spectra of all mice in a treatment group equally at each PEEP. Spectra were analyzed for significant differences using the null hypothesis that the data can be characterized by one three-parameter relationship or alternatively that the data are distinct enough to be characterized by two three-parameter relationships. The parameters of the R_L and E_L curves were estimated from non-linear regressions fitting to the spectra of each individual mouse within a treatment group at each PEEP. Then a mean and standard error for each parameter was taken for each treatment group [37, 41]. A 1-

way ANOVA was used to determine significant differences in the mean value of each parameter for treatment groups and PEEP. Pairwise comparisons were made using the Holm-Sidak method.

RESULTS

PARTICLE CHARACTERIZATION

In-house characterization analysis confirmed that as-received AgNPs had the physicochemical properties as shown in Figure 11; the zeta potentials are more similar than would be expected (the citrate capping may have surface-exchanged reducing the effective charge for these particles): all show a negative potential consistent with manufacturers specification. EDX spectra (Figure 12) showed that consortium particles (20nm) were gold-silver core-shell NPs. As expected the Au core could not be detected for 110nm NPs using EDX or high-angle annular dark-field scanning transmission electron microscopy (HAADF-STEM) as it is below the concentration limit for detection, buried in the Ag shell (the manufacturers MSDS state that the Au core is present, confirmed by ICP-MS at NCNHIR) (Figure 13 and 14).

The dissolution rates of the four types of AgNPs was examined at both pH 5 & 7 (inorganic buffers) by ICP. The dissolution rates were higher at pH 5 than at pH 7 (Figure 15 and 16). All particles, with the exception of 20nm citrate-capped particles, displayed less than 1% total release of silver to the solution over a three-day incubation period (Figure 15 and 16). Our results differ from the previous work of Bouwmeester, et al. (2011) using similar particles, where 5 to 15 % dissolution was observed with citrate stabilized particles. These differences are best explained by differences in methodology, dissolution medium, and separation techniques used by the different laboratories (Figure 17). The 20nm citrate-

capped particles displayed greater dissolution than the other particles at both pH 5 & 7; >4% Ag was released into the solution after three days of incubation (Figure 15). Having established that the particles were relatively stable against dissolution solution, we assessed their morphology and the effect of surfactant addition by TEM (Figure 18). Regardless of stabilization, or the presence of the model surfactant DPPC, 20nm AgNPs displayed a greater tendency to aggregate than the 110nm particles, as expected due to surface energy considerations. Evidence of particle aggregation and significant coarsening is also observed for the 20nm particles with both capping agents (Figure 18 C&G). The limited aggregation of 110nm AgNPs observed in buffer (Figure 18 A&E) was completely lost upon addition of DPPC (Figure 18 B&F). DPPC also had a dramatic effect on the 20nm AgNPs with only small clusters of NPs and no coarsening observed (Figure 18 D&H).

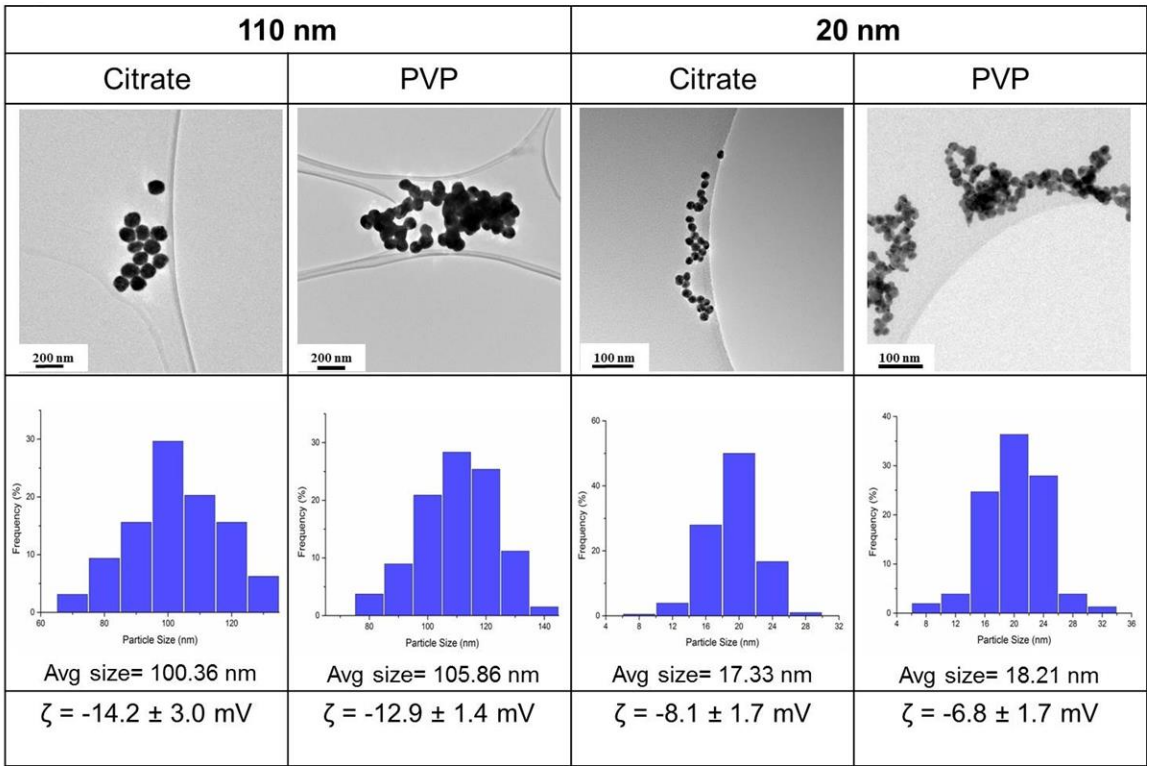

Figure 11. *AgNP Biophysical Characteristics:* Transmission Electron Microscopy (TEM) images, size distribution and zeta potential, ζ of as-received consortium AgNPs.

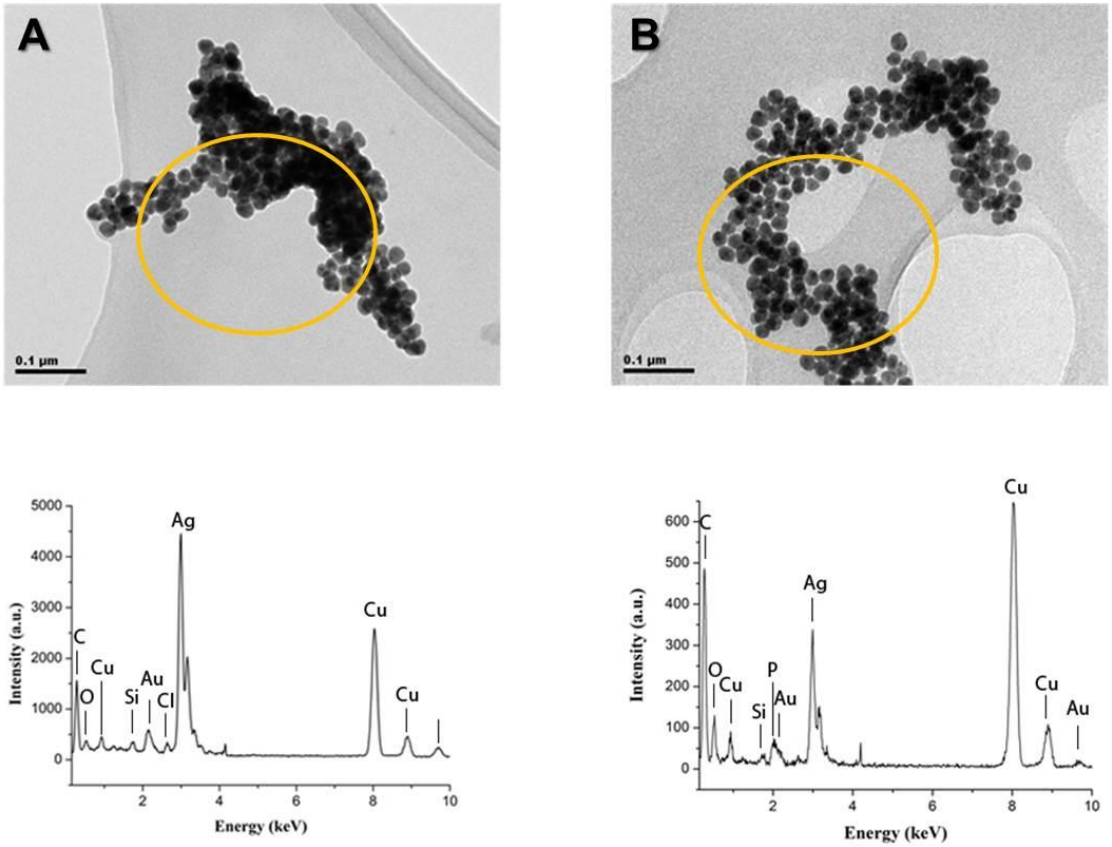

Figure 12. *Energy Dispersive X-Ray Spectroscopy (EDX) Particle Analysis:* Citrate AgNPs (20nm) incubated in pH 7 **A)** without DPPC **B)** with DPPC for 24 hours. Au was detected for both 20nm citrate and PVP coated AgNPs (Cu readings, background readings resulting from Cu plate).

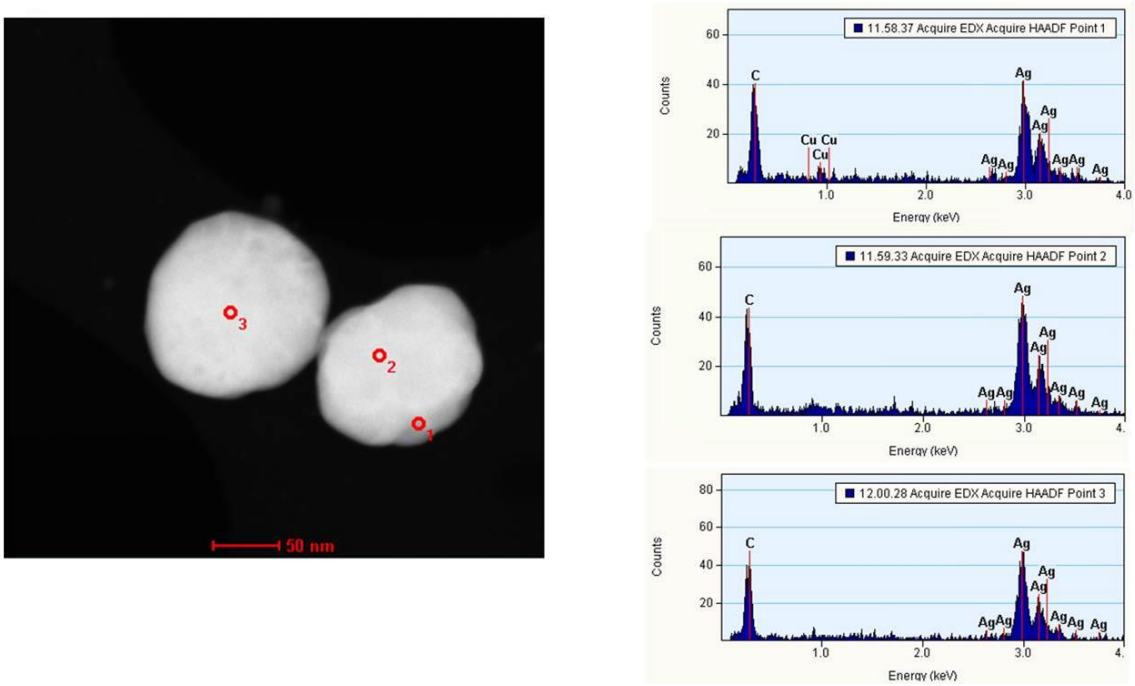

Figure 13. *High Angle Annular Dark Field Scanning Transmission Electron Microscopy (HAADF-STEM/EDX) Analysis:* Citrate coated AgNPs (110nm)

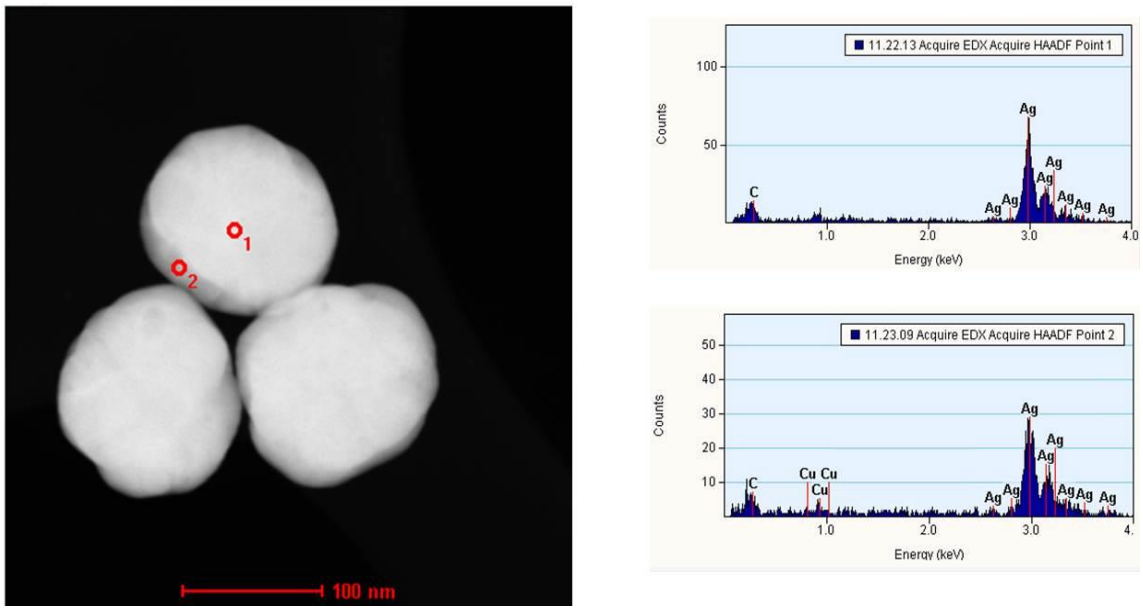

Figure 14. . *High Angle Annular Dark Field Scanning Transmission Electron Microscopy (HAADF-STEM/EDX) Analysis:* PVP coated AgNPs (110nm). Au cannot be detected for the 110 nm AgNPs (both PVP and citrate coating). This might due to the thick layer of silver coating around it.

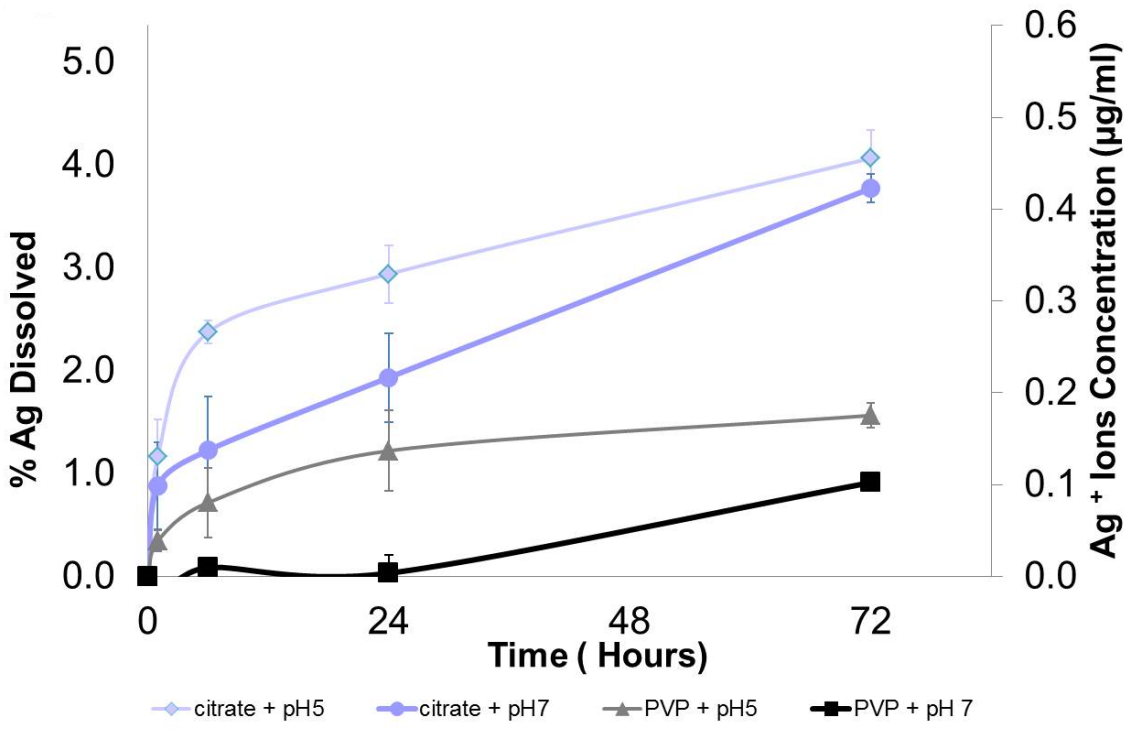

Figure 15. *Ag^{+} Ion Release Study:* 20nm AgNPs incubated in perchlorate acid/perchlorate buffer solutions (pH 5 and 7) over the course of 72 hours. Citrate stabilized particles demonstrated the greatest per cent Ag dissolved over the time course.

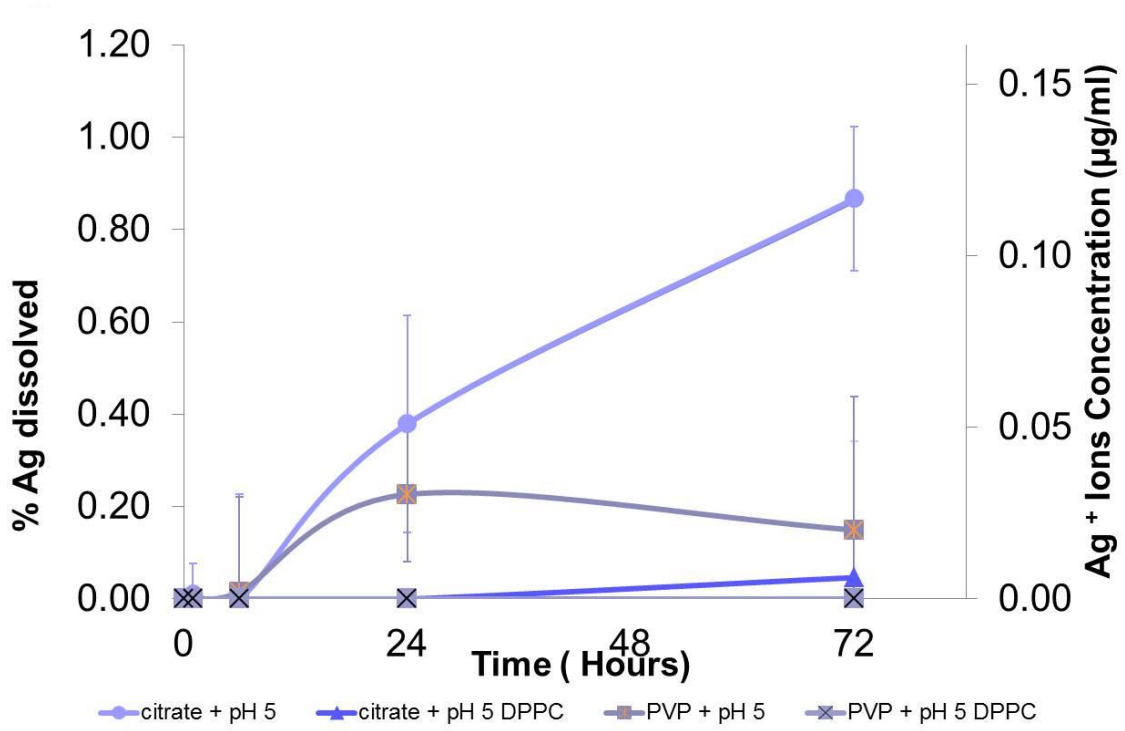

Figure 16. *Ag^{+} Ion Release Study with DPPC:* 110nm AgNPs incubated in perchlorate acid/perchlorate buffer solutions (pH 5 and 7) over the course of 72 hours with and without DPPC. Citrate stabilized particles demonstrated the greatest per cent Ag dissolved over the time course. 110nm citrate and PVP-stabilized AgNPs in pH 7 (with or without DPPC) were below 1%; negligible dissolution occurring.

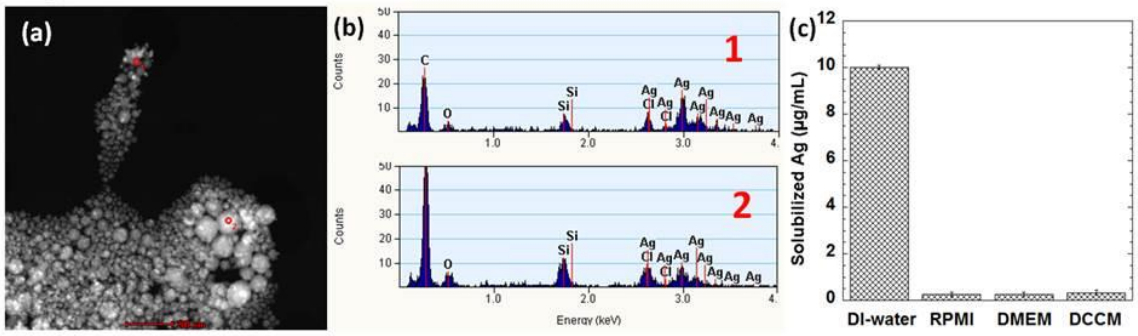

Figure 17. *Dissolution Techniques:* **(a)** A HAADF-STEM image of precipitates formed after the incubation of 17.0 µg/mL AgNO3 (equal to an Ag concentration of 10 µg/mL) in RPMI-1640 at 37°C for 0.5 h. **(b)** The corresponding STEM-EDX spectra 1-2 were collected from area 1-2 marked in **(a)**. The precipitation were collected by filtering the solution through 2 kDa filter membrane and washed 3 times by DI-water. **(c)** ICPOES analysis of solubilized silver concentrations of 17.0 µg/mL $AgNO_3$ in DI-water, RPMI-1640, DMEM and DCCM-1 cell culture media, incubated at 37°C for 0.5 h (n = 3).

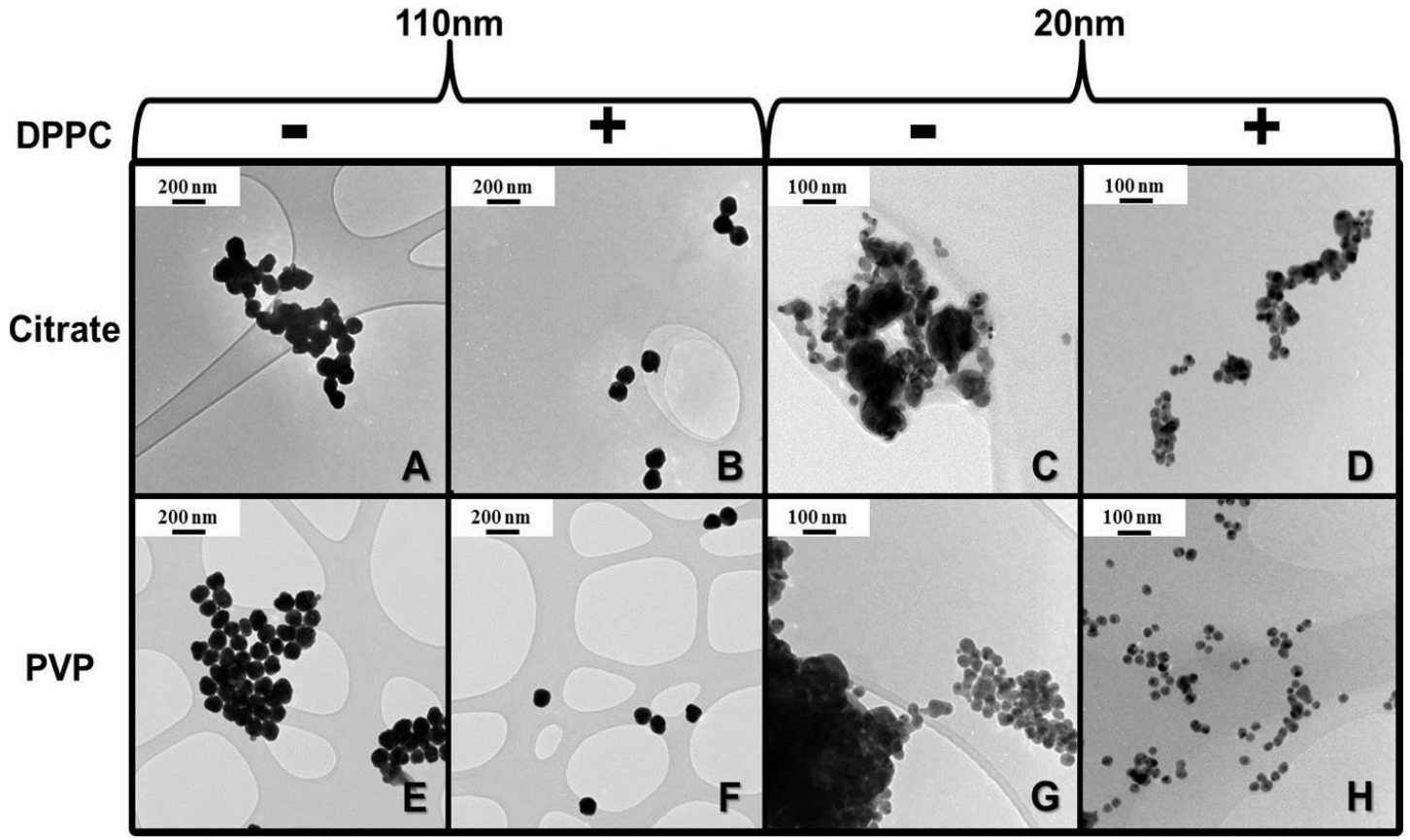

Figure 18. *AgNP Morphology and the Effect of Surfactant Addition by Transmission Electron Microscopy*: TEM images of citrate v. PVP stabilized AgNPs (20 and 110nm) incubated in pH 5 solution with and without DPPC at 37°C for 24 hours (magnification at 20x). Addition of DPPC decreased particle aggregation in all instances; however, size was the predominant factor in particle aggregation.

Acute Findings

Histology of the lung 1 day after particle administration demonstrated no significant injury. There was minor consolidation of the tissue and presence of airway thickening with all four types of AgNPs. The most significant consolidation and thickening appeared in PVP-stabilized AgNP treated mice as well as 110nm citrate-stabilized AgNP treated mice (Figure 19). Although in general there was minimal peribronchial or perivascular inflammation, there was observable cellular accumulation in the tissue of mice treated with PVP-stabilized AgNP; this accumulation was localized in the 20nm treatment group, but diffuse in the 110nm treatment group. Overall, there were no signs of injury or overt inflammation as evidenced by histology.

Cell count and cytology serve as quantitative and qualitative measures of inflammation. As expected with only minor tissue consolidation and airway thickening demonstrated in the histology of the AgNP treated mice, there was no significant change in BAL cell count (Figure 20) or alterations in the inflammatory cell population (in all conditions macrophages constituted >98% of the BAL cells), or increase in protein content within the BAL, indicating no loss of barrier function (Figure 21). To confirm that there was not significant injury to the lung lining, a LDH assay was performed using the BAL; LDH levels were not significantly different between treatment groups (data is not shown). Additionally, RT-PCR showed less than a two-fold change in mRNA expression of CCL2, IL1B, IL6, CXCL10, and IL12B in the BAL cells from AgNP treated mice as compared to the control (water) (Figure 22). NOS2 was not detectable in any of the conditions. These markers were chosen as indicators of macrophage activation.

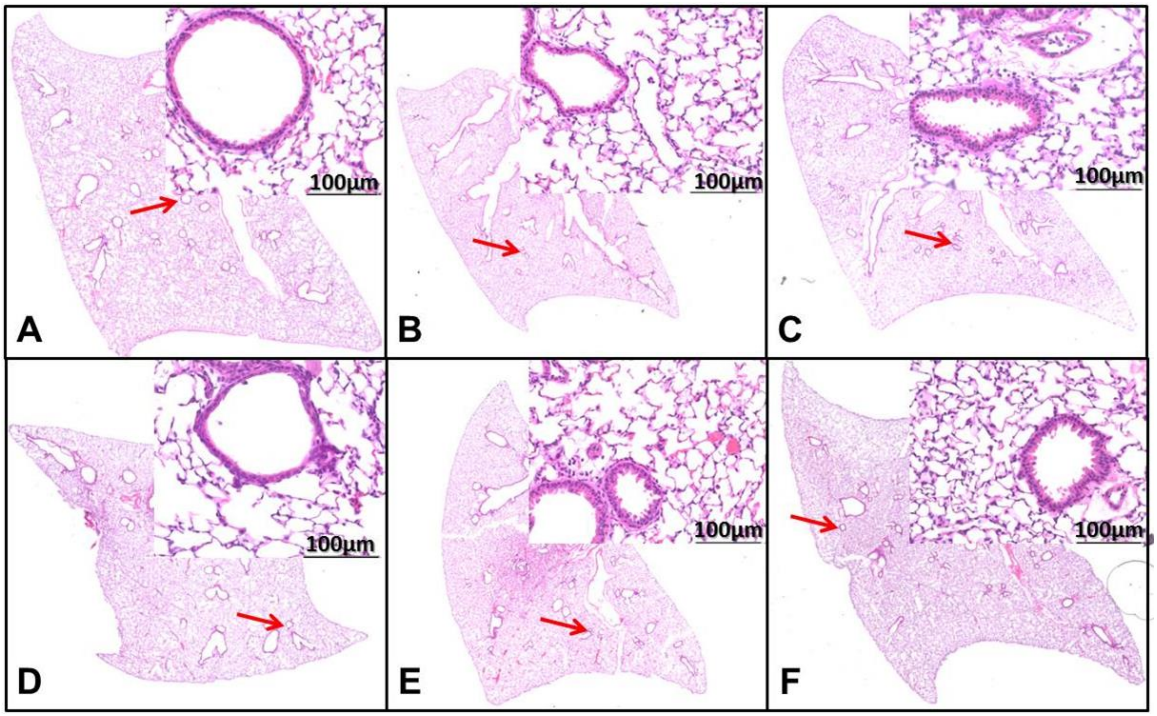

Figure 19. *Histology (H&E) 1 day post-instillation:* Post-mechanical ventilation, the left lung of the treated mice were inflation fixed, paraffin embedded, sectioned and stained with hematoxylin and eosin (whole lung image 0.8x, enlarged image 20x; red arrow marks site of interest) **A)** Untreated wild-type male mouse **B)** 20nm citrate-stabilized AgNP treatment **C)** 110nm citrate-stabilized AgNP treatment **D)** Water (control) treatment **E)** 20nm PVP-stabilized AgNP treatment **F)** 110nm PVP-stabilized AgNP treatment; all AgNP treated mice displayed slight tissue consolidation and airway thickening. This was most pronounced with 110nm citrate and both PVP-stabilized AgNP treated mice. But overall lung structure for all treatments was normal with no indication of overt inflammation.

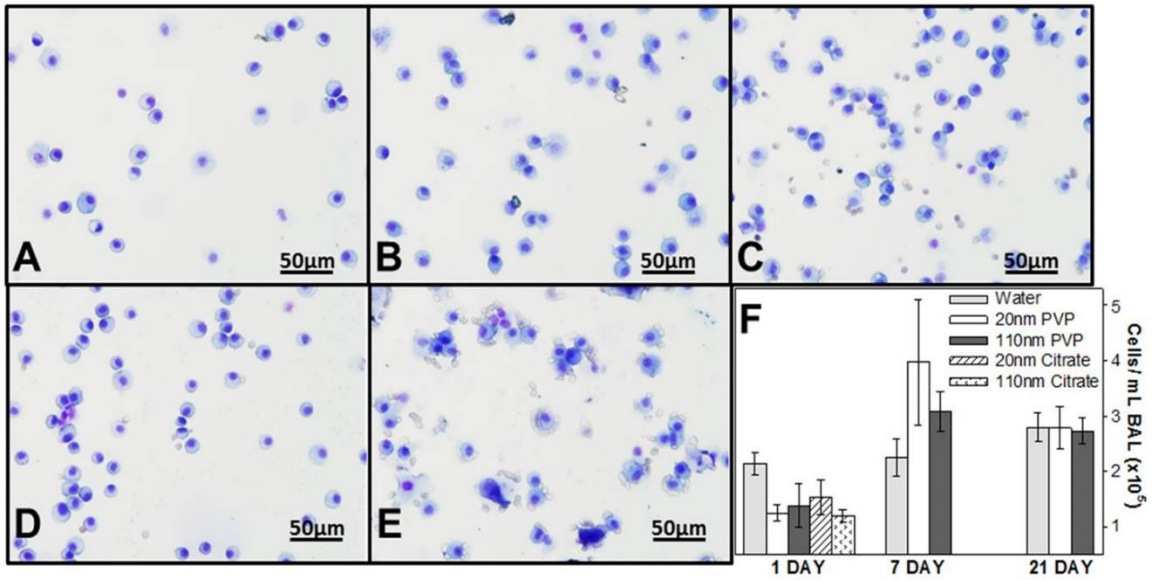

Figure 20. *Cell Count & Cytology using BAL:* Cell counts (mean ± standard error ($x10^5$)) were normalized to 1mL BAL and ~30 000 cells were used for cytology **A)** Water (control) treatment displayed slightly elevated cell count, but no sign of neutrophilia **B)** 20nm citrate-stabilized AgNP treatment **C)** 110nm citrate stabilized AgNP treatment **D)** 20nm PVP-stabilized AgNP treatment **E)** 110nm PVP-stabilized AgNP treatment (A-E all 1 day post-instillation); all AgNP treated mice displayed acute, decreased cell count as compared to the control with no signs of neutrophilia, but all treatments were within normal cell count range. The dominant cell type was macrophages in all treatments, neutrophils and lymphocytes <1% of cell population. **F)** The bar graph displays the cell count time course (n=4 for all treatment groups/time points).

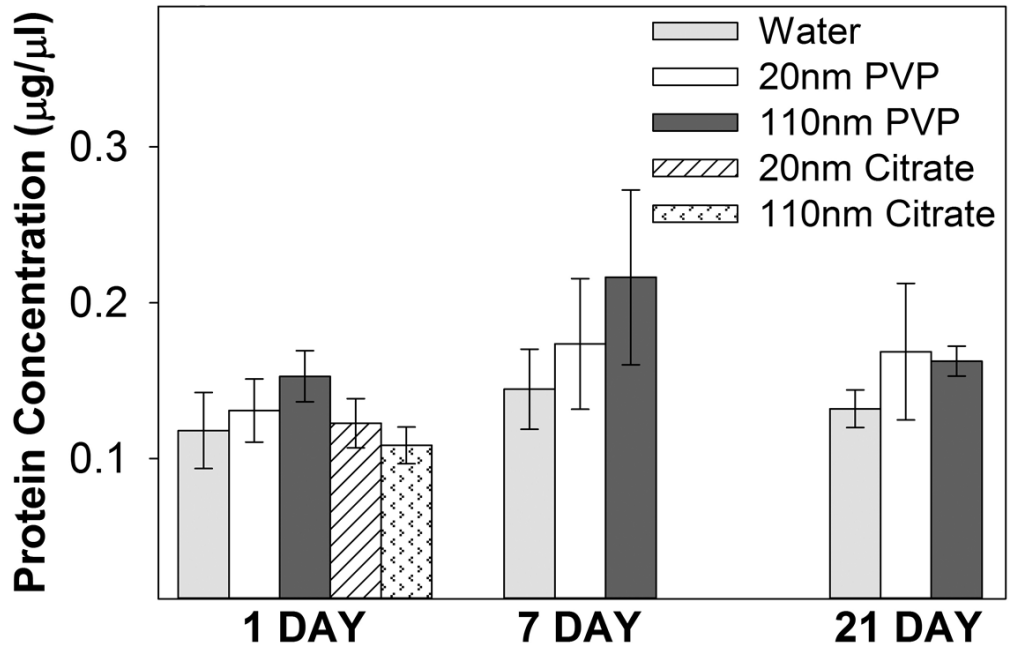

Figure 21. *BCA Assay for Protein Concentration:* Protein concentration was analyzed from BAL and used as indicator of barrier function. There was no significant change in protein concentration as compared to the control at any time point.

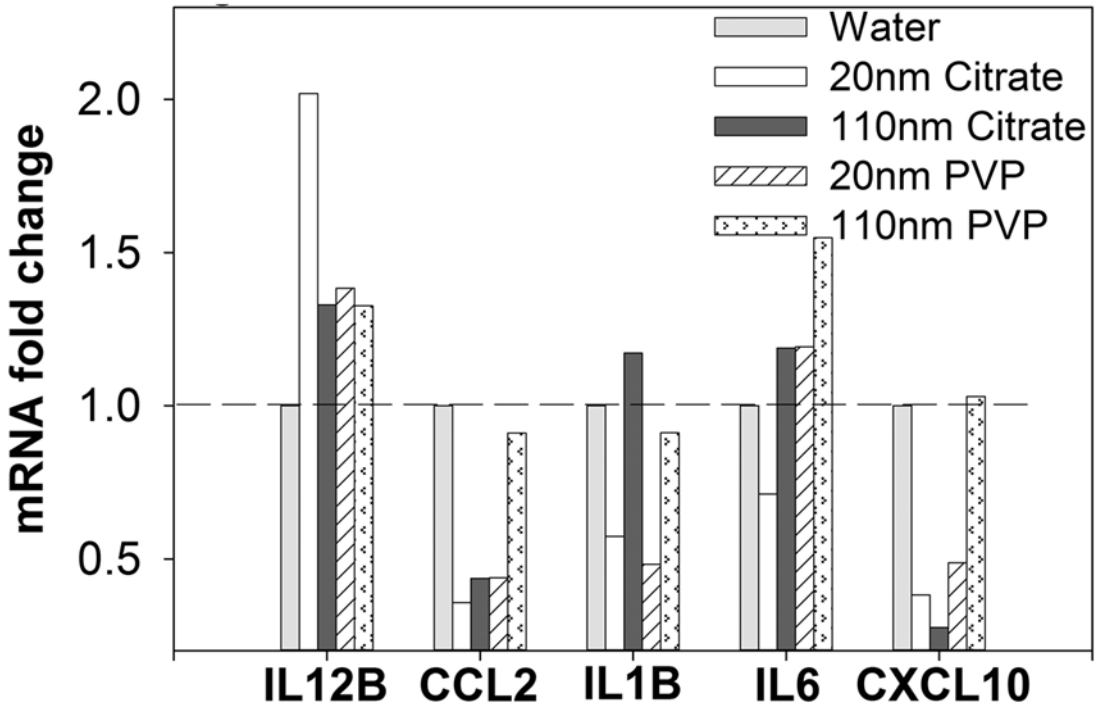

Figure 22. *Real-Time Polymerase Chain Reaction:* Analyzed mRNA expression of CCL2, IL1B, IL6, CXCL10, and IL12B. Less than a 2-fold change in expression for treated mice versus control at each marker (1 day post-instillation data only).

Macrophages are the principle phagocytic cells of the lung lining; a key point of interaction with AgNPs, and thus their activation is predicted in the presence of cellular injury. Characterization of the macrophage population by immunohistochemistry demonstrated that there were Cd11b+ cells present in all lung tissues (localized to both peribronchial and perivascular regions). However, this staining was independent of particle treatment (Figure 23). CD11b is a migratory integrin and is often used as a marker of immature or recruited cells. Therefore, this staining indicates that AgNP exposure does not increase inflammatory cell recruitment. As a whole these data indicate that there was no classic inflammatory response to any of the AgNP exposures.

In order to measure the effects of AgNPs on the lung lining fluid composition, both phospholipid content and surfactant protein content were measured. There was no significant increase in phosphate content with AgNP treatment, except within the 20nm citrate-stabilized particle group (Figure 24). To determine potential protein-particle effects, immunoblotting for both SP-D and SP-B was performed. There was no significant change in SP-B expression between treatment groups. However, there was a significant decrease in SP-D expression in mice treated with PVP-stabilized particles (both 20nm and 110nm Ag); this decrease was greatest in the 110nm treatment group (Figure 25). These changes in the composition of the lung lining fluid did not alter *in vitro* surface-active function as measured by capillary surfactometry. There were no significant differences between treatment groups for either percent capillary open or initial opening pressure (Figure 26).

Measuring mechanical impedance allows one to determine the frequency dependence of pulmonary resistance and elastance and hence to partition functional characteristics in terms of airway and parenchymal components. Lung mechanical function

was assessed by forced oscillation technique and R_L (resistance) and E_L (spectra) were fit to three component models, which have been used previously in assessing lung injury [37, 40, 41]. At PEEP of 3, all particle treated mice displayed a significant increase in both R_L and E_L spectra as compared to the control, with the exception of the 110nm citrate-stabilized particle treatment group in which only the elastance spectra were significantly increased (Figure 27 A, B & C). Furthermore, elastance was significantly greater in mice treated with 110nm PVP-stabilized AgNPs than in mice treated with other types of AgNPs (Figure 27C). The increases seen in the R_L and E_L spectra appear to occur predominantly in the low frequency ends of the spectra (Figure 27 D & E), indicating increased tissue resistance and inherent tissue elastance, with little effect on the main conducting airways.

Figure 27 D-G illustrates the parameter estimates from model fits made at PEEP 3. From the model one can calculate the parameter a/c, which is determined predominantly by low frequency behavior and thus is an estimate of tissue resistance, and the parameter b, which is an estimate of high frequency or airway resistance. Across all levels of PEEP a/c was significantly increased with all types of AgNP administration (Figure 27 D). However, b was not significantly altered by particle exposure at any PEEP (Figure 27 F). Furthermore, there was no significant alteration to a/c with increasing PEEP, except from PEEP 0 to 1. In contrast, with all treatments, parameter b decreased with increasing PEEP. These findings are consistent with our observation of no significant structural alteration as a result of particle administration.

In parallel with the resistance parameters one can estimate E0, as a measure of low frequency elastance, and ΔE, as a measure of the frequency-dependent increase in

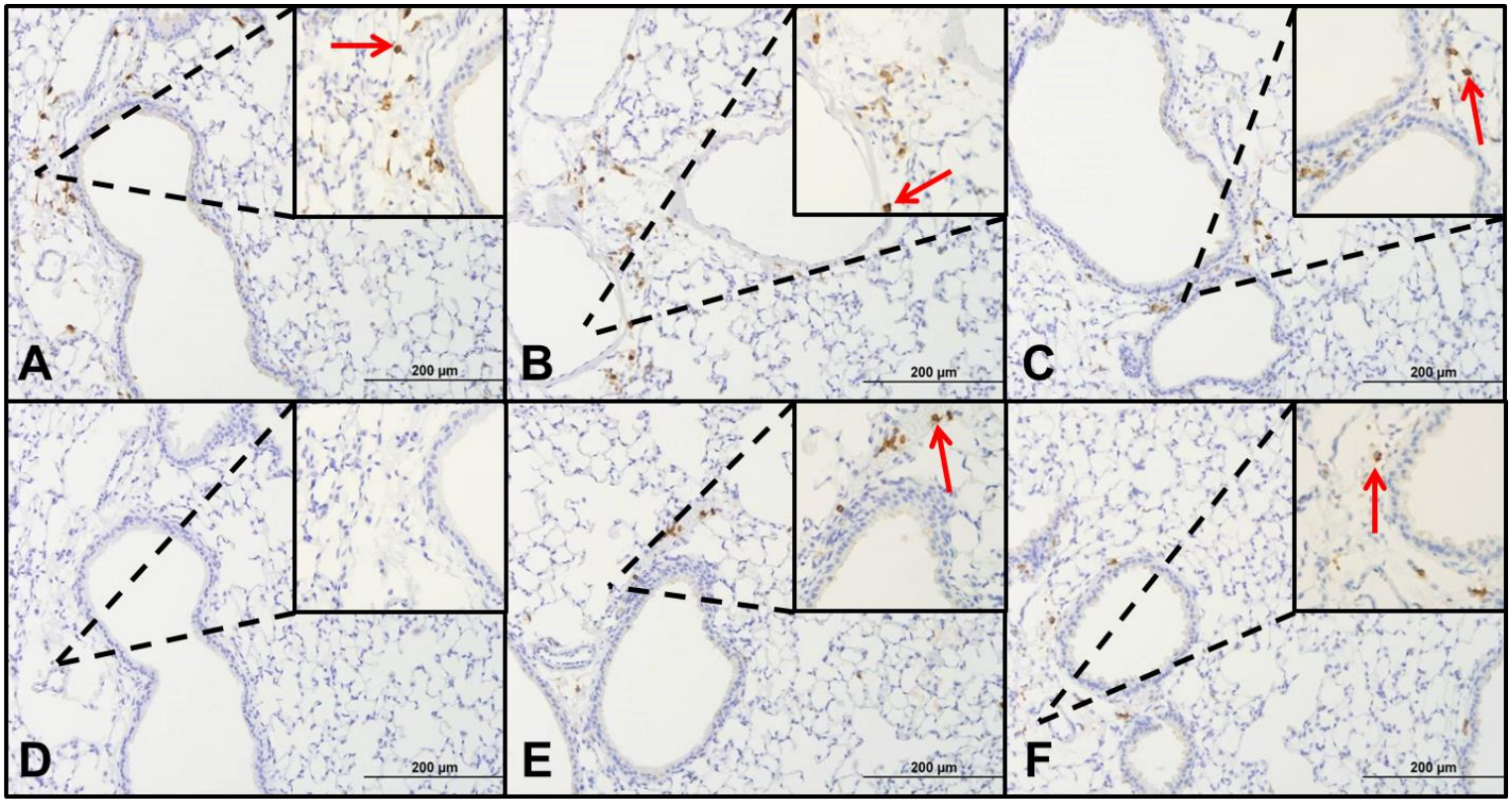

Figure 23. *Immunohistochemistry:* Lung tissue from 1 day post-instillation was stained with anti-Cd11b to assess cell recruitment (main image - 20x, enlarged image - 40x; arrows indicate uptake of stain) **A)** Water treatment **B)** 20nm Citrate-stabilized AgNP treatment **C)** 110nm Citrate-stabilized AgNP treatment **D)** IgG control using tissue from water treatment **E)** 20nm PVP-stabilized AgNP treatment **F)**110nm PVP-stabilized AgNP treatment. Brown stain indicates Cd11b+ cells. The staining is isolated to peribronchial and perivascular sections of the lung. Positive staining is independent of AgNP treatment.

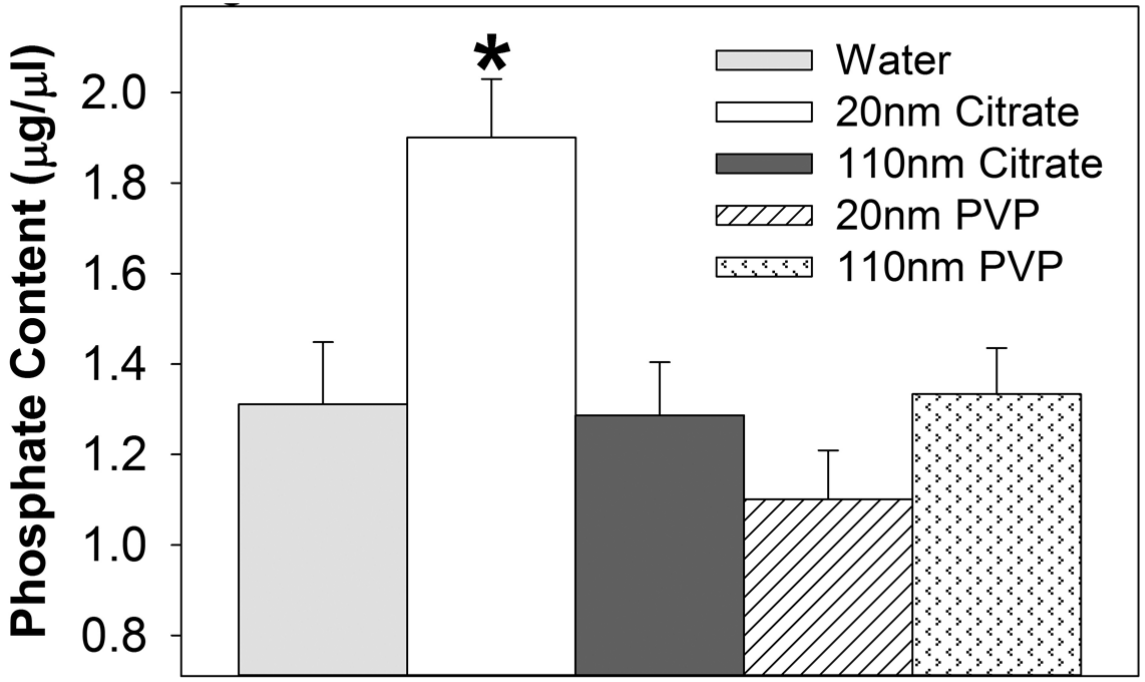

Figure 24. *Phospholipid Assay:* Inorganic phosphate from lipid-rich fractions was measured as an estimate of the phospholipid content. With the exception of 20nm citrate-stabilized AgNP treatment (ANOVA, HolmSidak method, $p<0.05$), there was no significant change in phosphate content as compared to the control (1 day post-instillation data only).

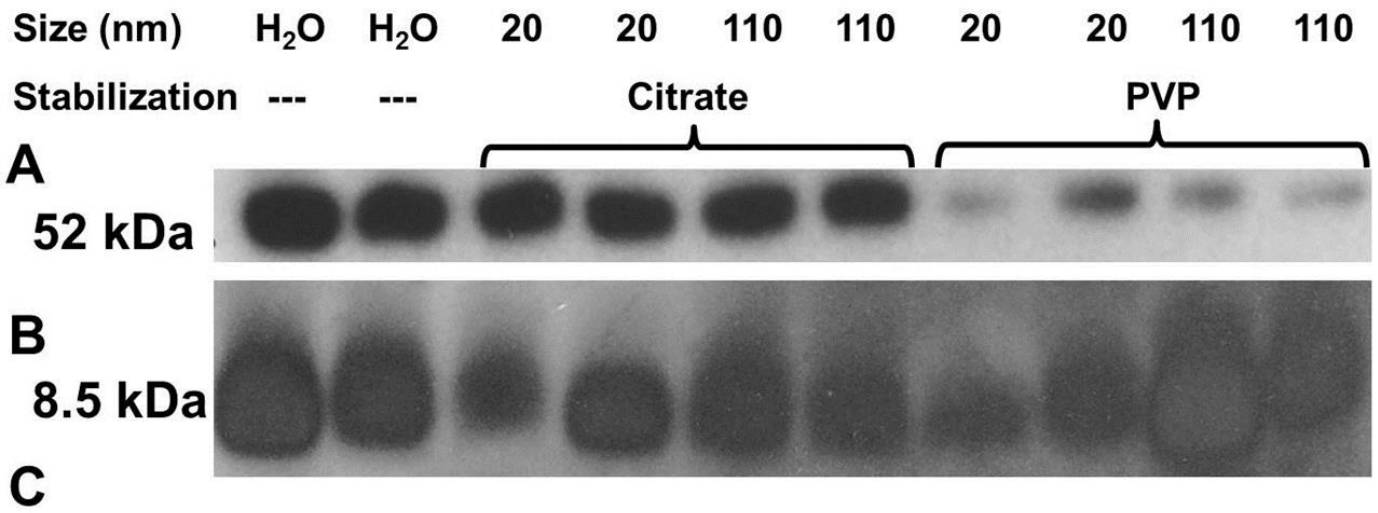

Treatment	SP-D/SP-B ratio compared to control	SP-D content compared to control	SP-B content compared to control
Water	1.00 +/- 0.091	1.00 +/- 0.072	1.00 +/- 0.026
20nm Citrate	0.900 +/- 0.096	0.936 +/- 0.063	1.05 +/- 0.050
110nm Citrate	0.902 +/- 0.072	0.944 +/- 0.036	1.05 +/- 0.047
20nm PVP	0.726 +/- 0.065	0.754 +/- 0.052*	1.04 +/- 0.043
110nm PVP	0.637 +/- 0.027*	0.661 +/- 0.028*†	1.04 +/- 0.053

Figure 25. *Surfactant Expression via Immunoblotting:* 1 day-post intratracheal instillation **A)** SP-D Immunoblot **B)** SP-B Immunoblot **C)** SP-D/SP-B ratios; SP-D expression decreases significantly when lungs are treated with PVP-stabilized particles, while SP-B expression is not significantly altered with particle exposure as compared to the control. Therefore, the SP-D/SP-B ratio decreases with PVP-stabilized particle exposure (*$p<0.05$ compared to the control, †$p<0.05$ compared to citrate-stabilized AgNP treatments; n=4 for all treatment groups).

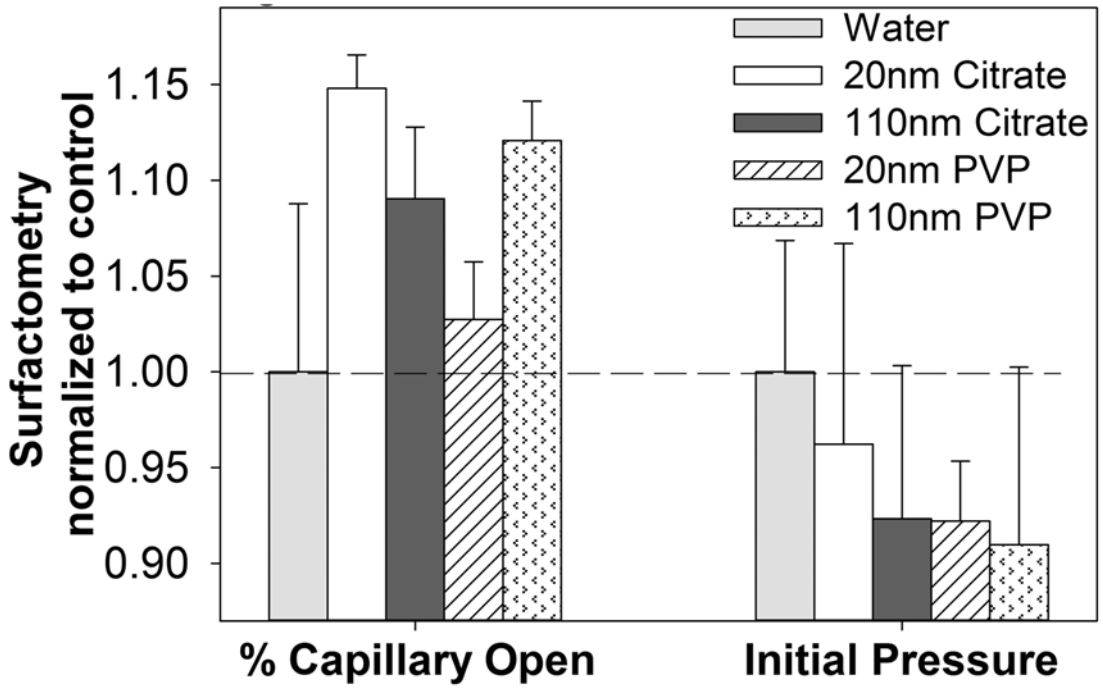

Figure 26. *Capillary Surfactometry:* Both the initial pressure to disrupt the LA BAL and percent capillary open were recorded to better examine any particle disruption of BAL surface tension. There was no significant difference between groups (1 day post-instillation data only).

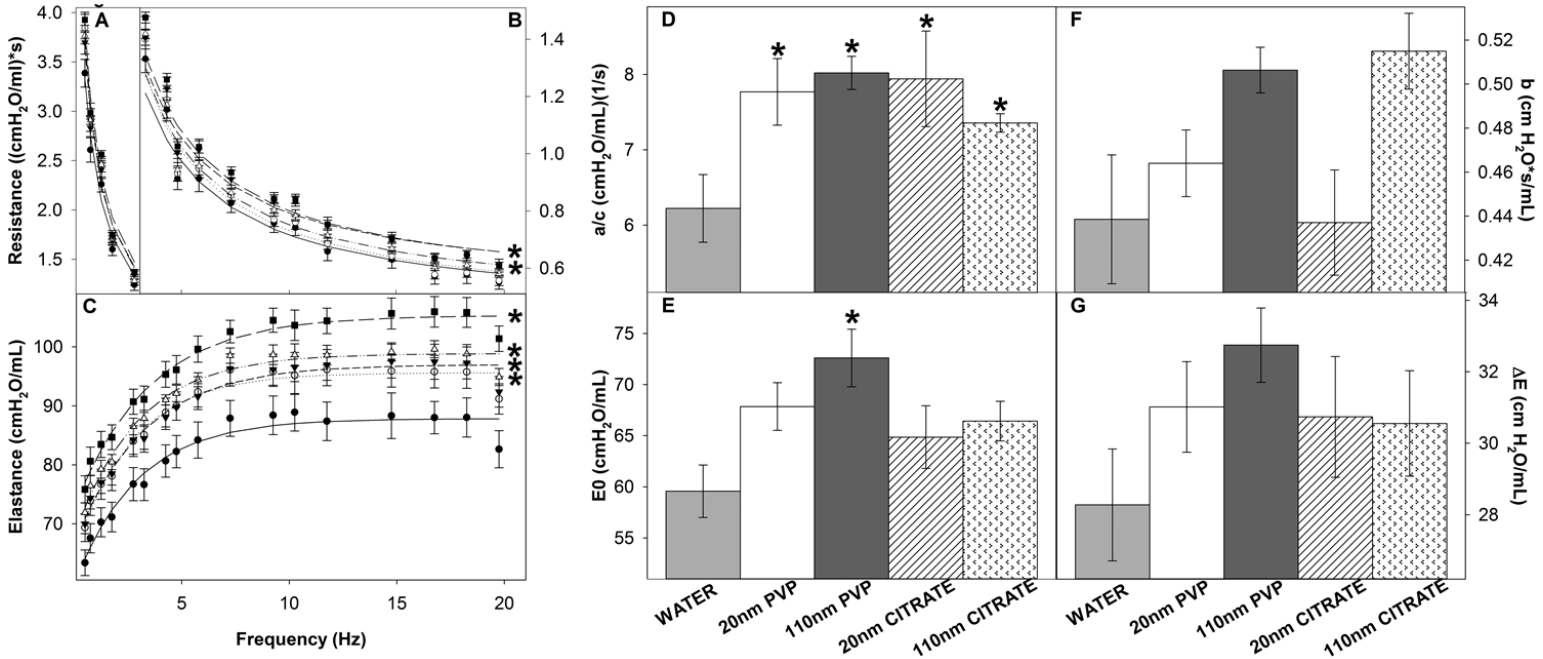

Figure 27. *Resistance (R_L) & Elastance (E_L) Spectra Using Forced Oscillation Technique:* Analysis of impedance measurements at PEEP 3—1 day post-instillation A&B) 20nm AgNP citrate & PVP stabilized, and 110nm AgNP PVP-stabilized treated mice were significantly ↑ v. control R_L spectra but C) all AgNP treated mice were significantly ↑ v. control E_L spectra (*$p<0.05$ compared to control) (●/solid line = Water/Model Fit; ○/dotted line = 20nm Citrate/Model Fit;▼/short dashed line = 110nm citrate/Model Fit; ▽/dashed & dotted line = 20nm PVP/Model Fit; ■/long dashed line = 110nm PVP/Model Fit) the D) low frequency resistance (a/c) E) low frequency elastance (E0) F) high frequency resistance (b) and G) magnitude of change in elastance (ΔE) were not PEEP dependent. Isolating the model parameters revealed that the greatest differences occur in the low frequency end of the spectra.

elastance (Figure 27 E & G). E0 was consistently raised by particle administration across PEEP values, although this increase was only statistically significant for 110 nm PVP-stabilized AgNP (PEEPs 1-6cmH2O). Similar to the resistance parameters, E0 responses to increasing PEEP were not altered by particle administration. In contrast, ΔE, which was raised at low PEEP within particle-administered mice (and to the greatest extent within 110 nm PVP-stabilized AgNPs), was completely resolved by increasing the PEEP.

Long-Term Effects

The most pronounced acute effects occurred within the PVP-stabilized AgNP treated mice. Therefore, longer-term studies to examine for the persistence of the responses focused on 20 and 110nm PVP instillations, and mice were examined at 7 and 21 days post instillation. Similar to the acute profile, there was no significant increase in protein concentration (Figure 21) as compared to control (water), and no injury or loss of structural integrity of tissue as evidenced by histology (data is not shown). Additionally, cytospins revealed a monocytic cell population from the BAL. While AgNP treated mice cell counts were not significantly increased as compared to the controls at 7 and 21 days, there was an increase in total cell count when comparing acute and chronic time points (Figure 21). However, the most significant difference between acute and chronic profiles was demonstrated in the respiratory mechanics. At 7 and 21 days there was no significant difference between 20nm PVP-stabilized AgNP treated mice compared to control in either resistance or elastance; all previous tissue stiffness seen at 1 day post-instillation had resolved by 7 days (Figure 28 B). 110nm PVP treated mice displayed significantly lower elastance at 7 days, but was similar to control by 21 days (Figure 28 C). Overall, all changes in lung function resolved by 21 days post-instillation.

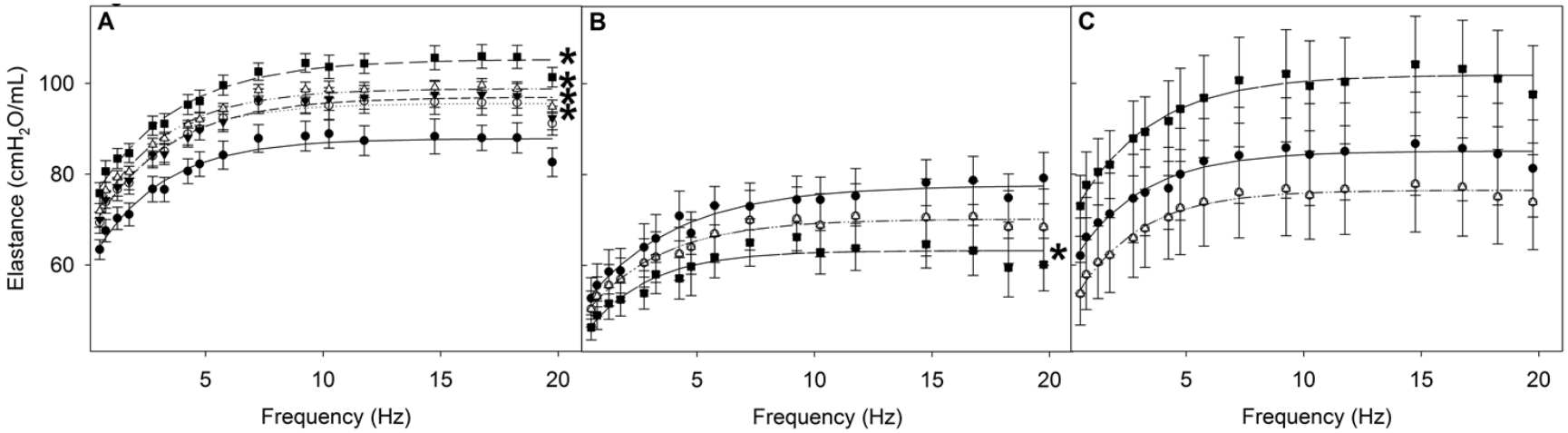

Figure 28. *Elastance (E_L) Spectra - All Time Points:* Analysis of impedance measurements at PEEP 3 **A)** 1 day, all AgNP treated mice demonstrated significantly increased elastance as compared to control (water) **B)** 7 day, acute tissue stiffness documented in 20nm PVP-stabilized AgNP treated mice resolves, 110nm group demonstrates significantly decreased elastance compared to control **C)** 21 day, AgNP mice are similar to control (*$p<0.05$ compared to the control) (●/solid line = Water/Model Fit; ○/dotted line = 20nm Citrate/Model Fit; ▼/short dashed line = 110nm citrate/Model Fit; ▽/dashed and dotted line = 20nm PVP/Model Fit; ■/long dashed line = 110nm PVP/Model Fit).

DISCUSSION

The goal of this study was to determine whether AgNPs, at a dose that does not elicit cellular toxicity, induces organ level toxicological effects. AgNPs are known to produce significant toxic effects when applied to cells *in vitro* [63, 64], although it is unknown whether the same toxic effects are elicited with an *in vivo* approach. The lung is a complex system, with potential for numerous interactions between AgNPs and its components including the lung lining fluid (alveolar cells, proteins, lipids, and surfactant). This system complexity and combination of potential interactions cannot be replicated in an *in vitro* system. Therefore, to truly examine the potential consequences of AgNP exposure it is necessary to measure organ level responses following *in vivo* exposure. This study demonstrates that, in the absence of cellular injury, there was an increase in work of breathing as a consequence of AgNP exposure. Additionally, we provide evidence of AgNP-lipid and protein interactions as well as changes in BAL composition that correlate with changes in respiratory effort, and may represent a mechanism for these responses.

From the respiratory mechanics data, one can observe that the elastance and resistance spectra do not change in parallel. This, in conjunction with PEEP failing to improve function, is best explained by increased tissue stiffness and heterogeneity, which leads to an increased work of breathing. One explanation for these observations is that particles are distributed unevenly within the lung; reaching some of the lower airways and reducing the airway opening. Both AgNP size and functionalization were significant factors in the extent of the increased work of breathing. There was a significant, acute increase in pulmonary elastance with AgNP administration that was not resolvable by PEEP and was most pronounced with 110nm PVP-stabilized particles. When examined at 7 and 21 days post-instillation, smaller PVP-stabilized particles demonstrated resolved

tissue stiffness by 7 days, while larger PVP-stabilized particles experienced dramatically decreased elastance at 7 days. All changes in work of breathing resolved by 21 days. Therefore in the absence of cellular injury, AgNPs acutely increase the work of breathing possibly via direct interactions with components of the lung lining fluid.

The lung lining fluid comprises a complex mixture of lipids and proteins that regulate both surface tension and innate immunity [12, 49]. The lung lining fluid is produced and recycled by the pulmonary epithelium while alveolar macrophages operate to absorb and degrade lining materials [65]. Loss of regulation of this intricate homeostatic system results from Type II epithelial cell injury or hyperplasia as well as macrophage activation. Both alveolar macrophages and Type II epithelial cells are key points of interaction for nanoparticles within the lung. Type II cells are responsible for the production of both the surface-active components of the lung lining, namely phospholipids and the proteins SP-B and C, and innate immune regulatory elements, such as SP-A and D [65]. Nanoparticle biophysics will affect interactions with components of the lung lining fluid and consequent interactions with alveolar macrophages as well as Type II epithelial cells.

Previous studies have shown that AgNPs interact with phospholipids [14] and given the high concentration of phospholipid in the lung lining these molecules represent likely targets for direct interaction. The association of AgNPs with lung lining phospholipids will alter surface active function and particle characteristics. Here, we demonstrate that size and functionalization alter particle aggregation within DPPC (the primary component of lung lining fluid) with larger PVP-stabilized particles being the most readily dispersed in DPPC. These *in vitro* data provide a potential explanation for the respiratory function effects. It

is reasonable to propose that by interacting with the phospholipids of the lung lining, AgNPs are capable of reducing surface active function. Thus as size and functionalization are key components of this interaction, it is reasonable to propose that these particle characteristics will determine *in vivo* outcome. Lipid-capped particles form strands in the presence of SP-B, increasing the surface tension of the lung lining fluid [16]. Although there was no change in SP-B content of the BAL, this does not preclude alterations in its aggregation status. One might predict a change in capillary surfactometry measurements with particle-lipid interactions. However, this technique is not sensitive to localized changes such as appear to occur with nanoparticle administration. The respiratory mechanics (a disproportionate increase in E_L v. R_L) indicate heterogeneity in the tissue response to particles [38]; indicating localized AgNP interaction with the lung lining. Such localized changes may go undetected when the whole BAL is analyzed.

A second significant component of the lung lining are the pulmonary collectins, including SP-D. These proteins are produced through an alternate secretory pathway to the surface active components and thus by measuring the relative content of SP-B and D one can gain insight into Type II cell function [49]. In this study, SP-B levels were unaltered by AgNP exposure, which correlates with a lack of change in the surfactometry assay. However, there was an acute, significant decrease in SP-D concentration in the BAL of mice treated with PVP-stabilized particles, indicating potentially reduced production or increased turnover of the collectins. As both SP-B and SP-D are derived from Type II cells and SP-B levels are unchanged, it seems most likely that this decrease results from increased SP-D turnover by alveolar macrophages, possibly as a result of binding to AgNP [19]. SP-D contains a carbohydrate recognition domain, which is predicted to bind such

molecular entities as the PVP functionalization group. Binding to the carbohydrate recognition domain of collectins results in aggregation and targeting towards macrophages and lung clearance [66]. The possibility of such a mechanism is supported by the work of Salvador-Morales, et al. (2007) who showed that nanoparticles have the potential to interact with the carbohydrate recognition domain of collectins *in vitro*, depending upon the NP biophysical properties. These acute changes in SP-D content may also have provided a trigger for the observed decrease in elastance at 7 days post-instillation by 110nm PVP treated mice. Resolution by 21 days implies restoration of surfactant composition. Importantly, there is no change in SP-D levels 7 and 21 days post-instillation of PVP stabilized particles.

One reason for the differences in pulmonary function observed between PVP and citrate-stabilized particles may be in their tendency to aggregate and dissolve. In this study, particles were suspended in water for delivery into the lung; and the spectrophotometry confirmed no silver particle aggregation when suspended in water over the course of many minutes, indicating we had achieved a homogeneous suspension during intratracheal delivery. However, once within the high ionic strength environment of the alveolar system, the citrate-stabilized particles are more likely to aggregate and precipitate. Although, our *in vitro* studies indicate that particle size is a more important factor in determining particle aggregation, especially within the context of a lipid environment (Figure 18). Furthermore, although citrate stabilized AgNPs do dissolve faster than PVP stabilized AgNPs, the loss of Ag^{+} within the time frame of this experiment was less than ~4% for any particle. Therefore it is unlikely that these properties explain the differential functional effects observed with PVP-stabilized AgNPs.

In the event that functionalization of particles results in inefficient clearance from the lung, there is the potential for AgNPs to prevent binding of SPs to receptors on the Type-II cells effecting SP production and recycling, leading to more chronic dysfunction. Further studies are required to investigate these possibilities. Importantly, the significant decrease in SP-D content following exposure to PVP-stabilized particles will compromise the effectiveness of the innate immune system if not cleared acutely, leaving the respiratory system more vulnerable to infection [67].

CONCLUSION

Low dose intratracheal exposure to AgNPs leads to significant changes in the lung lining components and in the mechanical function of the lung; without producing significant cellular injury. Such interactions were dependent upon size and AgNP-stabilization, but resolved over time. These changes may result from AgNP-lung lining fluid interactions including: phospholipid, SP-D, and alveolar macrophages. Further studies are required to better understand the mechanisms of action; however, from the increased work of breathing in the absence of injury and altered SP-D level, it becomes clear that the toxicology of such particles should be considered at the level of organ physiology in addition to direct cellular injury.

SPECIFIC AIM 3: EFFECTS OF SHAPE & INFLAMMATORY CONDITIONS

In this study, we aim to determine how nanoparticle shape and functionalization affects lung function and inflammation under physiological as well as inflammatory conditions. We propose that MWCNTs will elicit a persistent anti-inflammatory response to remove the nanomaterial over time, but will not alter work of breathing under physiological conditions; while when exposed to a baseline inflammatory environment, the MWCNTs will not be effectively cleared and disrupt the work of breathing. When a single high dose of carbon black nanospheres was delivered into the lung previously, there was an acute inflammatory response without a detectable change in lung function (Aim 1); in this study a similar dose of MWCNTs was administered (determined by surface area to volume ratio). Following exposure the lung function and inflammatory response was analyzed using the flexivent, bronchoalveolar lavage (BAL), and harvesting of the lungs for histology and molecular studies (1, 3, and 7 days post-single exposure). This provided an organ level assessment and allowed for correlation of respiratory mechanics (flexivent analysis) with changes in alveolar cells, proteins, lipids (BAL analysis) and lung tissue (histology) due to exposure from MWCNTs of varied functionalization.

RATIONALE

MWCNTs, like AgNPs, are increasingly being utilized in industrial processes and products, as well as for targeted drug delivery and diagnostics [68]. While occupational risks are of concern (production, processing, and disposal), a growing concern is exposure by break down of MWCNT materials purchased by consumers that may occur as a consequence of wear and tear over time and inappropriate storage/usage of materials [68]. There are conflicting reports regarding MWCNT carcinogenicity [29, 69, 70] which is likely due to differences in functionalization, experimental models, size, and dose. Prior

research has also demonstrated that SP-A and SP-D bind to functionalized carbon nanotubes [15, 21]. This may alter MWCNT clearance by alveolar macrophages, surfactant protein expression and Type II cell function, and ultimately lung function and inflammation. Additionally, as further nanomaterial studies are conducted, models of different pathologies must be explored. Aim 1 & 2 focused on healthy lungs and how the physiology is altered in response to particle exposure, while here in Aim 3 in addition to assessing physiological changes in the wild-type model, we assess the response to MWCNTs in an already low-level, chronic inflammatory environment.

METHODS

MULTI-WALLED CARBON NANOTUBES

Both types of MWCNTs (-COOH & acid-etched) were manufactured by CheapTubes, Inc. (Brattleboro, VT). The acid etching and functionalization of the MWCNTs was performed by Professor Som Mitra of the New Jersey Institute of Technology. The morphology and size of the particles was confirmed by the Nanotechnology Characterization Laboratory (NCL), National Cancer Institute at Frederick, Maryland using ICP-MS, SEM, TEM, and elemental analysis of carbon, hydrogen, nitrogen, oxygen, and sulfur. The MWCNTs were subsequently provided to our laboratory by the Consortium of NIEHS Centers for Nanotechnology Health Implications Research (NCNHIR). The two MWCNTs examined in this study are particle numbers: NIEHS-13-2 (-COOH functionalized: C-MWCNT) and NIEHS-13-3 (acid-etched: A-MWCNT). Both MWCNTs are approximately 30-50nm in outer diameter and 0.5-2μm in length.

Murine Model and Particle Instillation

Nine-week-old C57-BL6 Jackson wild-type male mice and SP-D$^{-/-}$ mice (male and female) were intratracheally instilled with MWCNTs following anesthesia using a ketamine/xylazine combination. SP-D$^{-/-}$ mice were made SP-D deficient and backcrossed onto the C57-BL6 background as described previously in the literature [34, 35]. Particles were first prepared in a stock solution: 1.25mg MWCNT/mL/g body weight, suspended into a Hank's balanced salt solution (HBSS) with 0.25% Triton and a native surfactant (0.13ng protein/µl). Particles were mixed using water bath sonication. Using this stock solution, 1.5µg MWCNT/g body weight were delivered by intratracheal instillation (a final volume of 50µl). Mice were left for 1, 3, or 7 days before being anesthetized and mechanical function assessed (see below). Following lung function assessment, tissues were harvested and analyzed as described below.

This protocol was approved by the Rutgers University Institutional Animal Care and Use Committee (IACUC) (Protocol Number: 06-028). The study was conducted in accordance with the recommendations in the Guide for the Care and Use of Laboratory Animals of the National Institutes of Health. Intratracheal instillations and mechanical ventilation were conducted under ketamine/xylazine anesthesia, and all efforts were made to minimize suffering. Animals were sacrificed using a lethal dose of ketmine/xylazine and exsanguination.

Bronchoalveolar Lavage

The whole lung of each mouse was lavaged (prior to inflation fixing with paraformaldehyde) with 10mM HEPES buffered saline in 1mL increments four times. Cells from the bronchoalveolar lavage fluid (BAL) were then centrifuged (300xg, 10

minutes). The supernatant was collected for further protein and lipid analysis, while the cell pellet was re-suspended in 1mL buffered saline for cytology and RT-PCR [36, 40, 49].

HISTOLOGY

The left lung was harvested and inflation fixed using a 3% paraformaldehyde in 2% sucrose solution. Lungs were then embedded in paraffin, sectioned and stained with hematoxylin and eosin (H&E). Lung images were captured using the Olympus VS120-SL Virtual Slide System [40, 49].

CELL COUNTS AND CYTOLOGY

Cell number was assessed using a Beckman Coulter™ Multisizer™ 3 Coulter Counter®. Approximately 30,000 cells were then centrifuged onto a glass slide at 800xg for three minutes, air dried, and then stained with Diff-Quik buffered modified Wright-Giemsa stain. Cell differentials were performed manually using a light microscope (1-way ANOVA, t-test) [36, 40, 49].

REAL-TIME POLYMERASE CHAIN REACTIONS

RNA was prepared from BAL cells using a QIAshredderTM kit and converted to cDNA. The cell samples for each treatment group were pooled into one larger sample for analysis. Thermocycling was used to analyze mRNA expression of IL1B, IL6, CCL2, IL4, IL13, IL10, and CXCL1. The ABI 7900HT Fast Real-Time PCR System by Applied Biosystems (Waltham, Massachusetts, USA) was used and primers were used from TAQman system. Fold expression was calculated by the ΔΔCT method normalizing to the HBSS (control) treatment group and using GAPDH as the control gene [41] .

PROTEIN AND PHOSPHOLIPID ASSAY

Whole BAL protein concentration was determined using a BCA Assay kit by Lamda Biotech, Inc (St. Louis, MO). To estimate phospholipid content whole BAL was

fractionated into small and large aggregate portions by centrifugation at 17,000xg for one hour at 4^0C. The supernatant is the protein-rich small aggregate fraction, while the pellet can be re-suspended in a small volume of saline (35µl) and was the lipid-rich large aggregate fraction. Inorganic phosphate from the lipid-rich fractions was measured as an estimate of the phospholipid content (1-way ANOVA, Holm-Sidak method) [49, 51].

IMMUNOBLOTTING

To determine surfactant protein content, reducing NuPAGE was performed using individual BAL samples. Gels were transferred to BioRad Immun-blot® PDVF membranes, incubated with SP-D or SP-B antibody (M.F. Beers, University of Pennsylvania), goatαrabbit linked to horseradish peroxidase, and imaged using Amersham™ ECL™ Prime Western Blotting Detection Reagent. Densitometry was performed to quantify the chemiluminescent signal (1-way ANOVA, Holm-Sidak method). Whole BAL was used for SP-D analysis; and sample load was normalized to volume. Large aggregate BAL (LA BAL) was used for SP-B analysis and sample load was normalized to phospholipid content as determined by the phospholipid assay [49].

MECHANICAL VENTILATION AND RESPIRATORY MODEL

Mice were anesthetized and ventilated using the flexiVent (SCIREQ, Montreal, Canada) at increasing positive end expiratory pressures (PEEPs) (0, 1, 3, and 6 cmH2O) to assay for resolution of lung function [62]. Mechanical ventilation with forced oscillation maneuvers was used to measure impedance broadband signal (0.5-20Hz) respiratory impedance [Z(f)] [39]. The flow [V(t)] is a known value input into the system while pressure [P(t)] output is unknown. As mechanical function varies with frequency of oscillation, a Fourier Transform was performed so that impedance could be expressed as a function of frequency, $Z(f) = P(f)/ V(f)$. Output impedance spectra were used to generate

resistance (R_L) and elastance (E_L) spectra across the frequency range, and fit to a model of heterogeneous lung function using the following equations [37, 40, 41]:

$$R_L = (a + bf)/(c + f) \text{ and } E_L = E0 + \Delta E\ (1\text{-}e^{-\beta f})$$

Statistical Analysis

All data (excluding respiratory mechanics) were analyzed using 1-way ANOVA and the Holm-Sidak Method, a p value of < 0.05 was considered statistically significant. In the case of respiratory modeling, model fits were estimated for each treatment group by fitting a non-linear regression curve to the spectra of all mice in a treatment group equally at each PEEP. Spectra were analyzed for significant differences using the null hypothesis that the data can be characterized by one three-parameter relationship or alternatively that the data are distinct enough to be characterized by two three-parameter relationships.

Results

1 Day Post-Instillation

Acutely, histology demonstrated clear baseline differences between genotypes: wild-type (WT) and SP-$D^{-/-}$ (KO). At baseline KO mice (Figure 29 E) displayed macrophages of increased size and of foamy cytoplasmic appearance in comparison with WT mice at baseline (Figure 29 A). Overall, there was no injury or destruction of tissue integrity in any treatment group or genotype. Macrophage morphological differences between genotypes were again evident in the cytospins: KO mice displayed enlarged macrophages with foamy cytoplasm (Figure 30). KO mice also displayed increased total BAL cell count as compared to WT mice (Figure 30). Additionally, C-MWCNT treated mice displayed neutrophilia in both genotypes (Figure 30). Analysis of BAL cells by PCR revealed a pro-inflammatory response in both genotypes, which was MWCNT

functionalization-specific in the WT mice (Figure 31). C-MWCNT treated WT mice displayed increased IL1B (16.9 fold) as compared to the HBSS control mice, a pro-inflammatory cytokine produced by activated macrophages [71]; anti-inflammatory cytokines, IL13 and IL10 were also elevated (4.2 and 5.4 fold) as compared to the control (Figure 31). IL13 is involved in the down-regulation of macrophage activation through inhibition of pro-inflammatory cytokines and chemokines, and IL10 is involved in blocking the NF-κB activity [72, 73]. Both C-MWCNT and A-MWCNT treated KO mice displayed increased IL1B (16.4 and 8.3 fold) as compared to the control mice, and unlike the WT mice CXCL1 was also elevated (6.0 and 3.2 fold) in MWCNT treated mice as compared to the control mice (Figure 31). CXCL1is a neutrophil chemoattractant produced by both macrophages and epithelial cells [74]. While there were no differences in BAL protein concentration between genotypes or treatments, KO mice displayed increased levels of organic phosphate at baseline as compared to WT mice (Table 2). C-MWCNT and A-MWCNT treated WT mice also demonstrated decreased organic phosphate levels as compared to the sham control mice (Table 2). Immunoblotting revealed significant changes in SP-B content in both genotypes for C-MWCNT treated mice as compared to sham control mice; while in the WT mice SP-B increased, SP-B decreased in KO mice (Figure 32). Lastly, respiratory mechanics demonstrated no change in lung function in either genotype as a result of MWCNT treatment.

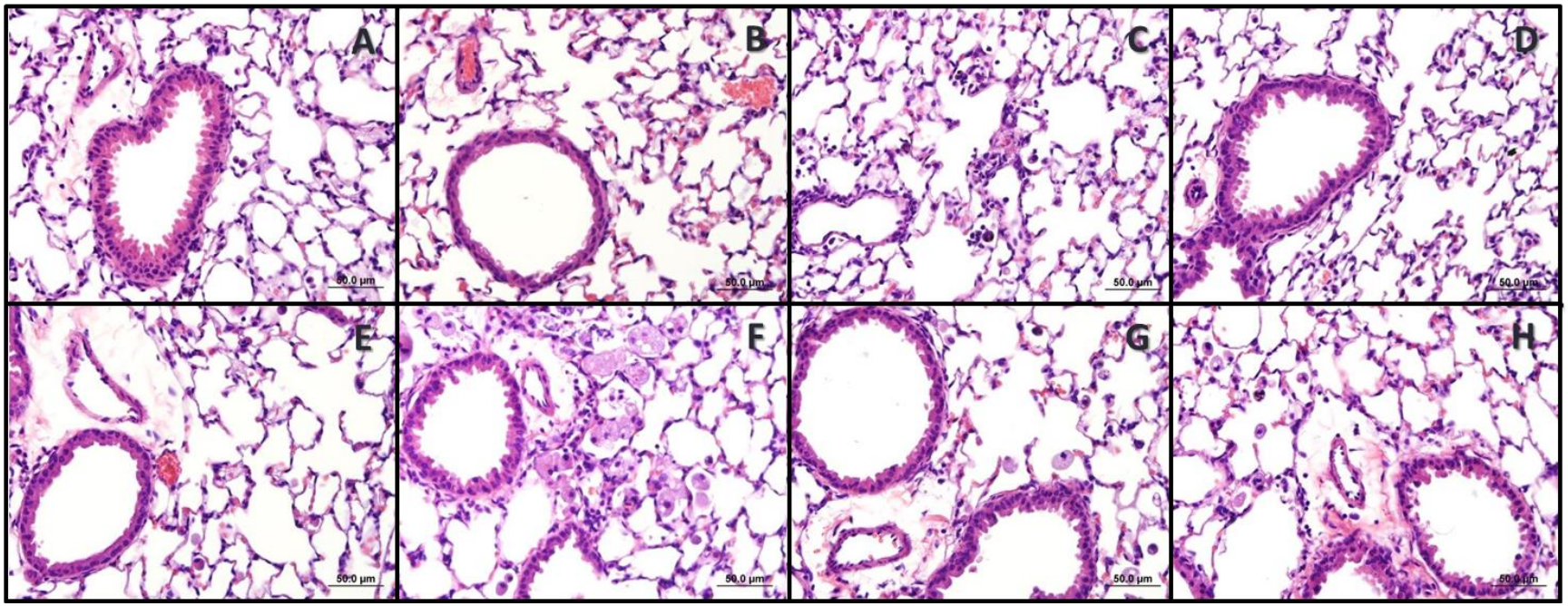

Figure 29. *Histology (H&E) 1 day post-instillation:* Post-mechanical ventilation, the left lung of the treated mice were inflation fixed, paraffin embedded, sectioned and stained with hematoxylin and eosin; **(A-D)** Wild-Type Mice **(E-H)** SP-$D^{-/-}$ (KO) Mice. **A)** WT Sham **B)** WT HBSS **C)** WT C-MWCNT **D)** WT A-MWCNT **E)** KO Sham **F)** KO HBSS **G)** KO C-MWCNT **H)** KO A-MWCNT. There is clear low-level baseline inflammation evidenced by size of macrophages in the sham KO mice. Overall lung structure is intact, and no signs of tissue injury. What is evident is the large size and foamy morphology of the macrophages in the KO compared with WT model in every treatment.

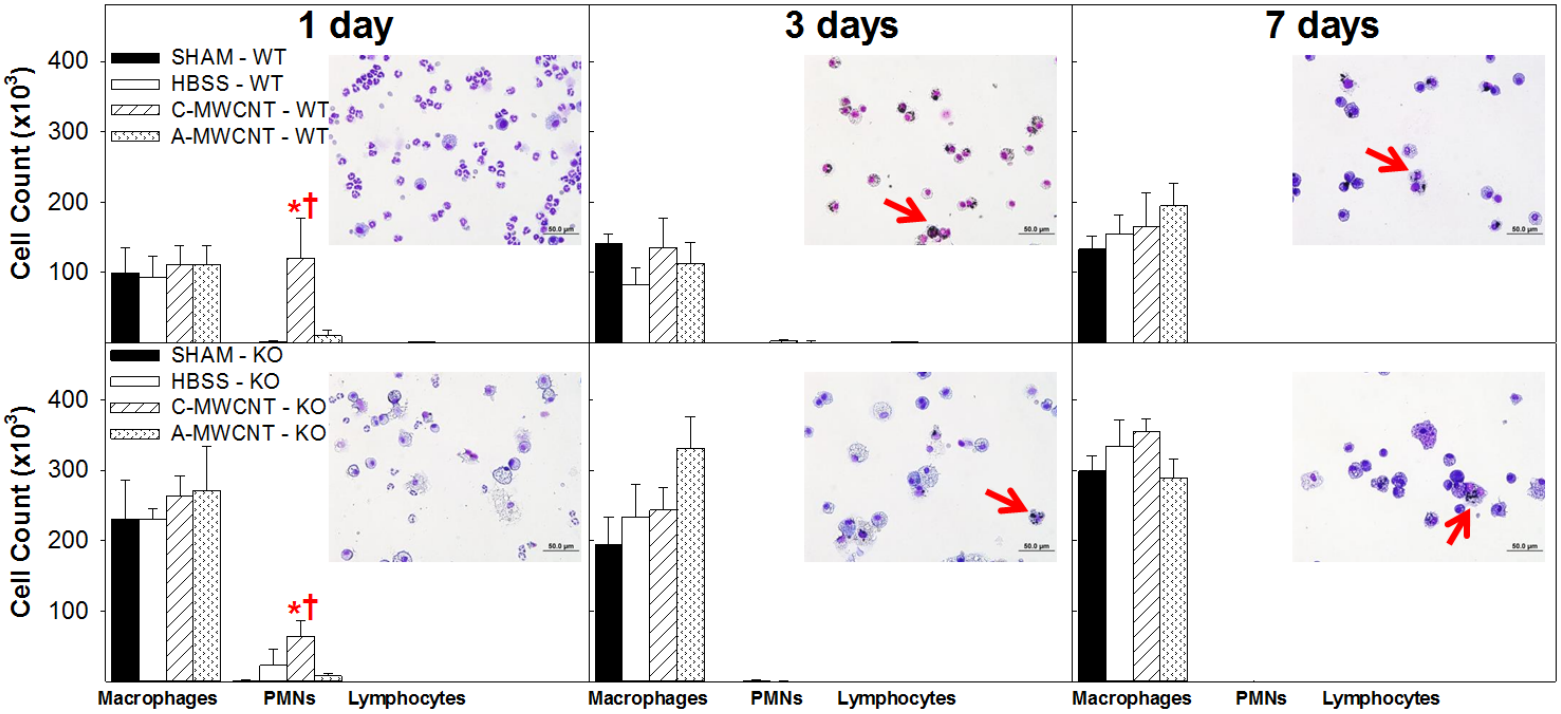

Figure 30. *Cell Count & Cytology using BAL:* Cell counts (mean ± standard error ($x10^5$)) were normalized to 1mL BAL and ~30 000 cells were used for cytology. C-MWCNT displayed neutrophilia acutely at 1 day, which resolved by 3 days post-instillation. MWCNTs were engulfed in macrophages acutely and persisted up to 7 days in BAL in both genotypes (as indicated by red arrows). Overall, macrophage morphology was different between genotypes at all time points and treatments (KO mice large, foamy macrophages). The dominant cell type was macrophages in all treatments, lymphocytes <1% of cell population (n=4-6 mice for all treatment groups/time points; *$p<0.05$ compared to sham †$p<0.05$ compared to HBSS and A-MWCNT).

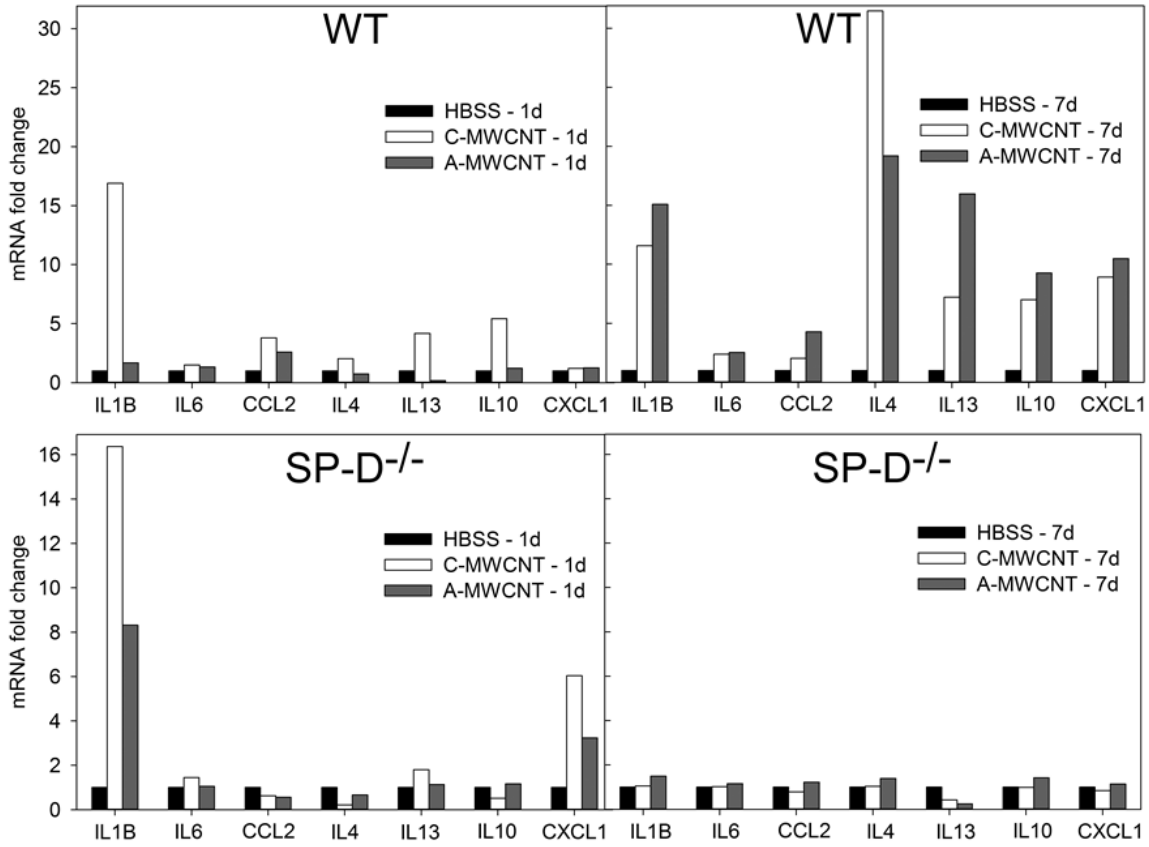

Figure 31. *mRNA expression by PCR*: 1 day post-instillation, IL1B is elevated as compared to the HBSS control mice in both genotypes, however in the KO model it is significantly elevated in both MWCNT treatment groups, while in the WT model only the C-MWCNT ILB levels are elevated. The KO model demonstrated elevated CXCL1 in both MWCNT treatment groups. While the acute inflammatory response is specific to C-MWCNT in the WT model with CCL2, IL13, and IL10 also at elevated levels of expression. After 7 days the inflammatory response as compared to the control resolved in the KO model, whereas in the WT model the inflammatory response persisted and evolved. ILB remained elevated, and IL4, IL13, IL10, and CXCL1 are increased in expression as compared to the control; however, this response was demonstrated in both MWCNT treatment groups (n=3 mice for all treatment groups/time points).

3 Days Post-Instillation

Again, there was injury to the lung tissue as a result of MWCNT treatment in either genotype. Total BAL cell count remained elevated at baseline in KO mice as compared to WT mice, but in both genotypes neutrophilia had resolved; additionally, Figure 30 shows a continued presence of MWCNTs being phagocytized by macrophages (as indicated by arrows, occurs in both MWCNT treatments). BAL protein concentrations were not significantly different from sham control mice in the KO model, however sham WT mice displayed increased BAL protein concentration as compared to particle treated WT mice (Table 2). While organic phosphate levels for KO mice remained elevated at baseline compared to WT mice, there were no treatment differences between groups in either genotype (Table 2). SP-B content was not significantly different between treatment groups in either genotype, however WT MWCNT treated mice displayed increased SP-D content as compared to sham WT control mice (Figure 32). At 3 days, there was still no change in lung function for MWCNT treated WT mice as compared to controls (sham and HBSS) (Figure 33). While in the KO model both MWCNT treated groups displayed decreased resistance and elastance as compared to controls that did not completely resolve with increasing PEEP (Figure 33).

		Protein Concentration (µg/µl)		Organic Phosphate (µg/µl)	
		WT	KO	WT	KO
1 DAY	SHAM	0.17 ± 0.025	0.18 ± 0.046	1.08 ± 0.183	6.87 ± 3.345
	HBSS	0.22 ± 0.032	0.16 ± 0.014	1.26 ± 0.301	6.28 ± 0.563
	C-MWCNT	0.22 ± 0.032	0.17 ± 0.020	0.64 ± 0.096*	6.92 ± 0.504
	A-MWCNT	0.24 ± 0.042	0.31 ± 0.15	0.72 ± 0.090*	5.85 ± 2.428
3 DAY	SHAM	0.43 ± 0.011*	0.22 ± 0.012	0.91 ± 0.202	5.34 ± 0.076
	HBSS	0.27 ± 0.069	0.19 ± 0.024	0.89 ± 0.189	4.30 ± 0.515
	C-MWCNT	0.29 ± 0.045	0.23 ± 0.032	0.94 ± 0.231	5.40 ± 1.025
	A-MWCNT	0.28 ± 0.060	0.19 ± 0.018	1.05 ± 0.232	6.60 ± 1.965
7 DAY	SHAM	0.15 ± 0.046	0.19 ± 0.030	1.23 ± 0.077	5.78 ± 0.893
	HBSS	0.10 ± 0.014	0.26 ± 0.059	1.50 ± 0.117	5.50 ± 0.255
	C-MWCNT	0.10 ± 0.012	0.19 ± 0.018	1.20 ± 0.092	5.30 ± 0.270
	A-MWCNT	0.11 ± 0.019	0.17 ± 0.023	1.30 ± 0.102	4.60 ± 1.068

Table 2. *Protein Concentration & Phospholipid Content in BAL*: There was no significant difference in protein concentration at any time point between any treatment groups (except the Sham 3 day mice did experienced elevated protein content in the BAL). Organic phosphate levels were higher in KO v. WT mice, but the only significant difference between groups occurred at 1 day post-instillation in the WT model. Both MWCNT groups contained significantly less organic phosphate than the controls (n=4-6 mice for all treatment groups/time points; *$p<0.05$ compared to control).

7 Days Post-Instillation

Though cytology revealed continued presence of MWCNTs at 7 days post-instillation (indicated by arrows Figure 30), tissue integrity remained intact in both genotypes regardless of treatment with MWCNTs. Total BAL cell count was still elevated at baseline in KO mice compared to WT mice, but there was no difference between treatment groups (Figure 30). BAL cell PCR analysis revealed resolution of pro-inflammatory cytokine expression in MWCNT treated KO mice as compared to HBSS control KO mice at 7 days post-instillation (Figure 31). Contrastingly, IL1B remained elevated in C-MWCNT treated WT mice (11.6 fold) compared to WT control mice (Figure 31). In addition to increased cytokine expression in the C-MWCNT treated mice, A-MWCNT mice also experienced increased pro- and anti-inflammatory cytokine expression (Figure 31). IL1B, IL4, IL13, IL10, and CXCL1 were all elevated in both MWCNT treatment groups as compared to control mice (Figure 31). There was no difference in protein concentration between treatment groups in either genotype, but KO mice still demonstrated elevated baseline levels of organic phosphate as compared to WT mice (Table 2). There were no significant differences between treatments in surfactant protein content evidenced by immunoblotting in either genotype (Figure 32). Lastly, respiratory mechanics revealed a persisting decrease in both resistance and elastance as a result of MWCNT treatment in KO mice that did not completely resolve with increasing PEEP, while WT mice demonstrated no change in lung function with MWCNT treatment (Figure 33).

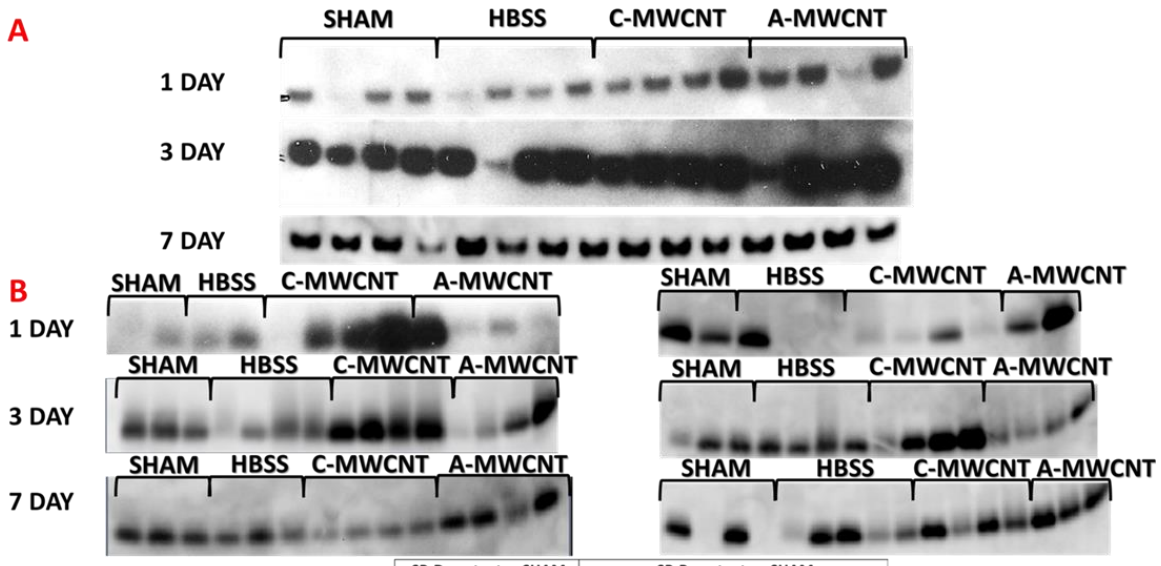

		SP-D content v. SHAM	SP-B content v. SHAM	
		WT	WT	KO
1 DAY	SHAM	1.0 ± 0.036	1.0 ± 0.045	1.0 ± 0.073
	HBSS	1.0 ± 0.038	1.1 ± 0.029	0.8 ± 0.154
	C-MWCNT	1.1 ± 0.067	1.3 ± 0.183*	0.5 ± 0.056*
	A-MWCNT	1.1 ± 0.104	1.1 ± 0.148	1.0 ± 0.201
3 DAY	SHAM	1.0 ± 0.021	1.0 ± 0.067	1.0 ± 0.139
	HBSS	1.1 ± 0.035	0.9 ± 0.142	1.2 ± 0.054
	C-MWCNT	1.2 ± 0.010*	1.6 ± 0.053	1.5 ± 0.216
	A-MWCNT	1.2 ± 0.015*	1.0 ± 0.226	1.1 ± 0.030
7 DAY	SHAM	1.0 ± 0.053	1.0 ± 0.028	1.0 ± 0.252
	HBSS	1.1 ± 0.044	0.9 ± 0.064	1.2 ± 0.177
	C-MWCNT	1.1 ± 0.028	0.8 ± 0.069	1.4 ± 0.103
	A-MWCNT	1.1 ± 0.043	1.2 ± 0.048	1.7 ± 0.041

Figure 32. *Surfactant Expression via Immunoblotting:* **A)** SP-D Immunoblot **B)** SP-B Immunoblot; Acutely, C-MWCNT treated WT & KO mice display a change in SP-B content; at 3 days both MWCNT treated WT mice experience an increases SP-D; and all alterations resolve by 7 days (*$p<0.05$ compared to the control; n=4-6 mice for all treatment groups).

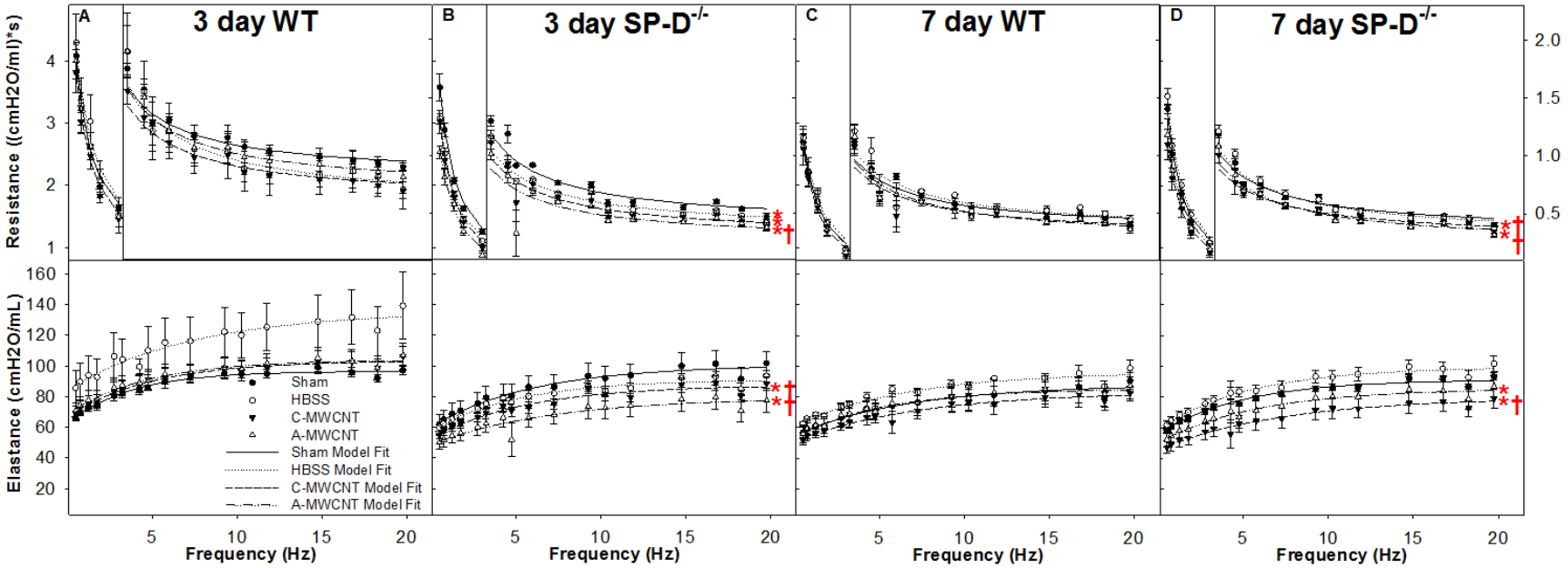

Figure 33. *Resistance (R_L) & Elastance (E_L) Spectra Using Forced Oscillation Technique:* Analysis of impedance measurements at PEEP 3 A) there are no significant differences between groups in the WT at 3 days B) in the KO model, MWCNT mice experience decreased resistance and elastance C) there are no significant differences between groups in the WT at 7 days D) in the KO model, the decrease in both elastance and resistance as a result of MWCNT treatment persists (*$p<0.05$ compared to the control, †$p<0.5$ compared to HBSS) (●/solid line = Sham/Model Fit; ○/dotted line = HBSS/Model Fit;▼/short dashed line = C-MWCNT/Model Fit; ▽/dashed and dotted line = A-MWCNT/Model Fit).

DISCUSSION

The goal of this study was to determine whether MWCNTs (C-MWCNT & A-MWCNT) induce organ level toxicological effects under physiological and inflammatory conditions. In our previous studies, carbon black nanospheres produced an acute inflammatory response that resolved by 7 days post-instillation, but they did not alter surfactant content or lung function (see Aim 1). Our studies examining AgNPs demonstrated nanosphere functionalization and increasing size leads to alteration of SP-D content and increased work of breathing that does not resolve until 21 days post-instillation (see Aim 2). Additionally, multiple *in vitro* studies provide evidence that MWCNTs interact with multiple components of the lung lining, including lipids and surfactant proteins [1, 15, 16, 21] and these interactions facilitate increased uptake of MWCNTs into macrophages [19, 20]. Two major points remain unclear in the current pool of literature: 1) organ level responses to MWCNTs following *in vivo* exposure and 2) lung function following MWCNT exposure in an inflamed respiratory system. This current study demonstrates that organ level response is dependent not only on nanoparticle shape and functionalization but on the inflammatory state of the respiratory system upon exposure.

Unlike carbon black nanospheres, which were cleared from the lung by 7 days post-instillation (as evidenced by cytospins, Figure 2), MWCNTs remained in the lung up to 7 days post-instillation (independent of functionalization & genotype, Figure 30). This is likely due to the higher aspect ratio of the MWCNTs and the similarity to more fibrous materials [68]. Prolonged exposure in the respiratory system due to ineffective clearance provides opportunity for continued interaction with components of the lung lining. These prolonged interactions lead to changes in the inflammatory response, which is demonstrated in our study when comparing carbon black nanospheres to MWCNTs. While

exposure to carbon black NPs led to a minor increase in IL1B acutely (3 fold increase over control) and inflammatory cytokine expression resolved by 7 days post-instillation (Figure 4), exposure to MWCNTs in WT mice produced a significant increase in IL1B (16.9 fold over control), IL13 (4.2 fold over control) and IL10 (5.4 fold over control) and both anti- and pro-inflammatory cytokines increased in expression at 7 days post-instillation (Figure 31).

In addition to shape as a factor in inflammatory response, particle functionalization also plays a large role as evidenced by this study. C-MWCNT treatment elicited acute neutrophilia in both genotypes, acute pro-inflammatory cytokine expression in WT mice, and acute alteration of SP-B content in both genotypes. These functionalization-dependent effects are all demonstrated acutely. The most likely reason for these effects is enhanced integration into the hypophase of the lung lining. As cited in other works, the more negatively charged the surface of a nanomaterial the more likely it is to interact with surfactant proteins and other surfactant materials [21]. Integration into the hypophase allows for interactions with alveolar cells (macrophages and epithelial cells) which then release chemoattractants for neutrophils. Additional interactions may occur with SP-D which can cause particle aggregation and phagocytosis by macrophages leading to the release of pro-inflammatory cytokines (IL1B) as well as anti-inflammatory cytokines (IL13 and IL10). Lipid-C-MWCNT interactions can also occur, leading to particles becoming coated by lipid; and once the lipid-particle ultrastructure is phagocytized, a decrease in not only in lipid content can occur, but also SP-B with associates with lipids to maintain surface tension.

Importantly, this study also demonstrates that the inflammatory state is a driving factor in organ level respiratory responses to MWCNT exposure. SP-$D^{-/-}$ mice are a model of low-level inflammation, as documented in this study by macrophage morphology, increased BAL cell counts, and increased concentration of BAL organic phosphate (in comparison to WT mice). While acute release of pro-inflammatory cytokines is functionalization-specific in WT mice, both types of MWCNTs elicited increased expression of ILB and CXCL1 as compared to the control in the KO model. Additionally, increased expression of anti-inflammatory cytokines was not demonstrated in response to the MWCNTs acutely as was the case for the WT model. By 7 days post-instillation, there was no increase in anti- or pro-inflammatory cytokines in response to MWCNTs in the KO model.

Differences in WT versus KO mice were evident in acute organic phosphate concentrations and SP-B content as well. In WT mice exposed to both types of MWCNTs, there was a significant decrease in BAL organic phosphate concentration acutely that resolved by 3 days. This indicates an acute decrease in phospholipid content as a result of MWCNT instillation. As previously cited, MWCNTs can become coated by lipids of the lung lining which enhances uptake into macrophages. If Type II cell function is normal, more lipids will be synthesized and released, allowing for resolution of the initial lipid loss as seen in this study. Though organic phosphate concentrations are not significantly different for MWCNT treated mice in the KO model, this does not prove that MWCNTs are not being coated by lipid and that there is no loss of lipid by phagocytosis of lipid-particle ultrastructure. At baseline, the KO model Type II cells are over-producing and

secreting phospholipids, therefore it may be difficult to determine any changes in phospholipid levels without significant injury or larger instilled doses of MWCNTs.

While both WT and KO C-MWCNT treated mice displayed an alteration in SP-B content, WT mice experienced an increase rather than a decrease in SP-B that is documented in the KO mice. The key to this differential response is likely Type II cell function. As previously noted, WT MWCNT treated mice experienced loss of organic phosphate. SP-B is associated with phospholipids to maintain surface tension of the lung lining fluid; and loss of phospholipid may result in loss of SP-B. An acute increase in SP-B may result as Type II cells work to produce and secrete additional SP-B and achieve surfactant homeostasis. In KO mice, with the absence of SP-D, surfactant homeostasis is compromised, and Type II cell response to SP-B alterations may be affected resulting in acute low levels of SP-B as MWCNTs aggregate with lung lining components and are phagocytized.

One of the most prominent differences between WT and KO mice response to MWCNT exposure in this study was demonstrated in respiratory mechanics. Similar to WT mice exposed to carbon black nanospheres, WT mice exposed to MWCNTs experienced no change in lung function at 1, 3 or 7 days post-instillation. Acutely, there was no change in lung function in the KO mice treated with MWCNTs as well. However, at 3 days post-instillation MWCNT treated KO mice displayed significant decreases in both resistance and elastance that did not resolve by 7 days. The most likely reason for this decrease in work of breathing is due to inefficient MWCNT clearance. SP-$D^{-/-}$ mice at baseline have increased number and size of alveolar macrophages, increased phospholipid content, and excess surfactant protein content (SP-A, B & C). With the introduction of MWCNTs, the

lower airways become “flooded” with material making it difficult to properly inflate the lower airways and achieve normal lung function. While 7 day data from cytospins demonstrate presence of MWCNTs persisting in the WT mice as well, we propose that there is inefficient clearance of MWCNTs in the KO mice due to the lack of SP-D and the resultant inhibition of a robust inflammatory response. Without SP-D to complex with MWCNTs, MWCNTs are not trafficked as efficiently into macrophages for clearance from the alveolar system; and without SP-D to bind to macrophage surface receptors, anti- and pro-inflammatory signaling is affected (as demonstrated by mRNA expression at 7 days in PCR analysis, Figure 18). Further studies are necessary to determine how long MWCNTs remain in the lung tissue of both genotypes, as well as any resulting chronic inflammation and injury due to MWCNT exposure.

CONCLUSION

Intratracheal exposure to MWCNTs leads to significant organ level toxicological effects including: inflammation, surfactant alteration, and changes in lung function. The magnitude and specificity of this response is highly dependent upon the shape and functionalization of the particle delivered and the inflammatory state of the lung it is exposed. SP-D is essential for efficient MWCNT clearance from the lung, however further study is needed to characterize the molecular mechanism of action.

SYNOPSIS & FUTURE DIRECTIONS

The data provided within this thesis validates the primary driving factors in organ level respiratory response to nanoparticle exposure are: core composition (metal v. carbon), zeta potential, shape, and host inflammatory state. These factors affect injury and inflammation, surfactant composition and lung function. Due to the nanoscale of these particles they reach the lower airways of the lung, making the lung lining a primary target and point of interaction. The three major potential NP-lung lining points of interaction include: lung lining lipids, airway cells, and collectins (SP-A/D). Considering the data in Specific Aims 1-3 together, zeta potential will determine the specificity and magnitude of the NP-lung lining interactions and consequent effects.

Overall, with each type of NP examined there was no evidence of tissue injury or loss of barrier function. Though NP exposure was not injurious, there were distinct inflammatory responses to the different NPs delivered into the lung. The inflammatory responses were acute or delayed depending upon the nature of the particle (carbon v. silver). Additionally, inflammatory response were affected by genotype (wild-type v. SP-$D^{-/-}$). Similarly, acute and delayed changes in surfactant protein content were core NP composition, functionalization and shape dependent, while alterations of lipid content was NP shape dependent (sphere v. tube). One of the most important observations regarding lung function measurements and modeling was that under physiological conditions (WT mice) neither carbon black nanospheres (low or high dose) or MWCNTs (A and C; at dose normalized to high dose spheres by surface area to volume ratio) elicited a change in lung function at any time point (1, 3 or 7 days). Comparatively, all types of AgNP sphere treatments elicited changes in lung function. When examining the model parameters

significant changes most often occurred in a/c—indicating changes in the lower airway function.

Zeta potential describes particle stability: the higher the zeta potential the more stable a nanoparticle is within a colloidal dispersion, and conversely the lower the zeta potential the less stable a nanoparticle becomes in colloidal dispersion [1, 57, 75]. Zeta potential is determined by particle shape, size, and hydrophobicity [57]. In general, larger, more hydrophilic nanoparticles have increased zeta potential, while smaller, more hydrophobic nanoparticles have decreased zeta potential. In a biological system, zeta potential of a nanoparticle will become altered depending upon interactions with the surrounding environment [57]. It has already been demonstrated within the literature that nanoparticles which bind with surfactant components (proteins and lipids) increase the ultrastructure zeta potential and consequently increase cell surface interactions [76]. The lung lining is a primary target and point of interaction for inhaled nanoparticles that reach the lower airways of the lung [53, 77]. The factors effecting NP zeta potential (shape, size and hydrophobicity) also affect the initial interactions at the air-liquid interface. More hydrophilic NPs, like silver nanospheres more easily integrate intro the lung lining hypophase versus non-metal, more hydrophobic NPs (i.e, carbon black nanospheres). Once incorporated into the hypophase, NPs with greater zeta potential more easily bind surfactant components—for example, 110nm PVP binds more efficiently with DPPC as demonstrated in Specific Aim 2. Therefore, these types of NPs and surfactant component interactions will lead to changes in surface active function (acute changes in lung function). Acute changes in lung function will then trigger cell signaling to mount an inflammatory response that decreases the work of breathing—may include cytokine expression to recruit

cells for particle clearance, as well as increases in Type II cell production and secretion of surfactant materials to decrease tissue stiffness effects.

NPs of lower zeta potential are less likely to bind with surfactant material and integrate into the hypophase of the lung lining. Their inability to efficiently repel adjacent NPs will lead to aggregation of NPs, and these larger structures will trigger an acute inflammatory response. Without disruption to the surface active portion of the lung lining, and so long as the NP aggregates are cleared efficiently, lung function will not be altered. Effective clearance of particles from the lung lining determines the inflammatory response and long term effects of lung function. In order for NPs to be trafficked and cleared they must interact with cell surfaces (epithelial cells and macrophages). As stated previously, these cell surface interactions are driven by the zeta potential of the NP. What is still poorly understood is how much of the change in particle zeta potential is due to the lipid versus the protein binding to the NP; however it is clear that zeta potential—or more specifically the factors that determine zeta potential—drive particle uptake by cells. These cellular interactions dictate inflammatory response through release of cytokines for chemoattractant signals as well lung function through Type II epithelial cell signaling for surfactant production, secretion and recycling.

The data provided within this manuscript provides evidence for the need to pursue organ level toxicological studies of nanomaterial exposures. Understanding molecular mechanisms and leveraging *in vitro* studies to examine focused questions concerning particle-protein, lipid, and cellular interactions is highly important; however, the field has become saturated with those exact types of studies. By shifting focus toward a more complex approach that relates molecular and physiological endpoints, more translational

work can be done that addresses both environmental and occupational exposure risks to the public concerning nanomaterials. It is clear that particle functionalization, shape, and size all play a role in the response mounted by the lung upon instillation of nanomaterials, but many avenues of exploration remain in the pursuit of characterizing the health risks, as well as benefits of nanomaterials.

INHALATION STUDIES

Aerosols containing nanomaterials are commonly used household products today; this presents the need for toxicological studies that consider both consumer and occupational exposures [78]. Silver nanoparticles are favored in aerosols due to their antimicrobial properties [78]. Future studies need to build upon these *in vivo* studies that have used intratracheal instillation by developing appropriate inhalation exposure models. Intratracheal instillation is limiting because it requires the suspension of NPs into solution which alters the particle biophysics and potentially the interactions within the lung lining. Inhalation study would allow for examination of NPs suspended in a gaseous phase versus a liquid phase. Our cross-laboratory collaborations have facilitated data sharing to develop a rat inhalation experimental design with silver nanopsheres as well as carbon nanotubes, and that work is currently underway. Considerations in this collaborative design include: analysis of impedance data, surfactant analysis, immunohistochemistry and silver staining to correlate inflammation with particle deposition in the lung.

Oftentimes dosing schemes in inhalation studies focus on high doses and occupational exposure models, while our data suggests that low dose exposures need to be considered as well. This becomes difficult to examine in rodent inhalation studies due to the convoluted nasal turbinates. A large portion of inhaled particles will first become

trapped in the nasal turbinates, rather than reaching the lungs. This must be taken into account in all future inhalation studies and modeling of rodent data.

A limitation of intratracheal instillation studies is a one-time exposure (multiple instillations risks injurious response due to delivery protocol). Repeat, low-dose inhalation exposures would more effectively mimic environmental exposure by consumers of nanomaterial-containing products. Repeat exposure to NPs would likely lead to bioaccumulation of particles, and the ability of the lung to mount an effective particle clearance response would determine chronic respiratory effects. It has been demonstrated in this thesis that even a single dose of MWCNTs in a normal lung (WT mice) leads to the presence of tubes a week later within the alveolar macrophages and BAL. If particles are not cleared, and the lung undergoes chronic inflammation it is likely that injury to tissue structure would occur, risking barrier damage as well as severe changes in lung function (increased work of breathing).

Defining Surfactant Protein-D – Nanoparticle Interactions

Further research beyond the SP-D$^{-/-}$ model presented in this manuscript needs to be performed to better define the interactions of SP-D with nanoparticles *in vivo*. The difficulty with the SP-D$^{-/-}$ model becomes that treatment effects due to low-level inflammation versus effects due to absence of SP-D are challenging to decipher. Future *in vivo* studies may benefit from the use of a conditional SP-D$^{-/-}$ model. Conditional knockouts allow for the gene of interest to be inactivated in a specific tissue, while retaining functional expression in all other tissues. A more targeted genetic approach to knockout SP-D would likely allow for a model without low-level inflammation; essentially eliminating the "background noise" to tease out particle – SP-D specific effects.

Exploring Nano-Drug Delivery Systems in the Lung

The Centers for Disease Control and Prevention currently sites 18.7 million cases of adult asthma in the United States, and 6.8 million cases of childhood asthma. Nanomaterials are being developed for targeted drug therapy and diagnostics [78]. Asthma is a chronic inflammatory disorder, and there is potential in nanomaterials for a therapeutic drug delivery system [78]. As demonstrated within this manuscript, nanoparticles can remain within lung tissue over the course of weeks, and depending upon surface chemistry can elicit differential immune and functional responses. Researchers can potentially utilize nanotechnology to target specific inflammatory cells to control chronic respiratory symptoms; work is currently being done to explore nano-therapies not only for asthma, but for chronic obstructive pulmonary disease (COPD) as well [78].

There may be difficulties however in utilizing nano-drug delivery systems in the lung. Inflammatory processes of asthma and other chronic respiratory disorders are easily triggered by inhaled irritants, and with an increase in environmental exposure to nanomaterials there are increasing opportunities to inhale unknown types and quantities of nanomaterials. This may lead to bioaccumulation within the lung of unknown nanomaterial that could potentially interact adversely with nano-therapies for lung disease. Another cause for caution, is the ability of nanoparticles to cross from the lung to into the blood [79]. Depending upon the biophysics of the nanomaterial and the structural integrity of the lung epithelial and endothelial barriers, there may be systemic effects to consider when using inhaled nano-drug delivery systems. Research models need to be developed that begin examining the effects of nanomaterials in various chronic respiratory disorders considering the above benefits and risks.

APPENDICES

A.1 PUBLICATION LIST

MANUSCRIPTS PUBLISHED

1. Mukherjee D, **Botelho D**, Gow AJ, Zhang J, Georgopoulos PG (2013) Computational multiscale toxicodynamic modeling of silver and carbon nanoparticle effects on mouse lung function. *PLoS One* 8(12):e80917.
2. **Botelho DJ**, Leo B, Massa CB, Sarkar S, Tetley T, Chung KF, Chen S, Ryan M, Porter A, Zhang J, Schwander S, Gow AJ (2015) Low dose AgNPs reduce lung mechanical function and innate immune defense in the absence of cellular toxicity. *Nanotoxicology* Jul 7:1-10. [Epub ahead of print].
3. Theodorou IG, **Botelho D**, Schwander S, Zhang J, Chung KF, Tetley TD, Shaffer M, Gow A, Ryan MP, Porter AE (2015) Static and dynamic microscopy of the chemical stability and aggregation state of silver nanowires in components of murine pulmonary surfactant provides insights into bio-nano interactions. *Environmental Science & Technology* Jul 7;49(13):8048-56. doi: 10.1021/acs.est.5b01214. Epub 2015 Jun 25.

MANUSCRIPTS IN PREPARATION FOR SUBMISSION

1. **Botelho DJ**, Leo B, Massa CB, Sarkar S, Tetley T, Chung KF, Chen S, Ryan M, Porter A, Zhang J, Schwander S, Gow AJ (2015) Exposure to metal nanospheres leads to altered respiratory mechanics & delayed immune response *in vivo*. (*In progress*).
2. **Botelho DJ**, Leo B, Mass CB, Taylor S, Tetley T, Chung KF, Chen S, Ryan M, Porter A, Zhang J, Schwander S, Gow AJ (2015) Surfactant protein-D mediated inflammatory response in murine multi-walled carbon nanotube respiratory exposure model. (*In progress*).

A.2 ABSTRACTS & CONFERENCE PROCEEDINGS

INTERNATIONAL MEETINGS

1. **Botelho DJ**, Chung F, Porter A, Gow AJ (2012) Nanoparticles disrupt lung function either directly or by inflammatory induction. Abstract accepted by the Interantional Conference on Biology, Chemistry and Therapeutic Application of Nitric Oxide, Edinburgh, Scotland. (Poster presentation 2012).

NATIONAL MEETINGS

1. **Botelho DJ**, Shaffer M, Porter A, Chung F, Tetley T, Zhang J, Gow A. (2015) Lung Lining Interaction Determines the Fate of Multi-Walled Carbon Nanotubes (MWCNTs) *in vivo*. Abstract accepted by the American Physiological Society, Boston, Massachusetts (Poster presentation 2015).
2. **Botelho DJ**, Porter A, Chung F, Tetley T, Zhang J, Gow A. (2014) Effects of Multi-Walled Carbon Nanotube Solubility on Inflammation & Lung Function.

Abstract accepted by the Society of Toxicology Annual Meeting, Phoenix, Arizona (Poster presentation 2014).

3. **Botelho DJ**, Sarkar S, Chung F, Porter A, Schwander S, Gow A. (2013) Resolution of inflammatory and surfactant alterations mediated by carbon black and silver nanospheres. Abstract accepted by the Society of Toxicology Annual Meeting, San Antonio, Texas (Poster presentation 2013).
4. **Botelho DJ**, Sieffert J, Zhao J, Sarkar S, Schwander S, Poter A, Ryan M, Tetley TD, Zhang J, Chung KF, Gow AJ. (2013) Effects of particle size and functionalization on the pulmonary response of rodents to silver nanoparticles. Abstract accepted by NIEHS Centers for Nanotechnology Health Implications Research (NCNHIR) Consortium Meeting, Research Triangle Park, North Carolina (Poster presentation 2013).
5. **Botelho DJ**, Sarkar S, Massa CB, Porter Alex, Ryan M, Zhang J, Schwander S, Chung KF, Gow AJ (2013) The effects of acute pulmonary exposure to silver and carbon nanospheres on lung function and inflammatory status. Abstract accepted by NIEHS Centers for Nanotechnology Health Implications Research (NCNHIR) Consortium Meeting, Research Triangle Park, North Carolina (Poster presentation 2013).

REFERENCES

1. Bakshi, M.S., et al., *Metal Nanoparticle Pollutants Interfere with Pulmonary Surfactant Function In Vitro.* Biophysical Journal, 2008. **94**(3): p. 855-868.
2. Comfort, K.K., et al., *Less is more: long-term in vitro exposure to low levels of silver nanoparticles provides new insights for nanomaterial evaluation.* ACS Nano, 2014. **8**(4): p. 3260-71.
3. Herzog, E., et al., *Dispersion medium modulates oxidative stress response of human lung epithelial cells upon exposure to carbon nanomaterial samples.* Toxicol Appl Pharmacol, 2009. **236**: p. 276 - 281.
4. Herzog, F., et al., *Mimicking exposures to acute and lifetime concentrations of inhaled silver nanoparticles by two different in vitro approaches.* Beilstein Journal of Nanotechnology, 2014. **5**: p. 1357-1370.
5. Richter, L., et al., *Monitoring cellular stress responses to nanoparticles using a lab-on-a-chip.* Lab on a Chip, 2011. **11**(15): p. 2551-2560.
6. Fehrenbach, H., *Alveolar epithelial type II cell: defender of the alveolus revisited.* Respiratory Research, 2001. **2**(1): p. 33 - 46.
7. Chang, C.-M. and Y.-L. Liu, *Electrical Conductivity Enhancement of Polymer/Multiwalled Carbon Nanotube (MWCNT) Composites by Thermally-Induced Defunctionalization of MWCNTs.* ACS Applied Materials & Interfaces, 2011. **3**(7): p. 2204-2208.
8. Clement, J.L. and P.S. Jarrett, *Antibacterial Silver.* Metal-Based Drugs, 1994. **1**(5-6): p. 467-482.
9. Shim, I.-K., et al., *An organometallic route to highly monodispersed silver nanoparticles and their application to ink-jet printing.* Materials Chemistry and Physics, 2008. **110**(2–3): p. 316-321.
10. Tolaymat, T.M., et al., *An evidence-based environmental perspective of manufactured silver nanoparticle in syntheses and applications: a systematic review and critical appraisal of peer-reviewed scientific papers.* Sci Total Environ, 2010. **408**(5): p. 999-1006.
11. Zhang, W., Z. Zhang, and Y. Zhang, *The application of carbon nanotubes in target drug delivery systems for cancer therapies.* Nanoscale Research Letters, 2011. **6**(1): p. 555-555.
12. Dhar, P., et al., *Lipid-Protein Interactions Alter Line Tensions and Domain Size Distributions in Lung Surfactant Monolayers.* Biophysical Journal, 2012. **102**(1): p. 56-65.
13. Foldbjerg, R., D. Dang, and H. Autrup, *Cytotoxicity and genotoxicity of silver nanoparticles in the human lung cancer cell line, A549.* Archives of Toxicology, 2011. **85**(7): p. 743-750.
14. Leo, B.F., et al., *The stability of silver nanoparticles in a model of pulmonary surfactant.* Environ Sci Technol, 2013. **47**(19): p. 11232-40.
15. Salvador-Morales, C., et al., *Binding of pulmonary surfactant proteins to carbon nanotubes; potential for damage to lung immune defense mechanisms.* Carbon, 2007. **45**(3): p. 607-617.

16. Tatur, S. and A. Badia, *Influence of hydrophobic alkylated gold nanoparticles on the phase behavior of monolayers of DPPC and clinical lung surfactant.* Langmuir, 2012. **28**(1): p. 628-39.
17. Davoren, M., et al., *In vitro toxicity evaluation of single walled carbon nanotubes on human A549 lung cells.* Toxicol in vitro, 2007. **21**(3): p. 438-448.
18. Chen, Z., et al., *Acute toxicological effects of copper nanoparticles in vivo.* Toxicol Lett, 2006. **163**(2): p. 109-120.
19. Ruge, C.A., et al., *The interplay of lung surfactant proteins and lipids assimilates the macrophage clearance of nanoparticles.* PLoS One, 2012. **7**(7): p. e40775.
20. Kendall, M., et al., *Surfactant protein D (SP-D) alters cellular uptake of particles and nanoparticles.* Nanotoxicology, 2013. **7**(5): p. 963-73.
21. Marchetti, M., et al., *Adsorption of surfactant protein D from human respiratory secretions by carbon nanotubes and polystyrene nanoparticles depends on nanomaterial surface modification and size*. Vol. 370. 2015.
22. Håkansson, K., et al., *Crystal structure of the trimeric α-helical coiled-coil and the three lectin domains of human lung surfactant protein D.* Structure, 1999. **7**(3): p. 255-264.
23. Braakhuis, H.M., et al., *Identification of the appropriate dose metric for pulmonary inflammation of silver nanoparticles in an inhalation toxicity study.* Nanotoxicology, 2015: p. 1-11.
24. Braakhuis, H.M., et al., *Particle size dependent deposition and pulmonary inflammation after short-term inhalation of silver nanoparticles.* Part Fibre Toxicol, 2014. **11**(1): p. 49.
25. Smulders, S., et al., *Toxicity of Nanoparticles Embedded in Paints Compared with Pristine Nanoparticles in Mice.* Toxicological Sciences, 2014. **141**(1): p. 132-140.
26. Kim, Y.S., et al., *Twenty-eight-day oral toxicity, genotoxicity, and gender-related tissue distribution of silver nanoparticles in Sprague-Dawley rats.* Inhal Toxicol, 2008. **20**(6): p. 575-83.
27. Ji, J.H., et al., *Twenty-eight-day inhalation toxicity study of silver nanoparticles in Sprague-Dawley rats.* Inhal Toxicol, 2007. **19**(10): p. 857-71.
28. Anderson, D.S., et al., *Influence of particle size on persistence and clearance of aerosolized silver nanoparticles in the rat lung.* Toxicol Sci, 2015. **144**(2): p. 366-81.
29. Muller, J., et al., *Respiratory toxicity of multi-wall carbon nanotubes.* Toxicol Appl Pharmacol, 2005. **207**(3): p. 221-31.
30. Han, S.G., et al., *Acute pulmonary effects of combined exposure to carbon nanotubes and ozone in mice.* Inhal Toxicol, 2008. **20**(4): p. 391-8.
31. Ma-Hock, L., et al., *Inhalation toxicity of multiwall carbon nanotubes in rats exposed for 3 months.* Toxicol Sci, 2009. **112**(2): p. 468-81.
32. Ryman-Rasmussen, J.P., et al., *Inhaled multiwalled carbon nanotubes potentiate airway fibrosis in murine allergic asthma.* Am J Respir Cell Mol Biol, 2009. **40**(3): p. 349-58.
33. Harkema, J.R., S.A. Carey, and J.G. Wagner, *The Nose Revisited: A Brief Review of the Comparative Structure, Function, and Toxicologic Pathology of the Nasal Epithelium.* Toxicologic Pathology, 2006. **34**(3): p. 252-269.

34. Atochina, E.N., et al., *Delayed Clearance of Pneumocystis carinii Infection, Increased Inflammation, and Altered Nitric Oxide Metabolism in Lungs of Surfactant Protein-D Knockout Mice.* Journal of Infectious Diseases, 2004. **189**(8): p. 1528-1539.
35. Botas, C., et al., *Altered surfactant homeostasis and alveolar type II cell morphology in mice lacking surfactant protein D.* Proceedings of the National Academy of Sciences, 1998. **95**(20): p. 11869-11874.
36. Casey, J., et al., *Alveolar surfactant protein D content modulates Bleomycin-induced lung injury.* Am J Resp Crit Care, 2005. **172**(6): p. 869-877.
37. Groves, A.M., et al., *Age-related increases in ozone-induced injury and altered pulmonary mechanics in mice with progressive lung inflammation.* Am J Physiol Lung Cell Mol Physiol, 2013. **305**(8): p. L555-68.
38. Bates, J.H. and G.B. Allen, *The estimation of lung mechanics parameters in the presence of pathology: a theoretical analysis.* Ann Biomed Eng, 2006. **34**(3): p. 384-92.
39. Moriya, H.T., J.C. Moraes, and J.H. Bates, *Nonlinear and frequency-dependent mechanical behavior of the mouse respiratory system.* Ann Biomed Eng, 2003. **31**(3): p. 318-26.
40. Groves, A.M., et al., *Prolonged injury and altered lung function after ozone inhalation in mice with chronic lung inflammation.* Am J Respir Cell Mol Biol, 2012. **47**(6): p. 776-83.
41. Massa, C.B., et al., *Acute chlorine gas exposure produces transient inflammation and a progressive alteration in surfactant composition with accompanying mechanical dysfunction.* Toxicol Appl Pharmacol, 2014. **278**(1): p. 53-64.
42. Fehrenbach, H., et al., *Keratinocyte growth factor-induced hyperplasia of rat alveolar type II cells in vivo is resolved by differentiation into type I cells and by apoptosis.* European Respiratory Journal, 1999. **14**(3): p. 534-544.
43. Gardai, S.J., et al., *By Binding SIRPα or Calreticulin/CD91, Lung Collectins Act as Dual Function Surveillance Molecules to Suppress or Enhance Inflammation.* Cell, 2003. **115**(1): p. 13-23.
44. Ikegami, M., et al., *Surfactant protein D influences surfactant ultrastructure and uptake by alveolar type II cells*. Vol. 288. 2005. L552-L561.
45. Korfhagen, T.R., et al., *Surfactant Protein-D Regulates Surfactant Phospholipid Homeostasis in Vivo.* Journal of Biological Chemistry, 1998. **273**(43): p. 28438-28443.
46. Fukuzawa, T., et al., *Lung surfactant levels are regulated by Ig-Hepta/GPR116 by monitoring surfactant protein D.* PLoS One, 2013. **8**(7): p. e69451.
47. Beers, M.F., et al., *Localization, synthesis, and processing of surfactant protein SP-C in rat lung analyzed by epitope-specific antipeptide antibodies.* Journal of Biological Chemistry, 1994. **269**(32): p. 20318-28.
48. Ingenito, E.P., et al., *Decreased surfactant protein-B expression and surfactant dysfunction in a murine model of acute lung injury.* Am J Respir Cell Mol Biol, 2001. **25**(1): p. 35-44.
49. Atochina-Vasserman, E., et al., *Immune reconstitution during Pneumocystis lung infection: disruption of surfactant component expression and function by S-nitrosylation.* J Immunol, 2009. **182**(4): p. 2277-2287.

50. Sarkar, S., et al., *Suppression of the NF-kB pathway by diesel exhaust particles impairs human antimycobacterial immunity.* J Immunol, 2012. **188**(6): p. 2778-2793.
51. Bligh, E. and W. Dyer, *A Rapid Method Of Total Lipid Extraction And Purification.* Can J Biochem Physiol, 1959. **37**: p. 911-917.
52. Sager, T.M. and V. Castranova, *Surface area of particle administered versus mass in determining the pulmonary toxicity of ultrafine and fine carbon black: comparison to ultrafine titanium dioxide.* Part Fibre Toxicol, 2009. **6**: p. 15.
53. Botelho, D.J., et al., *Low-dose AgNPs reduce lung mechanical function and innate immune defense in the absence of cellular toxicity.* Nanotoxicology, 2015: p. 1-10.
54. Seeger, W., et al., *Lung surfactant phospholipids associate with polymerizing fibrin: loss of surface activity.* American journal of respiratory cell and molecular biology, 1993. **9**: p. 213-213.
55. Shang, L., K. Nienhaus, and G.U. Nienhaus, *Engineered nanoparticles interacting with cells: size matters.* J Nanobiotechnology, 2014. **12**: p. 5.
56. Mu, Q., et al., *Chemical Basis of Interactions Between Engineered Nanoparticles and Biological Systems.* Chemical Reviews, 2014. **114**(15): p. 7740-7781.
57. Tejamaya, M., et al., *Stability of citrate, PVP, and PEG coated silver nanoparticles in ecotoxicology media.* Environ Sci Technol, 2012. **46**(13): p. 7011-7.
58. Warheit, D.B., K.L. Reed, and M.P. DeLorme, *Embracing a Weight-of-Evidence Approach for Establishing NOAELs for Nanoparticle Inhalation Toxicity Studies.* Toxicologic Pathology, 2013. **41**(2): p. 387-394.
59. Demokritou, P., et al., *An in vivo and in vitro toxicological characterisation of realistic nanoscale CeO2 inhalation exposures.* Nanotoxicology, 2013. **7**(8): p. 1338-1350.
60. Ding, N., et al., *Intratracheal administration of fullerene nanoparticles activates splenic CD11b+ cells.* J Hazard Mater, 2011. **194**: p. 324-30.
61. Dhaliwal, K., et al., *Monocytes Control Second-Phase Neutrophil Emigration in Established Lipopolysaccharide-induced Murine Lung Injury.* Am J Resp Crit Care, 2012. **186**(6): p. 514-524.
62. Allen, G. and J. Bates, *Dynamic mechanical consequences of deep inflation in mice depend on type and degree of lung injury.* J Appl Physiol, 2004. **96**(1): p. 293-300.
63. AshaRani, P.V., et al., *Cytotoxicity and Genotoxicity of Silver Nanoparticles in Human Cells.* ACS Nano, 2008. **3**(2): p. 279-290.
64. Park, E.J., K. Choi, and K. Park, *Induction of inflammatory responses and gene expression by intratracheal instillation of silver nanoparticles in mice.* Arch Pharm Res, 2011. **34**(2): p. 299-307.
65. Andreeva, A., M. Kutuzov, and T. Voyno-Yasenetskaya, *Regulation of surfactant secretion in alveolar type II cells.* Am J Physiol Lung Cell Mol Physiol, 2007. **293**(2): p. L259-L271.
66. Vuk-Pavlovic, Z., et al., *Carbohydrate Recognition Domain of Surfactant Protein D Mediates Interactions with Pneumocystis carinii Glycoprotein A.* Am J Respir Cell Mol Biol, 2001. **24**(4): p. 475-484.

67. Thacker, S., et al., *Restoration of lung surfactant protein D by IL-6 protects against secondary pneumonia following hemorrhagic shock.* Journal of Infection, 2014. **68**(3): p. 231-241.
68. Gasser, M., et al., *Pulmonary surfactant coating of multi-walled carbon nanotubes (MWCNTs) influences their oxidative and pro-inflammatory potential in vitro.* Particle and Fibre Toxicology, 2012. **9**(1): p. 17.
69. Nagai, D., K. Miyazaki, and H. Tsukamoto, *Molecular dynamics simulations on heat conduction in nano-porous Si.* Heat Transfer—Asian Research, 2013. **42**(3): p. 274-280.
70. Takagi, D., et al., *Mechanism of gold-catalyzed carbon material growth.* Nano Lett, 2008. **8**(3): p. 832-5.
71. Xuan, J., et al., *Relationship between IL-1β gene polymorphism and gastric mucosal IL-1β levels in patients with Helicobacter pylori infection.* Journal of Gastroenterology, 2005. **40**(8): p. 796-801.
72. Qiao, H.L., J. Yang, and Y.W. Zhang, *Relationships between specific serum IgE, cytokines and polymorphisms in the IL-4, IL-4Rα in patients with penicillins allergy.* Allergy, 2005. **60**(8): p. 1053-1059.
73. Sun, L., et al., *Dual role of interleukin-10 in the regulation of respiratory syncitial virus (RSV)-induced lung inflammation.* Clinical & Experimental Immunology, 2013. **172**(2): p. 263-279.
74. Moser, B., et al., *Neutrophil-activating properties of the melanoma growth-stimulatory activity.* The Journal of Experimental Medicine, 1990. **171**(5): p. 1797-1802.
75. Ma, P.C., et al., *Correlation between electrokinetic potential, dispersibility, surface chemistry and energy of carbon nanotubes.* Composites Science and Technology, 2011. **71**(14): p. 1644-1651.
76. Ruge, C.A., et al., *Uptake of nanoparticles by alveolar macrophages is triggered by surfactant protein A.* Nanomedicine: Nanotechnology, Biology and Medicine, 2011. **7**(6): p. 690-693.
77. Mukherjee, D., et al., *Computational multiscale toxicodynamic modeling of silver and carbon nanoparticle effects on mouse lung function.* PLoS One, 2013. **8**(12): p. e80917.
78. Vij, N., *Nano-based theranostics for chronic obstructive lung diseases: challenges and therapeutic potential.* Expert opinion on drug delivery, 2011. **8**(9): p. 1105-1109.
79. Choi, H.S., et al., *Rapid Translocation of Nanoparticles from the Lung Airspaces to the Body.* Nature biotechnology, 2010. **28**(12): p. 1300-1303.